A thermodynamic sea-ice model

Meijering, Laurens

Award date:
1993

ministerie van verkeer en waterstaat

koninklijk nederlands meteorologisch instituut

A Thermodynamic Sea-Ice Model

afstudeerverslag

Laurens Meijering

A THERMODYNAMIC SEA- ICE MODEL

Afstudeerverslag voor Technische Universiteit Eindhoven

Begeleiding KNMI: dr. R. Haarsma
Begeleiding TUE : dr. ir. B. van der Sijde
prof. dr. ir. G.J.F. van Heijst

Laurens Meijering,

KNMI, 21 januari 1993

Summary

Samenvatting

Sinds de industriele revolutie heeft de mens grote hoeveelheden CO_2 en andere, door de industrie geproduceerde, gassen in de atmosfeer gebracht. Deze gassen dragen bij tot een versterking van het natuurlijke broeikaseffect, wat mogelijk een temperatuurstijging op aarde veroorzaakt. Met behulp van klimaatmodellen, die bepaalde eigenschappen van het huidige klimaat simuleren, probeert men deze mogelijke temperatuurstijging enigzins te begrijpen en zelfs te voorspellen.

Huidige klimaatmodellen kunnen zeer gecompliceerd zijn, waarbij de verschillende klimaatcomponenten atmosfeer, oceaan, en zeeijs, aan elkaar zijn gekoppeld. Door de ingewikkeldheid van deze klimaatmodellen is het moeilijk inzicht te krijgen in de gevoeligheid voor de verschillende parameterisaties in deze modellen, zoals bijvoorbeeld de bewolkingsgraad en de warmte- uitwisseling tussen de atmosfeer en de oceaan. Een ander hiermee samenhangend probleem is de klimaatdrift die slechts in toom kan worden gehouden met behulp van een nogal rigoreuze fluxcorrectie vanuit de atmosfeer. Op het KNMI wordt een relatief eenvoudig klimaatmodel ontwikkeld om de gevoeligheid voor de verschillende parameterisaties te onderzoeken. Tevens wordt hiermee het probleem van de klimaatdrift bestudeerd. Onderdeel van dit klimaatmodel is een model dat de vorming van zeeijs simuleert.

Zeeijs bedekt ongeveer zeven procent van het oceaanoppervlak in de wereld. Het fungeert als een sterke barriere tussen de oceaan en de atmosfeer in de polaire gebieden, en belemmert daardoor de energie-uitwisseling tussen hen beiden. Zeeijs smelt en groeit als gevolg van de seizoensvariaties in de energiefluxen vanuit de atmosfeer en de oceaan. Omdat zeeijs relatief zoet is ten opzichte van het onderliggende oppervlaktewater, speelt het ijs ook een grote rol voor het zoutgehalte van de menglaag van de oceaan. Als gevolg van de zout- en temperatuur- effecten heeft de vorming van zeeijs invloed op de grootschalige oceaancirculatie. De sterkte en structuur van deze oceaancirculatie bepalen in belangrijke mate het wereldklimaat.

Dit verslag behandelt een thermodynamisch zeeijsmodel. Dynamica van zeeijs, zoals drift en deformatie, zijn niet meegenomen in de modellering. De theorie achter dit model wordt gepresenteerd en verschillende numerieke experimenten worden besproken. Het verslag geeft verder een kort overzicht van de huidige stand van zaken ten aanzien van het broeikaseffect.

CONTENTS

CHAPTER 1. GENERAL INTRODUCTION

The world's climate properties are immense and understanding how this climate system works seems rather impossible. As long as the earth exists the influence of climate has been enormous. Several ice ages occurred in which prehistorical animals could not survive. Now the climate has created surroundings in which mankind can live prosperously. However due to industrial activities, large energy use of fossile fuels, devestation of the tropical rain forests, and many reasons more, climate may be changing rather quickly compared to historical or natural changes in climate. Possible consequences and effects of this transformation in climate are only partially known. The most discussed subjects at the moment are the ozon hole at the poles of the earth and the greenhouse effect. Causes and consequences of the greenhouse effect are discussed in chapter 2. Social problems will also come up for discussion.

Many scientific institutes, such as the Royal Dutch Metereological Institute in de Bilt, study these subjects by using climate models. Current climate models consist of elaborate numerical procedures which can solve many of the equations encapsulating the physical laws that govern climate. Complete climate models should include the three major climatological components, the atmosphere, the ocean and the sea ice at both poles (actually, the biosphere and geosphere should also have to be included). However, the coupling of these climatological components is not a very simple and straightforward task. Their different timescales of relaxation make it very complicated. Greenhouse effect calculations with such coupled models are performed by computing temperature increments due to CO_2-concentration doubling in the atmosphere.

This report concentrates on the formation and melting of sea ice at the North Pole. Purpose of the presented sea ice model is not to understand its direct influence on the greenhouse effect. In first instance it is necessary to gain more insight in the mechanism responsible for the growth and decrease of sea ice, and the role of sea ice in the climate system. Only in that way climate changes concerning sea ice can be predicted well.

Sea ice covers roughly 7% of the Earth's oceans and forms a partial but at times very effective barrier between these oceans and the atmosphere. The configuration of sea ice and open water and the seasonal production of sea ice significantly affect variations of the atmosphere and oceanic circulation patterns on all climatic time scales. The interaction between atmosphere and ocean is influenced by the sea ice area (extent, concentration) and the sea ice thickness. The ice- covered area is important for the modification of the radiation budget because of the high albedo (reflectivity) of sea ice. Ice thickness and concentration, on the other hand, influence the exchange of heat and momentum between ocean and atmosphere. Sea ice exists as a result of the cooling of polar water below its freezing point, and varies from fine ice particles suspended in water to extensive stretches of ice with thicknesses up to 4 meters. In contrast to the distribution of the atmosphere and the oceans, the distribution of sea

ice undergoes large variations, both seasonally and interannually, thereby introducing additional complications to climate modeling studies.

The effect of ice growth or ice melt on the temperature and salinity patterns in the the upper ocean layer, called the mixed layer, probably has great impact on the thermohaline circulation. This thermohaline circulation is driven by temperature (thermo) differences and salinity (haline) differences. These differences induce density gradients and thus pressure gradients, which drive the oceanic flow. Important areas for the thermohaline circulation are the polar regions. In these regions deep convection occurs, as a result of unstable stratification due to surface cooling. A large part of the world's bottom water is believed to originate from the polar regions.

The thermohaline forcing consists of heat fluxes, i.e. solar radiance, infrared longwave radiation, latent and sensible heat fluxes, and salinity fluxes. In the open ocean these salinity fluxes are in fact freshwater fluxes, caused by precipitation and evaporation. However, underneath the ice slab the salinity fluxes arise due to melt and growth of the ice, which has a lower salinity contents than the surrounding fluid water. Thus sea ice acts not only as a kind of source for temperature differences but also for salinity differences. For climatological studies the thermohaline circulation is considered to be very important.

Sea ice models for use in large scale climate simulations have as primary goals to simulate, at each location and each time step, the amount of ice, including both ice thickness and areal ice concentration. There are plenty of good data on the sea ice extent, and the data on the ice concentration is improving, but there are very few data on sea ice thickness in the Arctic and nearly none in the Antarctic. Sea ice extent and concentration can be determined with satellite sensors, but the thickness has to be monitored by in situ instruments.

Sea- ice models can be divided into two categories: those which include only the thermodynamics of the ice cover, and those which also take ice dynamics into account. The thermodynamic sea- ice models determine the thickness and temperature structure of the ice, based on the principles of the conservation of energy. The sea- ice model presented here is based on the ice model of Semtner [1976], who adapted his model on a previous study performed by Maykut and Untersteiner [1971]. It is a one- dimensional thermodynamic sea- ice model. Ice dynamics are omitted. This choice was made with a view to simplicity and good understanding of basic physical principles and for later implementation of the ice model into the ocean model developed by Haarsma and Lenderink [1992]. The ice model is extended with an oceanic mixed layer, which is positioned immediately underneath the ice cover. Chapter 3 gives a description of the complete sea- ice model. Chapter 4 presents the most important results from numerical experiments involving quantities such as ice thickness, surface temperature, heat balance, mixed layer temperature and salinity, and ice margin. Chapter 5 discusses the quality of the model and uncovers the shortcomings and deficiencies of the model, paying much attention to the heat balance at the top of the ice shelf. Finally chapter 6 summarizes the most important features of the presented thermodynamic sea- ice model.

CHAPTER 2. THE GREENHOUSE EFFECT

2.1. Introduction

Since the industrial revolution in the nineteenth century, the emissions of carbon dioxide and other gases have increased tremendously due to human industrial activities. These massive emissions may be inadvertently changing the current climate and they may cause the temperature of the Earth's surface to increase, which is often referred to as the global warming. In other words, through our industrial activities humankind is creating an enhanced greenhouse effect next to the natural greenhouse effect. The global and local effects of this global warming are only known partially, but the consequences can have a large impact on all kinds of fields, such as agriculture, sea- level rise, ecosystems, cryosphere and for example precipitation.

To diminish the consequences of the global warming humankind should reduce the greenhouse gas emissions up to even 75%. However, according to current prognoses, economic activities will grow in the following 50 years to a five times larger magnitude or even more. Especially East- European and developing countries will have rapidly increasing energy usage. The world's population will increase very rapidly too, approximately to a stabilizing amount between 8 and 14 milliard people in the next century. This leads to large consumption rates, and thus requires an extensive increase in energy usage. The Earth's ecosystem will not be able to keep up with these rigorous changes. Thus the problems arising due to the human- induced greenhouse effect should not be underestimated, and future policy should require large international effort to minimize causes and consequences of the current global warming.

2.2. The mechanism of the Greenhouse effect

The driving energy for weather and climate is provided by the Sun. The Earth intercepts solar radiation and reflects about one third of it. The rest is absorbed by the different components of the climate system, being the atmosphere, ocean, ice, land, and biota. In the long term the energy absorbed from the solar radiation is balanced by outgoing radiation from the Earth and atmosphere. This terrestrial radiation takes the form of longwave invisible infrared energy, and its magnitude is determined by the temperature of the Earth- atmosphere system. This energy balance in the long term can be written as (see for example Mitchell [1989])

$$\pi a^2 (1-\alpha) S = 4\pi a^2 \sigma (T_e)^4$$

where a stands for the Earth's radius,
α is the fraction of radiation reflected by the Earth and atmosphere, α=0.30,
S is the solar constant, S=1353 Wm^{-2},
σ is the Stefan- Boltzmann constant, $\sigma = 5.67 \cdot 10^{-8}$ Wm^{-2},
and T_e is the effective radiating temperature of the system.

In case of the above parameterizations T_e corresponds to a value of approximately 254 K. In the absence of an atmosphere, T_e will be the Earth's surface temperature. However in reality the mean global temperature is about 33 K higher. This is due to the greenhouse effect. The solar radiation can pass through the clear atmosphere relatively unimpeded. But longwave terrestrial radiation emitted by the surface of the Earth is partially absorbed and then re-emitted by a number of trace gases, known as the greenhouse gases. Since, on average, there should be a balance of the outgoing longwave radiation and the incoming solar radiation, both the atmosphere and the surface will be warmer than they would be without the greenhouse gases. Figure 1 schematically illustrates the greenhouse effect.

The main natural greenhouse gases are not the major constituents, nitrogen and oxygen, but water vapour (the biggest contributor), carbon dioxide, methane, nitrous oxide, and ozone in the troposphere and stratosphere. Aerosols or small particles in the atmosphere can also affect climate because they can reflect and absorb radiation. Explosive vulcanic eruptions can increase concentrations of aerosols in the lower stratosphere.

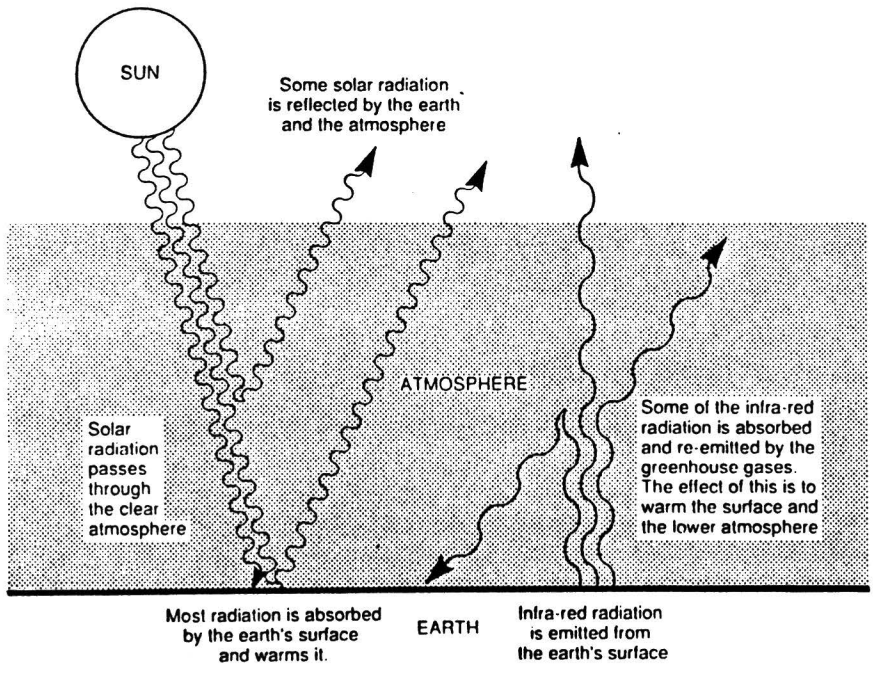

Fig.1 A simplified diagram illustrating the greenhouse effect.

The energy balance of the earth- atmosphere system can be disturbed by changes in the radiative forcing on climate. For example, the Sun radiance has some variability on an 11-year time scale, and also longer solar cycle periods may occur. Even slow variations in the Earth's orbit affect the distribution of the solar radiation. These orbit variations were probably responsible for initiating the ice ages according to the Milankovitch theory. Slow changes in the geometry of the Earth's orbit occur in response to predictable changes in the gravitational field experienced by the Earth, see Berger et al. [1984]. Furthermore, the climate has its own natural variability on all timescales and changes occur without any known external influence.

The greenhouse effect, caused by the occurrence of the greenhouse gases in the atmosphere, has also been observed with the help of satellites at other planets, such as Venus and Mars. Their surface temperatures are in general agreement with the greenhouse theory. Other evidence of the greenhouse effect goes back 160.000 years and originates from measurements from ice cores. They show us that the Earth's temperature is closely parallel to the amount of carbon dioxide and methane in the atmosphere. This correspondence is illustrated in figure 2. Cause and effect are difficult to distinguish. An increase in temperature can cause an increase in the amount of carbon dioxide, and vice versa. This seems to imply that temperature and carbon dioxide concentration are highly correlated and can amplify each other. For sure is that changes in the greenhouse gases were partly responsible for the large global temperature changes between the ice ages and the interglacial periods.

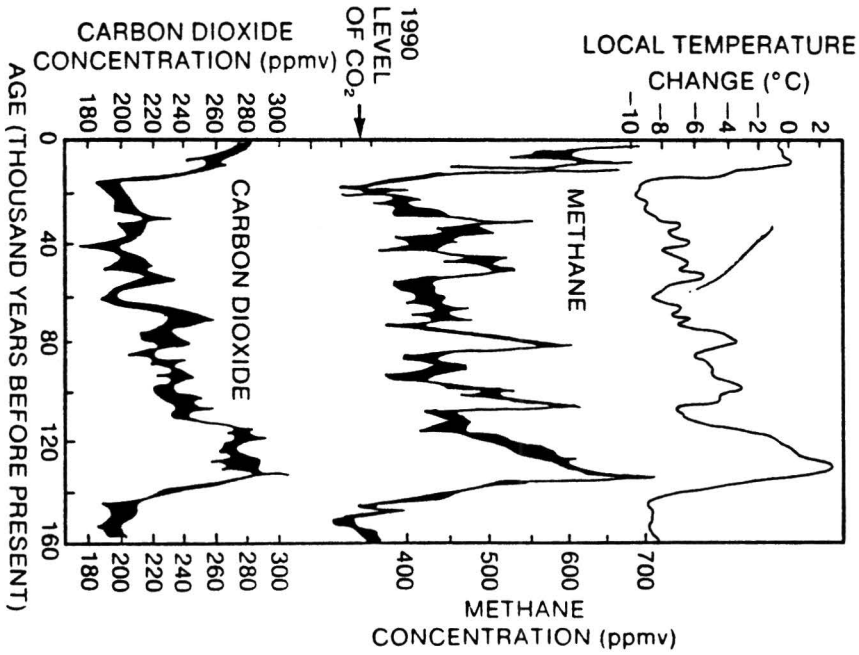

Fig.2 Methane and carbon dioxide concentrations and the closely correlated local temperature over the last 160.000 years. Also the present day concentration of carbon dioxide is indicated.

Nowadays the greenhouse gas concentrations are increasing rapidly due to human industrial activities. Humankind also added new greenhouse gases like chlorofluorocarbons to the Earth's atmosphere. In this way the global mean temperature will probably rise due to human interference. Strictly spoken, this effect is an enhanced greenhouse effect, namely above that occurring due to the natural greenhouse gas concentrations. Other human activities also have the potential to affect climate. A change in the albedo (reflectivity) of the land, due to desertification and/or deforestation affects the amount of solar radiation absorbed at the Earth's surface. Furthermore, human- made aerosols, coming from sulphur, are injected into the atmosphere and also ozone concentrations in the stratosphere are changed due to CFC emissions.

There are many uncertainties about the rate at which the climate of the Earth is changing. Many elaborate processes are involved and many feedbacks exist and global and local effects can be significantly different. This makes climate modelling concerning the greenhouse effect a very difficult task.

2.3. Greenhouse gases and feedbacks

Table 1 summarizes the emission rates of the most important greenhouse gases which are affected by human activities (IPCC report [1990]). Pre-industrial and present- day atmospheric concentrations are depicted, as well as the atmospheric lifetimes, which are quite different for each of the greenhouse gases. The pre- industrial concentrations of CFC11 and CFC12 equal zero, because they are pure industrial products. Water vapour is not included in the model, although it is the biggest contributor to the greenhouse effect. But water vapour is determined internally within the climate system, and, on a global scale, its concentration is not affected by human sources and sinks. The water vapour concentration will increase in response to global warming and thus enhances the greenhouse effect. The influence of ozone is very uncertain. Its concentration changes in the stratosphere and troposphere due to human CFC- emissions. Present observed ozone concentrations are too scarce to give a good estimation of its changing contribution to the greenhouse effect.

CO_2- concentrations are increasing due to the combustion of fossile fuels and due to deforestation. The current proportion is about 80% CO_2-concentration increase by combustion and 20% by deforestation. The mean proportions taken over the total industrial period are about 50-70% and 30-50% respectively. The way in which CO_2 is absorbed by the oceans and biosphere is not known very well.

CFC- concentrations have increased very fast after their invention around 1930. They are commonly used as aerosol propellants, solvents, refrigerants and foam blowing agents. Their emission rates are very well known. CFC-concentrations also diminish the ozone concentrations in chemical reactions. In this way it may contribute to the cooling of the Earth's surface.

Probably the source of methane originates from rice production, cattle rearing, biomass burning, coal mining and ventilation of natural gas. The cause of the increase of the nitrous oxide concentration is presumably also due to human activities; it seems likely that agriculture plays a part.

Other greenhouse gases, which only have a small contribution, are SO_2 and NO_x.

Table 1. Summary of greenhouse gases affected by human activities

	Carbon Dioxide	Methane	CFC-11	CFC-12	Nitrous Oxide
atmospheric concentration	ppmv	ppmv	pptv	pptv	ppbv
pre-industrial (1750-1800)	280	0.8	0	0	288
present day (1990)	353	1.72	280	484	310
current rate of change per year	1.8 (0.5%)	0.015 (0.9%)	9.5 (4%)	17 (4%)	0.8 (0.25%)
atmospheric lifetime (years)	50-200	10	65	130	150

ppmv=parts per million by volume;
ppbv=parts per billion (thousand million) by volume;
pptv=parts per trillion (million million) by volume.

The different lifetimes of the greenhouse gases, whose concentrations are influenced by human activities, are shown in table 1. Especially CO_2-emissions are important: emission rates are high and lifetimes of the gas are long. If humankind would stop the human CO_2- emission immediately, then still about half of the increase in CO_2- concentration caused by human activities would be evident by the year 2100. The lifetimes of CFC and CH_4 are much shorter. The longer we continue with the large present- day CO_2-emission rate, the larger the reductions of CO_2- emission rates are necessary to establish atmospheric stabilisation. The term atmospheric stabilisation is often used to describe the limiting of the concentration of the greenhouse gases at a certain level (for example the present- day atmospheric concentrations as depicted in table 2).

The effectivity of each of the greenhouse gases is quite different. For example, for one molecule of CO_2, CH_4 or CFC-11, the effectivity proportion concerning the global warming is 1:21:12,000. On a kilogram base the equivalent values are 1:58:4,000. The total radiative forcing at any time is the sum of those from the individual greenhouse gases. For simplicity this radiative forcing can be expressed in carbon dioxide units only, which would lead to a same forcing magnitude: this CO_2- concentration is called the equivalent carbon dioxide concentration. Since industrial times the greenhouse gases have increased to an amount of a 50% equivalent CO_2-concentration. Actually the CO_2- concentrations have increased 'only' 26%. Other greenhouse gas emissions are responsible for the other 24%. Figure 3 shows the radiative forcing and corresponding equivalent CO_2- concentrations from 1900 to 2100. Four scenarios have been worked out: the steepest line belongs to the Business-as-Usual (BaU) scenario, which implies that no steps

Table 2. Stabilisation of atmospheric concentrations. Reductions in human- made emissions of greenhouse gases required to stabilise concentrations at present- day levels (IPCC report [1990]).

greenhouse gas	reduction required
Carbon dioxide	> 60%
Methane	15-20%
Nitrous oxide	70-80%
CFC-11	70-75%
CFC-12	75-85%
HCFC-22	40-50%

are taken to limit greenhouse gas emissions. The other three scenarios B, C, and D assume that progressively increasing levels of controls reduce the growth of emissions. These scenarios are extensively described in the IPCC report [1990]. Appendix E gives a short description of the four emission scenarios.

Figure 4 shows the contribution of each of the human- made greenhouse gases to the change in radiation forcing from 1980 to 1990. The contribution of ozone may also be significant, but cannot be quantified at present. As can be seen carbon dioxide is responsible for about half of the decadal increase.

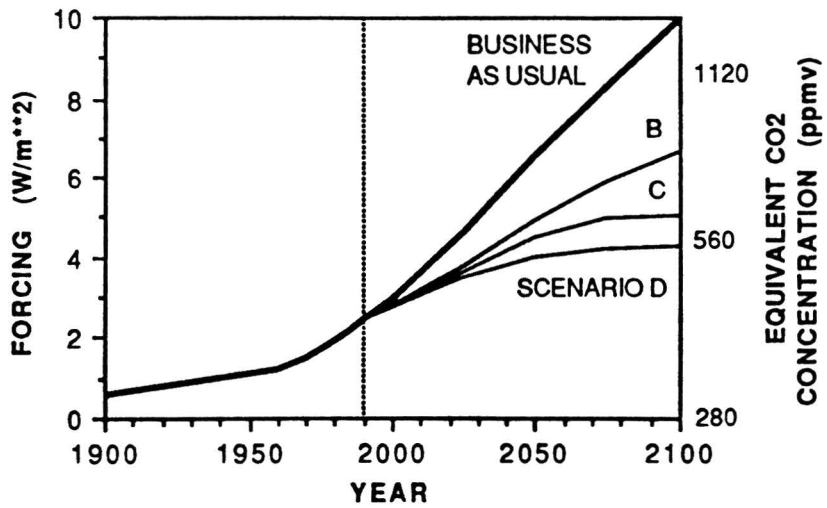

Fig.3 The radiative forcing and corresponding equivalent CO_2 concentration from 1900 to 2100 according to four different future scenarios.

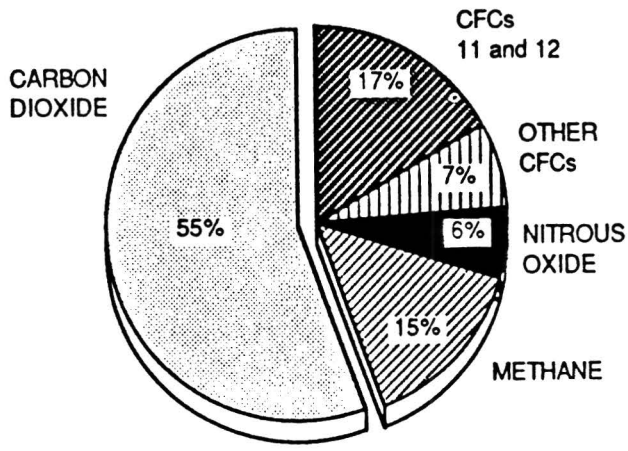

Fig.4 The relative contribution of each of the human- made greenhouse gases to the change in radiative forcing in the period 1980-1990.

To evaluate the consequences of the different greenhouse gases, the concept of relative Global Warming Potential (GWP) has been introduced in many models to account for the different types of gases with different lifetimes. The global warming potential of a greenhouse gas is an index which stands for the time integrated commitment to climate forcing from the instantaneous release of 1 kg of a trace gas expressed relative to that from 1 kg of carbon dioxide. The GWP can be written as

$$GWP = \frac{\int_0^n a_i c_i dt}{\int_0^n a_{co_2} c_{co_2} dt}$$

where a_i is the instantaneous radiative forcing due to a unit increase in the concentration of trace gas, i, and c_i is the concentration of trace gas i, remaining at time t, after its release and n is the number of years over which the calculation is performed. The corresponding values for carbon dioxide are in the denominator.

GWPs can be defined for different time horizons, reflecting the need to consider the cumulative effects on climate over various time scales. The longer time horizon is appropriate for the cumulative effect; the shorter time scale will indicate the response to emission changes in the short term.

Table 3 gives an estimate of the GWPs of the most important, by humankind influenced, greenhouse gases on a 100 year time horizon. It also shows the 1990 emission rates of the different gases. Although the GWP of carbon dioxide is the smallest, its relative contribution to the greenhouse effect is by far the greatest, due to its very large emission rate.

Table 3. Global Warming Potentials and 1990 emission rates of human- made greenhouse gases (IPCC report [1990]).

	GWP (100 yr time scale)	1990 emission (Tg)
Carbon dioxide	1	26000
Methane	21	300
Nitrous oxide	290	6
CFC's	various	0.9
HCFC-22	1500	0.1
Others	various	

Thus to compose an effective policy to reduce the global warming, one should carefully take into account the characteristics of each of the greenhouse gases, such as its relative contribution, its lifetime, and knowledge of its sources (and sinks).

Greenhouse gas emissions also can increase or decrease due to natural greenhouse gas feedbacks. In case of carbon dioxide several feedbacks are known. For example, when the Earth's temperature is rising, the CO_2-emission will increase due to the increase of the respiration at a faster rate than the increase in photosynthesis of the terrestrial ecosystems. Some plant and forest populations cannot adapt quickly enough to the environmental changes. In case of warmer conditions in a tundra area there will be a net flux of CO_2 to the atmosphere, because in these regions large amounts of carbon are stored. However an increase in the CO_2- concentration can also enlarge the productivity of some natural ecosystems, for example caused by an increased soil moisture in dry areas. The effectivity with which ecosystems can remove CO_2 is unknown. Furthermore, for higher oceanic temperatures, the CO_2 uptake will be diminished due to changes in the chemical an biological activities in the seawater and in the exchange rate of CO_2 between the upper ocean and deep ocean layers.

Methane emissions also increase at higher global temperatures and soil moisture, especially on natural wetlands and rice field areas or from methane that is stored in permafrost at high northern latitudes.

As can be seen there exists a high correspondence between the temperature and the greenhouse gas concentrations (as was also illustrated in figure 2). Although its rate is very uncertain, it is believed that greenhouse gas concentrations will increase in a warmer world caused by several natural feedback mechanisms.

2.4. (Possible) consequences of global warming

2.4.1. General consequences

The main consequence of the increase in the concentrations of the greenhouse gases is an increasing global mean averaged temperature. Under the IPCC Business-as-Usual scenario emissions of greenhouse gases, the average rate of increase of global mean temperature during the next century is estimated to be about 0.3 °C per decade (with an uncertainty range of 0.2 °C to 0.5 °C). Figure 5 displays the realised temperature rise from 1850 to 1990 according to observed increases in greenhouse gases. Figure 6 shows the simulated realised temperature rise and predictions of the future temperature rise between 1990 and 2100 for the four different scenarios. In case of the BaU- scenario also the uncertainty range is depicted. The realised temperature rise over the past 100 years is approximately 0.5 °C. However, we are also committed to a further temperature rise toward the equilibrium temperature. Due to the coupling of the atmosphere and the ocean, the temperature rise forced by the greenhouse effect will act to slow down as a result of the heat exchange between the atmosphere and the ocean. Because of their thermal capacity this takes decades to centuries. For the BaU scenario in the year 2030, for example, a further rise of 0.9 °C would be expected. Realisation of this enhanced temperature increase would become apparent decades to centuries afterwards.

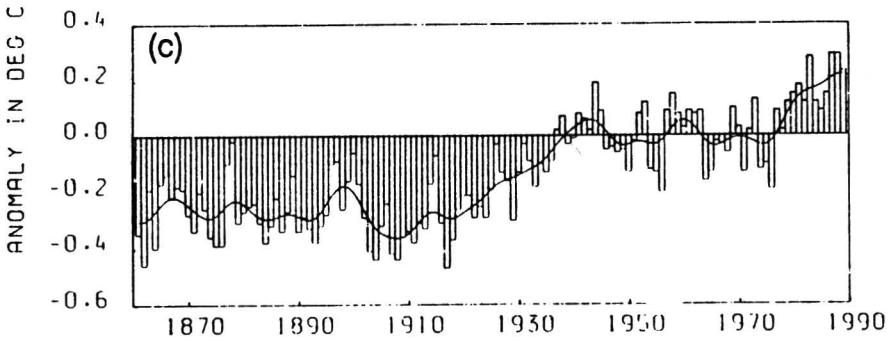

Fig.5 Combined land air and sea surface temperatures, 1861-1989, relative to 1951-1980, on a global scale.

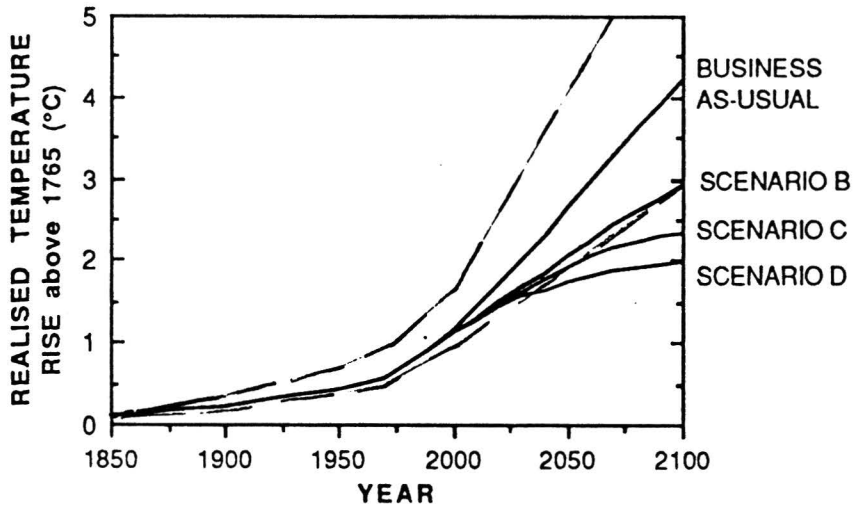

Fig.6 Simulated global mean temperature rise from 1850-1990 and future simulated temperature rise until the end of the 21th century.

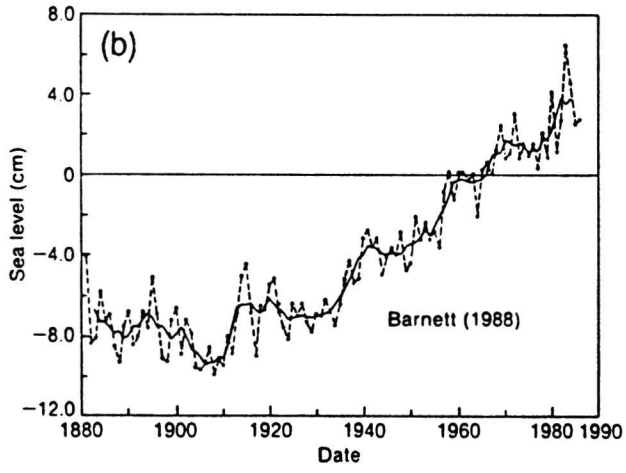

Fig.7 Global mean sea- level rise over the last century. The dashed line represents the annual mean, and the solid line the 5-year running mean.

Due to the global mean temperature increase the following effects can be expected:

1. **Sea- level rise.**

Figure 7 displays the global mean sea- level rise over the last century. The baseline is obtained by setting the average for the period 1951-1970 to zero. It shows us clearly that the sea level has been rising over the past 100 years. There has not been observed an acceleration in the sea- level rise. The most important contributing factors for the sea- level rise are:

* the thermal expansion of the oceans;
* the melt of glaciers and small ice caps;
* the melt of the Greenland ice sheet;
* the Antarctic ice sheet (including the special case of the West Antarctic ice sheet).

In the following section, concerning the cryosphere, the role of the glaciers and ice sheets will be discussed in relation to its possible contribution to past and future sea- level rises. Other possible factors that can contribute to a certain sea- level change are net increases or decreases in surface and groundwater storage. Groundwater depletion and drainage of soils and wetlands would contribute to a mean sea- level rise. On the other hand, increases in surface storage capacities, for example large dams, would detract from sea level. Overall, the estimates of the groundwater contribution appear to be too imprecise and insufficient, to conclude much about the possible net effects on past sea- level rise.

Table 4 gives a survey of the contributing factors to a mean sea level rise over the past 100 years with low and high estimates.

Figure 8 shows the expected future global sea- level rise for the next century in case of the BaU scenario. The best estimate calculation for the global sea level rise in 2030, starting in 1985, equals 18 cm (±10 cm). The thermal expansion accounts for 10 cm of sea- level rise, the mountain glaciers take care of approximately 7 cm. Greenland produces a slight positive effect, while Antarctica leads to a negative contribution to sea-level rise of about -0.6 cm due to a large increase in precipitation over the Antarctic polar area.

The thermal inertia of the oceans and the continuing response of land ice to climate changes creates a very substantial sea- level rise commitment on large time scales. Even if greenhouse gas emissions would be reduced to zero from now on, still a quite large sea- level rise will occur caused by the lag effects of the ocean.

The consequences of a rising sea level can be enormous (on the long term):

* large floods are more likely to occur;
* some low- level islands will disappear:
* wetlands, where large populations are settled, will disappear (Bangladesh);
* migrations of population groups in affected regions.

Table 4. Estimated contributions to sea level rise over the last 100 years (in cm).

	low	best estimate	high
Thermal expansion	2	4	6
Glaciers/ small ice caps	1.5	4	7
Greenland ice sheet	1	2.5	4
Antarctic ice sheet	-5	0	5
Total	-0.5	10.5	22
Observed	10	15	20

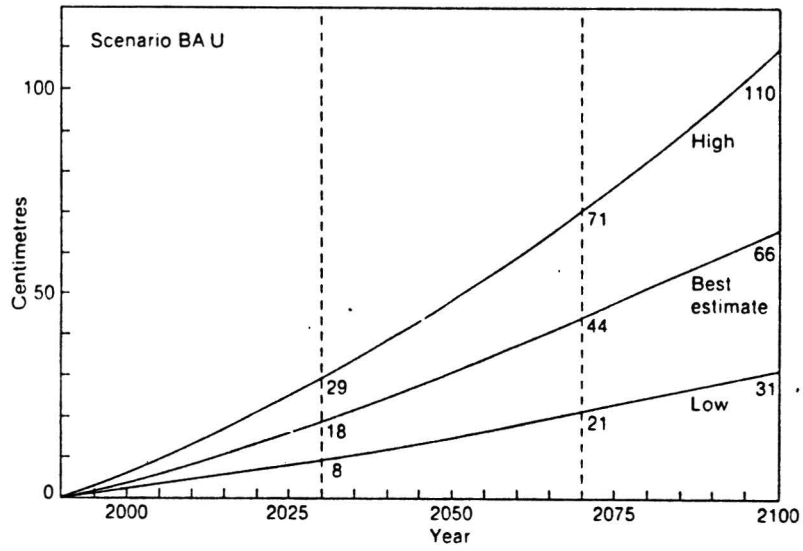

Fig.8 Global sea- level rise for the 21th century.

2. Changes in ecosystems.

Processes like photosynthesis and respiration depend on climate factors and carbon dioxide concentrations on the short term. On the long term the climate factors can influence total ecosystem structures, such as species composition, in which the strong species probably will survive. Furthermore, ecosystems will also respond to changes in local temperature, precipitation, soil moisture and extreme events.

Photosynthesis captures atmospheric CO_2, water and solar energy and stores it for later usage as plantgrowth, growth of animals or microbes in

the soil. Via respiration all these organisms release CO_2 again. Most of the land plants react positively on an increase in the CO_2- concentration. But due to several feedbacks, such as nutrient availability, there can still occur a negative trend.

The forests of the Earth, of course including the tropical rainforests, are capable of storing large amounts of carbon only when they are mature enough in the warmer climate. However the present large deforestation, especially in the tropics, due to human activities and also due to adapting problems, and the small amount of reforestation, with only little maturity, contributes to an actual increase in the atmospheric CO_2- concentration. The deforestation also has further consequences for the climate system, via reflectivity changes caused by new surface types, via changes in the hydrological cycle and via changes in surface roughness and thus atmospheric circulation.

Thus ecosystems will change in structure and in composition. Some organisms will move to other latitudes or altitudes, or they will be forced to live in more local regions. Some weak and vulnerable species will not survive.

3. **Changes in the hydrological cycle.**

The hydrological cycle consists of precipitation, evaporation and runoff. Probable consequences of the global warming for the hydrological cycle are:

* more precipitation with large regional differences;
* transformations of humid and dry regions with eventual consequences for the harvest;
* changes in the runoff of some rivers.

4. **Other effects:**

* an increase of erosion processes;
* desertification due to human and/or natural causes;
* eventual increase of meteorological calamities, such as storms or long lasting drought periods.

2.4.2. Consequences for the cryosphere

The climate system consists of five components, as illustrated in figure 9, -atmosphere, -ocean, -cryosphere, -biosphere, and -geosphere. Because this report describes a thermodynamic sea- ice model, an element which belongs to the climate component cryosphere, this section will pay much attention to the effects of global warming to the different cryosphere elements.

The terrestrial cryosphere can be classified into five components. For each of the components their response to actual global warming will be described and/or their contribution to sea- level rise is elucidated. The cryosphere consists of the following parts:

* **Sea ice.** Sea ice affects climate on timescales of seasons and longer. It works as an insulator for the heat exchange between the atmosphere and the ocean. Furthermore it can influence deep- water formation by salt extrusion during the freezing period and by generation of fresh water layers in the melting period. Measurements of the sea- ice extent anomalies in the Northern and Southern Hemisphere do not show clear trends which could be

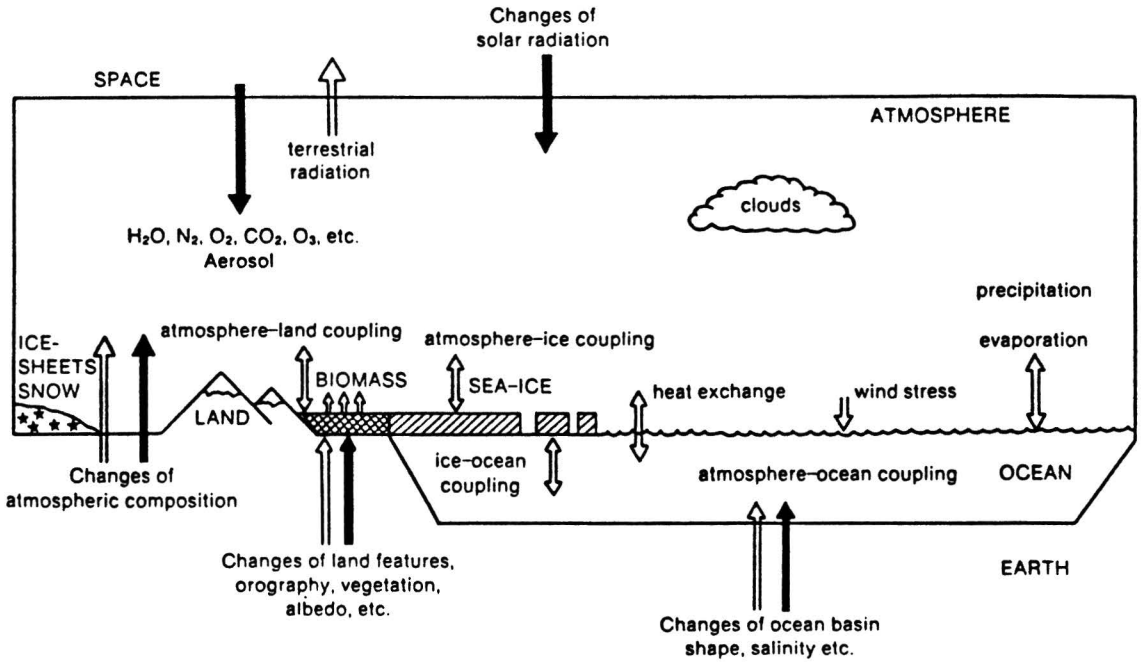

Fig.9 Schematic illustration of the components of the coupled atmosphere-ocean- ice- land climate system. Full errors stand for external processes, open arrows for internal processes in climate change.

caused by the global warming. Figure 10 displays the sea- ice extent for both hemispheres.

Other independent measurements showed a little change in total global ice area, but a significant decrease of open water within the ice. Because of the short time series, it is uncertain wether the decrease is real. Sea- ice extents can 'easily' be measured by satellites. However sea- ice thicknesses are very difficult to determine. Some data indicate a 15% decrease in mean ice- thickness values between 1976-1987 over a large area in the neighbourhood of Northern Greenland. Lack of a continuous set of observations makes it impossible to judge whether observed changes are part of a long- term trend.

An important feature of a decreasing ice (or snow) cover is the positive feedback mechanism to the greenhouse effect. A warmer Earth leads to less ice and snow cover and thus diminishes the reflectivity of the planet, due to its lower mean albedo. So it will absorb more incoming solar radiation, which again leads to higher temperatures of the lower atmosphere, etc.

* **A seasonal snow cover.** The rate of snowfall responds quickly to changing atmospheric dynamics (timescales of days). The seasonal heat storage is quite small. But its high albedo has large influence on the reflectivity of the surface and thus on the amount of reflected solar radiation. There exist some reasonable good observational data of snow extent anomalies from 1975 until now. The data sets show a clear descending trend starting in 1980.

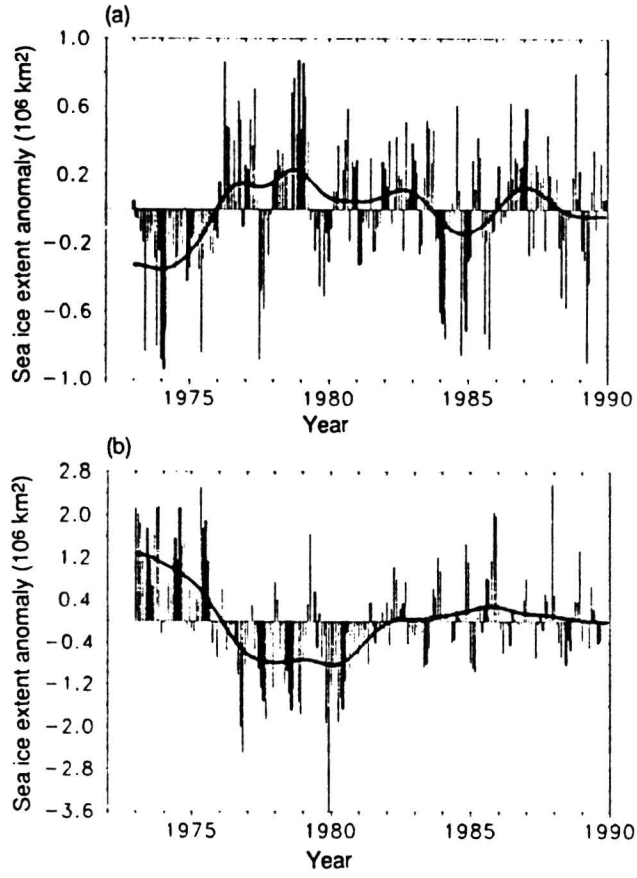

Fig.10 (a) Northern Hemisphere, and (b) Southern Hemisphere sea- ice extent anomalies.

* **Ice sheets of Greenland and Antarctica**. Both ice sheets have quasi-permanent topographic features. They contain about 80% of the fresh water contents of the Earth, thus they represent a fresh water reservoir on the long term. A change in the magnitude of this reservoir will influence the global sea level. The Greenland and Antarctic ice sheets show different reactions to a global temperature rise. To understand their different behaviour, it is necessary to consider the mass- balance curve of the ice sheets as a function of the annual surface atmospheric temperature, as depicted in figure 11. For low temperatures, in region (a), accumulation of snow due to an increased precipitation rate is dominant. There is a positive gradient in the mass balance in this region. At higher atmospheric temperatures, in region (b), evaporation and runoff play a very important role. Now the mass balance gradient becomes negative, and thus an increase in the surface temperature will lead to smaller ice sheets. The Greenland ice sheet appears to be in range (b) of the mass balance, thus the global sea level will rise due to melt of the Greenland ice sheet. Its contribution is somewhat lower than the one caused by glacier melt and thermal expansion of the oceans (see table 4).

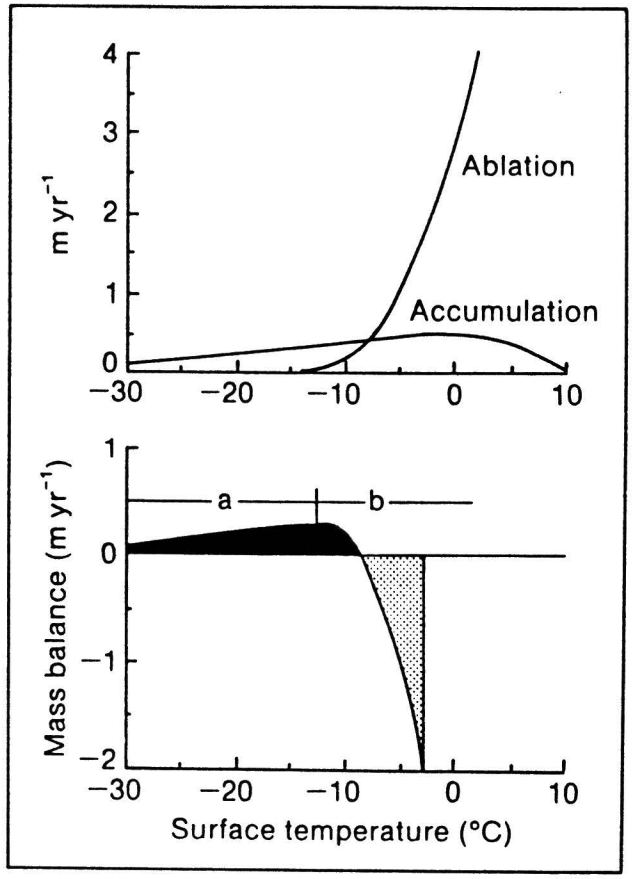

Fig.11 (a) Dependence of ablation (evaporation and runoff) and accumulation on annual surface temperature. (b) The dependence of the net annual mass balance on temperature changes sign, which complicates the response of glaciers and ice sheets to climate change.

The balance situation of the Antarctic ice sheet is very uncertain. It is believed that the net mass balance is positive, thus the Antarctic ice sheet is situated somewhere in region (a). Thus it contributes to a sea level lowering, approximately equal to -0.6 mmyr^{-1}. It is unknown if the Antarctic ice sheet is now in a steady balance and whether it has contributed to the sea- level rise in the past 100 years. Accumulation plays a very important role in the Antarctic area, and depends strongly on temperature and latitude, with a strong mutual correlation. An ablation zone does not effectively exist in Antarctica, and probably a large warming would be required in order for ablation to influence the mass balance.

Much attention is paid to the possible instability of the West Antarctic ice sheet. Parts of this ice sheet are grounded far below sea level and therefore may be very sensitive to changes in sea level rise. A very quick disintegration of this ice sheet may occur due to a small sea- level rise. Much of the drainage of the West Antarctic ice sheet goes through a number of fast flowing ice streams on a century to decadal time scale. Thus this part of the ice sheet has the potential to react quickly to any change in the boundary conditions. However, model results show that the bulk of the increased mass outflow would occur between 100 and 200 years from now.

* **Glaciers and small ice caps.** Glaciers also account for a certain percentage of the fresh water reservoir on Earth. Glaciers are very important diagnostic 'tools' to register climate changes. They react quickly to new environmental circumstances. Glaciers show the same behaviour as a function of surface temperature as the Greenland ice sheet as illustrated in figure 11. All of the current glaciers are situated in region (b). Figure 12 illustrates the decrease in glacier length of some selected glaciers all over the world. The response time of glaciers depends on their extensiveness; the bigger the glacier, the slower their response. The rate of glacier recession appears to have been generally the largest between about 1920 and 1960. Between 1960-1980 some glaciers were advancing again and thus the number of retreating glaciers decreased. However, the proportion of retreating glaciers has increased sharply since the early 1980s, at least for sure in the Alpine area. This behaviour in these decades may be related to the atmospheric temperature course in this period. During 1960-1980 there occurred a relatively cool period in the Northern Hemisphere. After 1980 the mean temperature rapidly started to increase again.

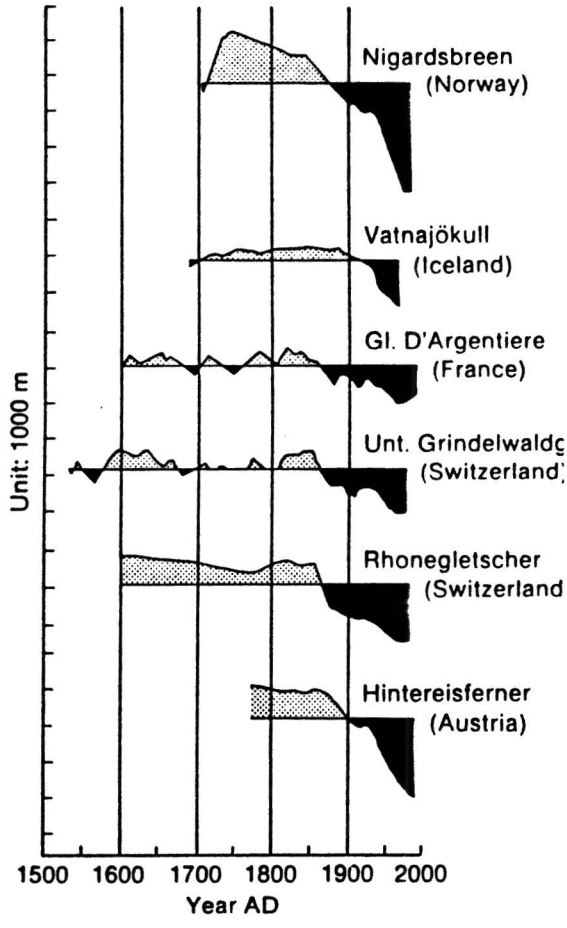

Fig.12 Variations of some selected glaciers measured by their length.

* **Permafrost.** Permafrost appears at mean annual air temperatures lower than -1 °C and will continuously occur at temperatures lower than -7 °C. Vertical temperature profiles in the ground respond within decades to environmental changes. Changes in permafrost can affect surface ecosystems and river discharges. It can also influence the thermohaline circulation of the ocean.

2.5. Climate modelling concerning the global warming

The most highly developed tool which we have to predict future climate is known as a General Circulation Model or GCM. These models are based on the laws of physics and use descriptions in simplified physical terms of the smaller- scale processes such as those due to clouds and deep mixing in the ocean. In a climate model an atmospheric component, essentially the same as a weather prediction model, is coupled to a model of the ocean, which can be equally complex. To make a climate forecast, the model should be run for a few (simulated) decades. Then the model must be run again with increasing concentrations of the greenhouse gases in the model. The difference between the statistics of the two simulations (for example in mean temperature) provides an estimate of the accompanying climate change.

The long- term change in surface air temperature following a doubling of carbon dioxide (referred to as climate sensitivity) is generally used as a benchmark to compare models. The range of the results from model studies is 1.9 to 5.2 °C, with a best estimate of climate sensitivity of 2.5 °C.

There exist also much simpler climate models, known as box- diffusion models, which contain highly simplified physics but give similar results as the GCMs when globally averaged.

Another possibility to predict future climate is to consider similar climate situations in the past. However, the forcing factors and all other conditions of the past should resemble to the current situation, but analogues of present greenhouse- gas concentrations have not been found. Still, palaeo- climatological information can provide useful insights into climate processes, and can assist in the validation of climate models.

There are many uncertainties in the climate predictions because of our imperfect knowledge of, for example, future rates of human- made emissions, how these changes will change the atmospheric concentrations of greenhouse gases and how the climate will respond to these changed concentrations. The climate models are far from perfect. There are a lot of uncertainties due to model imperfections. Large problems arise when atmosphere models are coupled to ocean models. The main problem of coupling is the resulting climate drift in the ocean. The oceanic surface fluxes need to be adjusted so that the ocean temperature and salinity remain close to the present climatology. If no flux corrections are included, significant systematic errors may be introduced due to imperfections in the coupled simulation models. These flux corrections are comparable in magnitude to the atmospheric fluxes, but they tend to be opposite in latitude, as can be seen in figure 13, and also in time. This flux correction substantially reduces the net effective flux to the ocean. The large flux adjustments distort the model's respons to perturbations such as those associated with increasing CO_2. To overcome the problem of climate drift, one could try to work with much simpler models than extensive GCM's. This approach also applies to this paper, where a

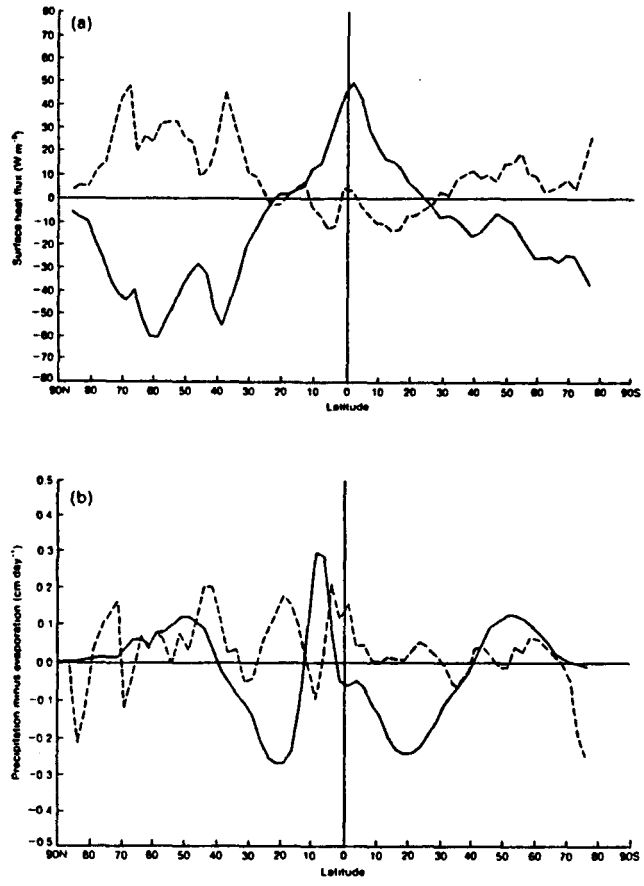

Fig.13 The zonal mean of the surface fluxes of a) heat and b) precipitation minus evaporation, simulated by the atmosphere in a coupled GCM (solid line) and the corresponding flux corrections (dashed line).

simple sea- ice model is presented, which is meant to be coupled to a simple ocean model.

The most important problems in climate modeling arise in the field of

* clouds: cloud formation and dissipation, radiative cloud properties which influence the response of the atmosphere to greenhouse gases,
* oceans: energy exchange between the ocean and the atmosphere, as mentioned earlier, and between the upper layers of the ocean and the deep ocean, which affect the rate of global and regional climate change.
* greenhouse gases: uptake and release, chemical reactions, and influence on climate change,
* polar ice sheets: which affect predictions of sea level rise.

Studies of land surface hydrology, and of impact on ecosystems are also important.

For a good and confident prediction of future climate, international coordinated research is necessary. This should include long- term observations, such as satellite measurements concerning atmospheric constituents, clouds, the Earth's radiation budget, wind, sea surface

temperature, etc. New climate models should be coupled completely, thus an atmosphere-land-ocean-ice configuration and the resolution of the models must be improved to account for regional effects. Rapid results from current scientific programmes cannot be expected, although computers are becoming faster and faster.

2.6. Future policy

The Earth's climate system already has responded to the current global warming in several ways:

1. Over the past 100 years the global temperature has increased over 0.5 °C;
2. The temperature of the stratosphere is decreasing;
3. Glacier surfaces are decreasing;
4. The sea level is rising;
5. There is a mean increase in precipitation;
6. The polar ice topography is changing; Greenland's ice cover is probably decreasing, and the Antarctic ice cover will probably grow.

Future climatological circumstances depend on our future policy concerning the greenhouse gas emissions. We can carry out several measures to diminish the release of greenhouse gases:

1. The most important and effective way is to spare energy, thus lowering the use of fossile fuels and searching for more effective energy usage. However, current energy prices are very low, so nowadays not much effort is made to diminish fossile fuel usage; on the contrary, we need more energy every year for our expanding economies.
2. We will have to decrease deforestation extensively and stimulate reforestation.
3. Alternative energy sources, such as solar and wind energy, have great potential. However high costs, technical difficulties and general acceptance are common problems concerning alternative energy.
4. Usage of nuclear energy is a possibility, but it gives rise to problems as:
   * the total amount of Uranium is unknown, but probably it is not sufficient for more than the coming 50 years;
   * safety problems of nuclear power plants;
   * storage of nuclear waste products;
   * proliferation danger (development of nuclear weapons).
5. There are some possibilities of chemical and physical absorption of CO_2 and of storage of CO_2 in empty natural gas fields.

Economic growth at the current rate shows little responsibility towards forthcoming generations. Fossile fuel stocks are decreasing rapidly and greenhouse gas concentrations continue to rise faster than ever before. We can state that the measures concerning the greenhouse effect cannot be established by means of technological operations and inventions only. Social solutions are necessary, thus quantity restrictions concerning consumption, mobility, and of course limiting the growth of the Earth's population is of great importance too.

Chapter 3. A THERMODYNAMIC ICE MODEL

3.1. Description of the thermodynamic ice model

The one-dimensional sea- ice model that will be described in this chapter, is based on the ice model of Semtner [1976]. This model simulates the thickness of sea ice, by using a balance of heat fluxes at the top and bottom of the ice. The model includes diffusion processes in the ice and has an additional snow cover on top of the ice during certain periods of the year. Semtner based his model on a previous study of sea ice performed by Maykut and Untersteiner [1971], and made a more simple numerical version without losing much accuracy for a wide variety of environmental conditions.

This paragraph will essentially describe the '0-layer model' as described in the appendix of Semtner's article.

A schematic diagram of the ice model is depicted in figure 14. The ice model consists of a single layer of sea ice with a variable thickness equal to h_i. On top of the ice there is a layer of snow, with thickness h_s, which depends on the seasonal snow- fall during autumn and winter and the snow melt in late spring and summer. Beneath the sea ice the upper ocean is represented by a slab of fixed thickness, called the mixed layer with a depth equal to h_m. This layer is left out of consideration in this section, but will be discussed later in section 3.3.

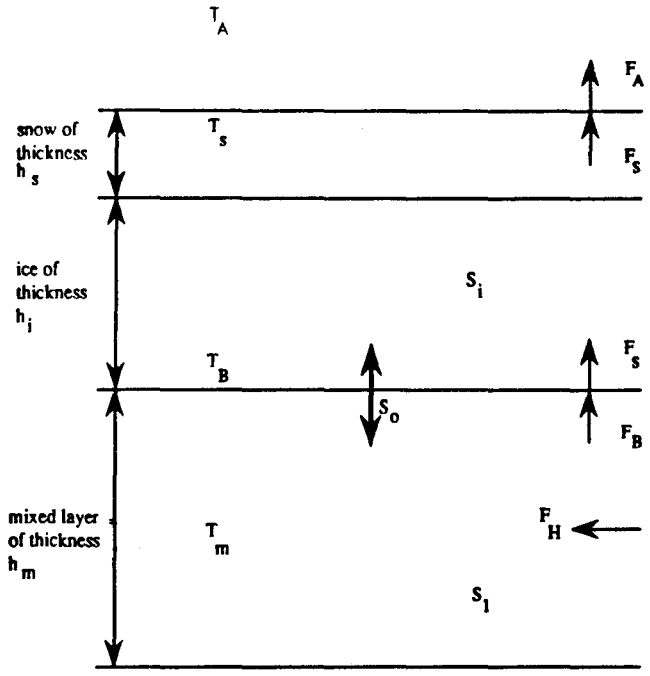

Fig.14 Schematic diagram of the '0-layer model' of A.J. Semtner, consisting of an ice and snow layer. Also represented is the oceanic mixed layer with a constant thickness of 100 m.

At equilibrium there exists a balance of fluxes at the top and the bottom of the ice layer, expressed by

$$F_A - F_s = 0 \qquad (1a.)$$

$$F_B - F_s = 0 \qquad (1b.)$$

where F_A stands for the atmospheric fluxes at the top of the ice,
F_s is the conductive flux through the ice and snow layers,
and F_B is the oceanic heat flux from the mixed layer below the ice.

In case of no snow-cover on top of the ice, the atmospheric flux F_A consists of the following components:

$$F_A = H + E + I + (1-\alpha_1)\,(1-\beta P_0)\,Q + \sigma\,(T_s)^4, \qquad (2.)$$

where E stands for the flux of latent heat, caused by differences in humidity between the surface air and the air at anemometer level,
H for the flux of sensible heat, caused by temperature differences between the air and the surface of the ice layer,
I for the incoming long-wave radiation from the atmosphere and clouds,
Q for the incoming solar short-wave radiation,
α_1 is the albedo of ice (the albedo is an indication for the percentage of incident solar radiation that is reflected at the surface of the ice-cover), $\alpha_1 = 0.64$,
P_0 is the fraction of the net incoming solar radiation which penetrates into the interior of the snow-free ice, P_0=17%,
β is an additional reflectance term that roughly imitates an increase in brine volume and effectively increases the ice albedo, β=0.4,
$\sigma(T_s)^4$ is the outgoing long-wave radiation with σ the Stefan-Boltzmann constant, $\sigma = 5.67 \cdot 10^{-8}$ $Wm^{-2}K^{-4}$, (the emissivity ε is set equal to one) and T_s the surface temperature of the ice slab.

In case of an additional snow cover the atmospheric flux F_A changes into:

$$F_A = H + E + I + (1-\alpha_s)\,Q + \sigma\,(T_s)^4, \qquad (3.)$$

where α_s is the albedo of snow, given by monthly mean values in appendix A, and other terms are defined as before.

The conductive flux in equation (1.) is assumed to be linearly dependent on the ice thickness and the temperature difference between the top and the bottom of the ice layer:

$$F_s = \frac{k_s\, k_i\, (T_B - T_s)}{k_s\, h_i + k_i\, h_s} \qquad (4.)$$

where h_i is the ice-layer thickness,
h_s the snow-layer thickness,
k_i the thermal conductivity of ice, k_i=2.034 $Wm^{-1}K^{-1}$,

k_s the thermal conductivity of snow, $k_s=3.097 \cdot 10^{-1}$ $Wm^{-1}K^{-1}$ and
T_B stands for the bottom temperature of the ice-layer and is always equal to the freezing point of sea water, T_B = 271.15 K.

In case of no snow cover (thus h_s equals zero) equation (4.) simplifies to:

$$F_s = \frac{k_I}{h_I} (T_B - T_s) \tag{5.}$$

The oceanic heat flux F_B in equation (1.) is assumed to be proportional to the temperature difference between the mixed layer and the bottom of the ice slab:

$$F_B = b\ (T_m - T_B) \tag{6.}$$

where b is a constant which equals 200 $Wm^{-2}K^{-1}$ and
T_m is the mixed layer temperature.

By solving (1.) we obtain the equilibrium values of T_s and h_I:

$$T_S = \left(\frac{F_B - K}{\sigma} \right)^{1/4} \tag{7.}$$

$$h_I = \frac{k_I}{F_B} \left(T_B - \left(\frac{F_B - K}{\sigma} \right)^{1/4} \right) - \frac{k_I}{k_s} h_s \tag{8.}$$

where in case of no snow accumulation (h_s=0)

$$K = H + E + I + (1-\alpha_I)(1-\beta P_0)\ Q \tag{9a.}$$

but in case of an additional snow cover

$$K = H + E + I + (1-\alpha_s)\ Q. \tag{9b.}$$

For time- varying atmospheric fluxes the sea ice responds by changing T_s and by melting and ablation at the top and bottom of the ice layer respectively, to keep the heat fluxes at the top of the ice layer in balance according to equation (1a.), so

$$F_g = F_A - F_s = 0. \tag{10.}$$

After each time step a new T_s can be calculated by searching the zero point of $F_g(T_s)$. This is done by using the Newton- Raphson method as explained in Numerical Recipies [1986]. The new T_s is calculated with use of the surface temperature at the previous time step, T_p, in the following way:

$$T_s = T_p - \frac{F_g(T_p)}{F_g'(T_p)} \tag{11.}$$

The derivative of F_g, F_g', is determined numerically as follows:

$$F_g'(T_p) = \frac{F_g(T_p+\Delta T_s) - F_g(T_p)}{\Delta T_s} \qquad (12.)$$

where ΔT_s is a very small ice surface temperature increase.

If the new value of T_s exceeds the melting point at 0°C (273.15 K), then it must be reset to 0°C. The imbalance that now exists between the atmosferic flux F_A and the conductive flux F_s will be used to melt the ice or snow. In case of no snow-cover, the ice thickness then changes during a timestep Δt with a value corresponding to

$$\Delta h_i = \Delta t \frac{(F_A - F_s)}{q_i} \qquad (13.)$$

With an additional snow-cover the snow thickness will diminish due to melting according to

$$\Delta h_s = \Delta t \frac{(F_A - F_s)}{q_s} \qquad (14.)$$

with q_i the latent heat of fusion of sea-ice, $q_i=3.014\cdot10^8$ Jm^{-3}, and q_s the latent heat of fusion of snow, $q_s=1.097\cdot10^8$ Jm^{-3}.

At the bottom of the ice, there can also be ablation or accretion of ice which changes the ice thickness during a time step Δt according to

$$\Delta h_B = \Delta t \frac{(F_s - F_B)}{q_B} \qquad (15.)$$

where q_B is the heat of fusion at the bottom of the ice slab, $q_B=2.679\cdot10^8$ Jm^{-3}.

When ice is melting relatively fresh water will enter the mixed layer, because ice has a very low salinity percentage in proportion to the salinity content of the mixed layer. When ice is growing the salinity of the mixed layer will increase because ice accretion leads to salt rejection. The salt flux S_o (see also figure 12) can be written as:

$$S_o = \frac{\rho_i}{\rho_o}\left(S_1 - S_i\right)\left(\frac{\partial h_i}{\partial t} + \frac{\partial h_B}{\partial t}\right) \qquad (16.)$$

where ρ_i equals the sea ice density, $\rho_i = 0.9\cdot10^3$ kgm^{-3},
ρ_o is the sea water density, $\rho_o = 1.025\cdot10^3$ kgm^{-3},
S_1 is the mixed layer salinity,
S_i is the sea ice salinity, S_i = 5 PSU,
$\partial h_i/\partial t$ is the ice melt at the top of the ice slab and

$\partial h_B/\partial t$ is the ice melt at the bottom of the ice slab.

Evaporation of sea ice at the top of the ice slab is neglected.

3.2. The atmospheric forcing

3.2.1. Introduction

The heat fluxes from the atmosphere, respectively the solar radiation Q, the infrared longwave radiation I, the latent heat E and the sensible heat H, have a great influence on the melt and growth of sea ice. In the ice models, as discussed by Maykut and Untersteiner [1971] and Semtner [1976], these atmospheric heat fluxes are given as monthly averaged fluxes. Instantaneous values of these surface fluxes were deduced using linear interpolation between these monthly averaged values. The values of these fluxes are depicted in appendix B (the heat fluxes are positive when directed upwards). In order to use the sea ice model in a climate model, these fluxes have to be parameterized. Haney [1971] and Parkinson and Washington [1979] parameterized these heat fluxes in terms of the atmospheric temperature T_a and the surface temperature T_s. These parameterizations will be described in the following sections 3.2.2. to 3.2.4. Section 3.2.5. will define the atmospheric temperature, which is the only variable forcing parameter which still has to be prescribed.

3.2.2. The solar radiation

The most important heat flux is the incoming solar radiation. The parameterization of the solar radiation given by Parkinson and Washington [1979] is somewhat simplified here. The solar radiation absorbed at the surface is given by

$$Q = - (1-\alpha_{sfc}) Q_o (1-0.6 f_c) (1-0.6 \alpha_{sfc} f_c) \qquad (17.)$$

with

$$Q_o = S \cos(Z) \qquad (18.)$$

where α_{sfc} stands for the surface albedo,
Q_o is the solar radiation incident on the surface under cloudless skies,
f_c represents the percentage of cloud cover, $f_c = 0.5$,
S is the solar constant, $S = 1353\ Wm^{-2}$ and
Z is the zenith angle.

The factors involving f_c represent multiple reflections between the ground surface and the clouds, with a cloud albedo of 0.6. The surface is either sea ice, snow or open ocean.

The cosine of the zenith angle Z is calculated by the standard geometric formula

$$\cos(Z) = \sin(\phi)\,\sin(\delta) + \cos(\phi)\,\cos(\delta)\,\cos(HA) \qquad (19.)$$

where ϕ, δ, and HA are latitude, declination and hour angle, respectively (Sellers [1965]). The approximate declination and the hour angle are determined as

$$\delta = 23.44^{\circ}\,\cos[(172 - \text{day of year})\,\pi/180] \qquad (20.)$$

$$HA = (12 \text{ hours} - \text{solar time})\,\pi/12 \qquad (21.)$$

In the current ice model a time step of 5 days is chosen, because the ice model will be implemented in the ocean model which uses the same time step. For this reason the incident solar radiation Q_o has to be averaged over this period. Therefore the cosine of the zenith angle has to be averaged over a day time (it is assumed that the daily averaged incident solar radiation only differs slightly from a five days averaged incident solar radiation):

$$\langle\cos(Z)\rangle = \frac{1}{2\pi}\int_{HA_1}^{HA_2}(\sin(\phi)\sin(\delta) + \cos(\phi)\cos(\delta)\cos(HA))dHA \qquad (22.)$$

where HA_1 is the time of sun rise and HA_2 is the time of sun set. Above the polar circle, the sun will not go down for some days during the summer. Exactly at the north pole during half a year the sun will shine, but during the other half of the year the sun is down (the polar night). For these cases, ($HA_1=-HA_2=-\pi$), the integral in equation (22.) gets the form

$$\langle\cos(Z)\rangle = \sin(\phi)\,\sin(\delta) \qquad (23.)$$

In case of a normal day and night rhythm, both the hour angles must be determined. This can be done by putting $\cos(Z) = 0$ or in other words

$$\cos(HA) = -\tan(\phi)\,\tan(\delta) \qquad (24.)$$

Now solving the integral (22.) gives us the other averaged expression for the cosine of the zenith angle,

$$\langle\cos(Z)\rangle = \frac{1}{2\pi}\Big[\sin(\phi)\sin(\delta)\,(HA_1-HA_2) + \cos(\phi)\cos(\delta)\,(\sin(HA_1)-\sin(HA_2))\Big] \qquad (25.)$$

In this way the daily averaged incident solar radiation Q_o can be determined at every latitude during every period of the year.

3.2.3. The infrared radiation

The net infrared longwave radiation consists of two parts. The first part is the incoming infrared radiation out of the atmosphere and the second the outgoing infrared radiation from the surface. The parameterization for the

incoming infrared radiation, developed by Idso and Jackson [1969], is represented by

$$I = - I_o \, (1 + 0.275 \, f_c) \tag{26.}$$

with

$$I_o = \sigma \, T_a^4 \left(1 - 0.261 \, e^{(-7.77 \, 10^{-4} \, (273-T_a)^2)} \right) \tag{27.}$$

where σ is the Stefan- Boltzmann constant,
T_a is the atmospheric temperature at the surface and
f_c is the cloudiness factor as mentioned earlier.

The exponential term in equation (27.) has been deduced from experimental considerations and statistical analysis of data at different latitudes and during different seasons. It appears that the effective emittance of the atmosphere is a minimum at 273 K and that it increaeses symmetrically to approach unity exponentially at higher and lower temperatures. Although there are many other parameterizations for the incoming longwave infrared radiation, as will be discussed in section 5.3.2., the parameterization of Idso and Jackson seems to be most reliable one.

The outgoing infrared radiation can be written as a blackbody radiation term (with the emissivity ε equal to 1), $\sigma(T_s)^4$, as in equation (2.) and (3.).

3.2.4. The latent and sensible heat

The fluxes of latent and sensible heat in terms of the surface temperature T_s and prescribed atmospheric parameters, can be parameterized as

$$E(T_s) = \rho_a L_v C_D v_a \, (q_s(T_s) - q_a) \tag{28.}$$

$$H(T_s) = \rho_a c_a C_D v_a \, (T_s - T_a) \tag{29.}$$

where ρ_a is the air density, $\rho_a = 3.48 \cdot 10^2 / T_a$,
L_v is the latent heat of vaporization, $L_v = 2.49 \cdot 10^6$ Jkg^{-1},
c_a is the heat capacity of air, $c_a = 1.005 \cdot 10^3$ Jkg^{-1}K^{-1},
C_D stands for the drag coefficient, $C_D = 1.75 \cdot 10^{-3}$ in case of an ice- or snow- cover and $C_D = 1.40 \cdot 10^{-3}$ in case of an open ocean,
v_a is the wind speed at anemometer level, $v_a = 5$ ms^{-1},
$q_s(T_s)$ is the saturation specific humidity at the temperature of the surface T_s and
q_a is the specific humidity of the air at anemometer level.

The humidity difference in (28.) can be rewritten as a temperature difference between surface temperature and atmospheric temperature as is done by Haney [1971]. This formulation of the latent heat flux is very useful, because in that way the atmospheric temperature is the only

prescribed time- dependent parameter in the ice model. If E is expanded in a truncated Taylor series about the atmospheric temperature T_a, we get

$$E(T_s) = E(T_a) + \left(\frac{\partial E}{\partial T} \right)_{T_a} (T_s - T_a). \tag{30.}$$

Since $q_a/q_s(T_a) \approx e_a/e_s(T_a) \equiv r$ with e_a the vapour pressure, e_s the saturation vapour pressure and r the relative humidity in decimal form, (28.) can be written in case of the atmospheric temperature as

$$E(T_a) = \rho_a L_v C_{D_a} v_a \, q_s(T_a) \, (1-r). \tag{31.}$$

Furthermore, from (28.) we can deduce

$$\left(\frac{\partial E}{\partial T} \right)_{T_a} = \rho_a L_v C_{D_a} v_a \left(\frac{\partial q_s}{\partial T} \right)_{T_a}. \tag{32.}$$

The relation between the saturation specific humidity and the saturation vapour pressure is given by

$$q_s(T) = \frac{0.622}{p_a} \, e_s(T) \tag{33.}$$

where p_a is the pressure which equals $1.01325 \cdot 10^5$ Pa. According to Washington and Parkinson, the saturation vapour pressure $e_s(T)$ is given by

$$e_s(T) = 611 \cdot 10^{\,a(T-273.16)/(T-b)} \tag{34.}$$

where (a,b) = (9.5,7.66) if an ice cover exists and (7.5,35.86) if no ice cover exists. Haney used the following formulation for the saturation vapour pressure

$$e_s(T) = 100 \cdot 10^{\,(9.4051-2353/T)}. \tag{35.}$$

Definitions (34.) and (35.) will show to lead to almost no different behaviour. If we now differentiate equation (33.) with respect to T, we have (using definition (34.))

$$\frac{\partial q_s}{\partial T} = \frac{0.622}{p} \ln(10) \left(\frac{273.16a - ab}{(T-b)^2} \right) e_s(T). \tag{36.}$$

Now insert (36.) into (32.) and then substitute (31.) and (32.) into equation (30.). The result is

$$E = E_1 + E_2 \, (T_s - T_a) \tag{37.}$$

where

$$E_1 = \rho_a L_v C_D v_a \frac{0.622}{p_a} e_s(T_a) (1-r) \qquad (38a.)$$

$$E_2 = \rho_a L_v C_D v_a \frac{0.622}{p_a} \ln(10) \left(\frac{273.16a-ab}{(T_a-b)^2} \right) e_s(T_a) \qquad (38b.)$$

The parameterization of the sensible heat H in (29.) already contains the temperature difference (T_s-T_a), so this relation needs no further adjustment.

3.2.5. The atmospheric temperature

As can be seen from the definitions of all the atmospheric fluxes, the only prescribed time- dependent variable left is the atmospheric temperature T_a. In 'Physics of Climate' of Oort and Peixoto [1989], horizontal surface temperature distributions are given for January and July all over the world. In order to test the performance of the sea ice model, we extracted from these data a simplified, longitude- independent time- varying temperature distribution. We choose the temperature in the Northern Hemisphere at 170°W as the most appropriate one. At this longitude no land surface is crossed in the Northern Hemisphere when going up from the Equator to the North Pole. It passes in between the continents of Russia and Northern America. In this region also no warming Gulf Stream exists. Figure 15 displays the atmospheric temperature in July and January as a function of latitude at 170°W longitude as deduced from Oort and Peixoto with a corresponding fitted trigonometric cosine function. The fitted curves are represented by

$$T_{Jan} = -3.5 + 30.5 \cos(2.4\ \phi - 36^\circ) \qquad (39a.)$$

$$T_{Jul} = 13 + 15 \cos(2.25\ \phi - 22.5^\circ) \qquad (39b.)$$

with ϕ the latitude in degrees. Equation (39a.) corresponds with the minimum atmospheric temperature in the year at a certain latitude, (39b.) with the maximum value during summer time. The time dependence of the atmospheric temperature is given by

$$T_a = 273.15 + \frac{T_{Jul}+T_{Jan}}{2} + \frac{T_{Jul}-T_{Jan}}{2} \sin\left(\frac{2\pi\ (t-105\ \text{days})}{360\ \text{days}} \right) \qquad (40.)$$

where t stands for the time of the year in seconds. The extrema in temperature are assumed to occur 15 days after the solstices.

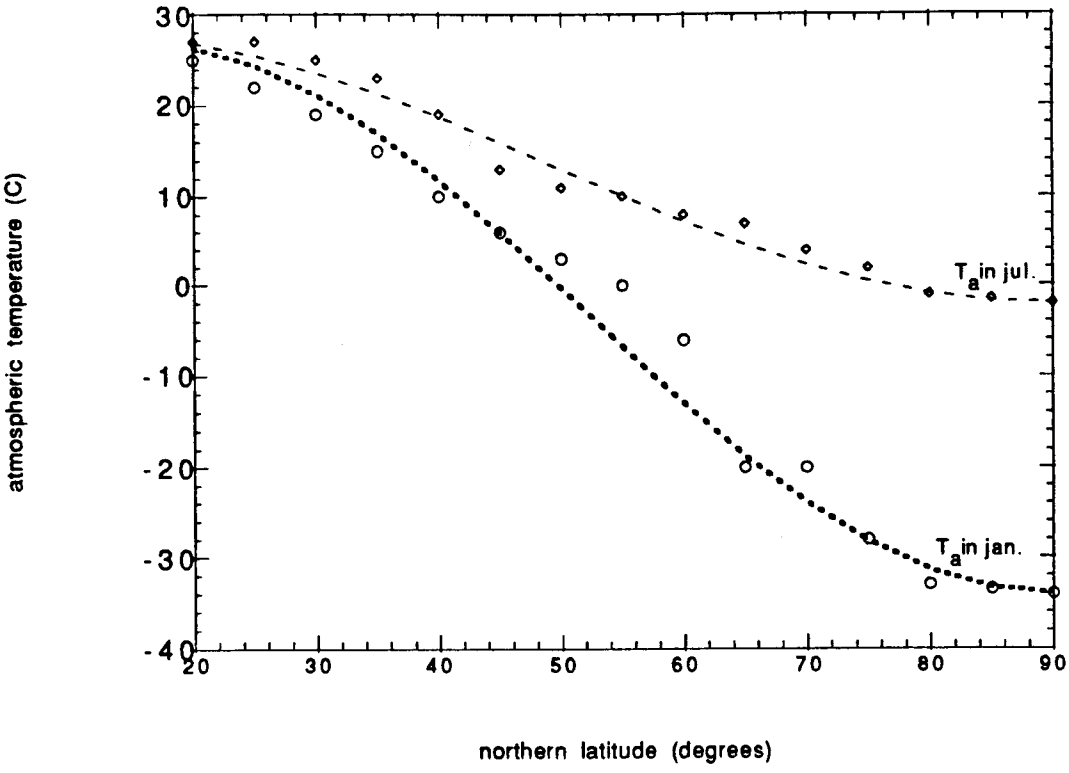

Fig.15 Atmospheric temperature in July and January as a function of latitude at 170°W longitude with data from Oort/Peixoto and cosine curve fit.

3.3. The heat and salt balance of the mixed layer

In case the mixed layer is covered with an ice slab, see figure 14, the heat balance of the mixed layer can be written as a balance of the oceanic bottom flux F_B, the advection flux and diffusion flux F_H and the heat capacity of the mixed layer with thickness h_m:

$$\rho_o c h_m \frac{\partial T_m}{\partial t} = - F_B + F_H \qquad (41.)$$

where c is the specific heat of sea water, $c=4.089 \cdot 10^3$ $Jkg^{-1}K^{-1}$, and with F_B defined as in equation (6.). The advection flux F_H is taken as a constant equal to 4 Wm^{-2}, unless otherwise described. It represents the advection and diffusion of sea water from nearby regions and from deeper oceanic layers. In reality F_H is not a constant at all. The ocean model in which the ice model will be implemented will compute values for the advection flux.

If during the entire year no open ocean will appear at a certain latitude, the mixed layer temperature will tend to go to an equilibrium value which follows from the equality $F_B = F_H$. The mixed- layer temperature can then be written as

$$T_m = \frac{F_H}{b} + T_B \qquad (42.)$$

T_m will have a value just above the freezing point of sea water, which is equal to T_B (-2 °C).

In case there is no ice layer on top of the mixed layer, the thermodynamic energy equation (Pollard et al. [1983]) equals

$$\rho_o c h_m \frac{\partial T_m}{\partial t} = - F_A + Q\, e^{-\gamma h_m} + F_H , \qquad (43.)$$

where γ is the solar extinction coefficient taken as 0.2 m^{-1}. The incoming solar radiation Q times the exponential term with γ represents the fraction of solar radiation that penetrates through the mixed layer and disappears into the deep ocean. For a mixed- layer depth of 100 m, the contribution of this term in the heat balance is negligible and can therefore be omitted in the computations. In the situation of no ice cover, the mixed- layer temperature has a seasonal variation due to the seasonal variation of the atmospheric fluxes which are included in F_A.

The salt balance of the mixed layer is given by

$$\frac{\partial (h_m S_1)}{\partial t} = S_o \qquad (44.)$$

where S_1 is the mixed- layer salinity and S_o the salinity flux as formulated in equation (16.). Discretising (44.) we get

$$S_1(t) = S_1(0) + \frac{\Delta t}{h_m} S_o \qquad (45.)$$

where $S_1(0)$ stands for the initial value of the mixed- layer salinity.

3.4. Description of the input parameters

For convenience the year is divided into twelve months of each 30 days. Time steps in the numerical procedure are taken equal to 5 days, except for ice thicknesses smaller than 20 cm and unequal to zero. In that case the time step is lowered to 8 hours. The reason for this is that numerical instabilities occur at small latitudes for these small ice thicknesses (h_1 appears in the denominator of the conductive flux F_s).

In the case of very small ice thicknesses, e.g. less than 5 cm, the ice thickness and snow thickness are set equal to zero and the oceanic mixed layer is in direct contact with the atmosphere. If ice accretion occurs after a period of no ice cover at all, the initial ice thickness is set to 5 cm and the surface temperature to 273.15 K. The error made by introducing this numerical construction is very small.

The albedo of melting snow is not equal to the albedo of accumulating

snow. It is assumed that the albedo of melting snow decreases linearly with the snow thickness. If all the snow has vanished the albedo corresponds to the albedo of bare ice, which equals 0.64.

Snowfall is also prescribed. Between 20 August and 30 October snowfall is taken to consist of a linear accumulation of 30 cm, between 1 November and 30 April another 5 cm, and in the month of May also 5 cm of snowfall. Snowfall accumulates only when the surface temperature is below freezing.

The thermal conductivities of ice and snow, k_I and k_s respectively, have been multiplied by a factor ζ=1.065 which makes the ice slightly thicker than before. This factor ζ was implemented by Semtner to compensate for the assumption of a linear equilibrium profile of temperature. This assumption causes the ice thickness to be too small. Because a net positive amount of heat that would normally warm the interior of the ice goes into additional melting, the ice is thinner than it should be.

Values of all the constant parameters have already been given in the previous sections.

Initial values of the ice thickness, snow thickness, ice- surface temperature and mixed- layer temperature have no influence upon the final annual equilibrium cycle of temperature and ice thickness. However, the initial values are chosen to have reasonable realistic values, because then the time constants of the ice model will be small and thus integration towards equilibrium will only take a 'few' integration steps (see section 4.7.). The initial value of the mixed- layer salinity coincides with the initial defined salinity in the ocean model and depends on latitude:

$$S_1(0) = 34.5 \qquad \text{for } \phi \geq 70^\circ N \qquad (46a.)$$

$$S_1(0) = 35.75 + 1.25 \cos(3.6\,\phi - 72) \qquad \text{for } \phi \leq 70^\circ N \qquad (46b.)$$

Annual equilibrium cycles of salt do depend on the initial values of the ice thickness h_I, as can be seen from equation (16.).

The grid size used in experiments with latitudinal dependence equals 2.5°.

Chapter 4. EXPERIMENTAL RESULTS

4.1. The seasonal ice, snow and temperature cycle

Using the atmospheric forcing as described in section 3.2., one expects a seasonal cycle of ice thickness, snow thickness and surface layer temperature after the transients in the first years of integration have vanished. The integration of the ice model starts at the first day of January. Figure 16 displays the seasonal ice thickness, snow thickness and surface temperature for the first 20 years of the time integration at a latitude of 80° N. After an integration time of about 18 years the sea ice model has reached an equilibrium situation with a seasonal cycle. The equilibrium situation is reached from the moment that the time extrema of the ice thickness will keep the same value each year within an accuracy of 5 cm. The equilibrium values are independent from the initial chosen values for the ice thickness, snow thickness, or surface temperature.

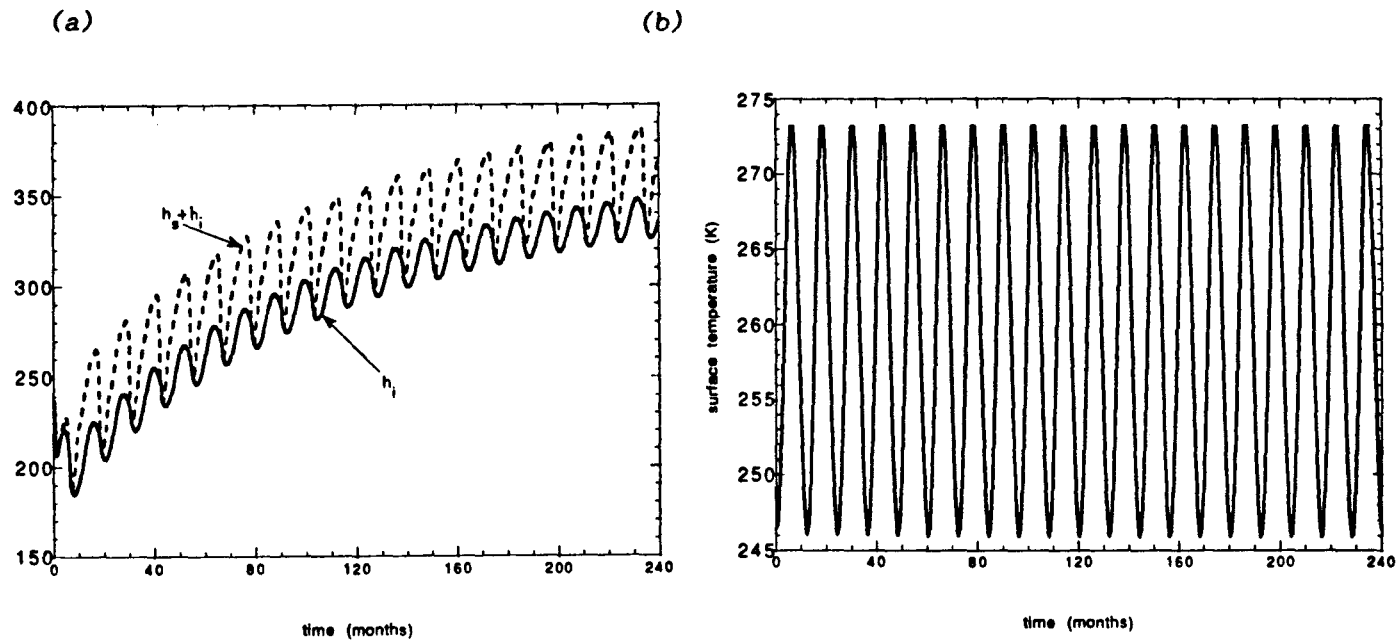

Fig.16 Seasonal cycles of (a) the ice thickness and the snow thickness and and (b) the surface temperature. Equilibrium ice thickness cycles are reached after an integration time of about 18 years.

Figure 17 displays the three seasonal cycles all together in one picture during an equilibrium cycle. In the first part of the year, the ice thickness becomes thicker and the snow accumulates. The surface temperature is rising, until it equals the melting point of sea ice, 0° C, which roughly occurs at the end of June. From that moment on temperature does not change any more until the beginning of August. The upper snow layer will start to melt when the difference between the atmospheric and the conductive heat flux becomes negative. When the snow cover has entirely vanished, the ice

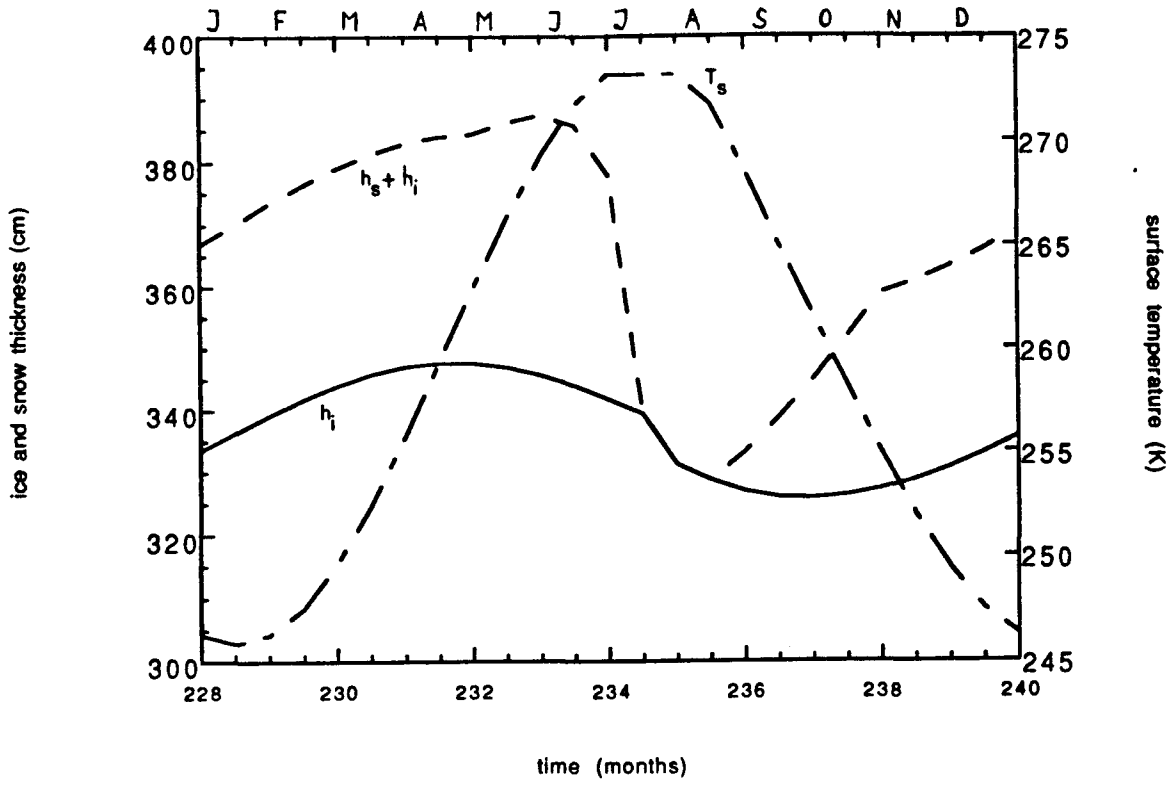

Fig 17 Seasonal cycle of ice thickness (solid line), snow thickness (dashed line) and the surface temperature (dotted- dashed line) during an equilibrium cycle.

thickness will decrease more rapidly than before. Approximately at the end of September the ice melting stops. The ice- layer thickness increases again and snow accumulates on top of the ice layer. One seasonal cycle is now completed and will repeate as long as the input parameters keep the same annual values.

4.2. Multi- year equilibrium cycles

The thermal conductivity of snow is about a factor 7 smaller than that of ice. The isolating property of snow diminishes sea ice growth. Equation (8.) shows that in equilibrium the sea- ice thickness is decreased by k_i/k_s times the snow- layer depth. Due to these large differences between k_i and k_s multi- year cycles in ice and snow thickness will occur when the environmental conditions are specified in such a way that during a certain period of the integration the ice slab will vanish completely. These cycles repeat themselves exactly, and an open ocean appears only once in each multi-year period (see figure 18a). If an open ocean appears in a given summer, the upper ocean starts refreezing when the mixed- layer temperature has become smaller than the freezing point of sea water (271.15 K). In the subsequent winter the ice will grow rapidly because of the absence of an additional snow cover, to such a thickness that several years with the usual snow cover must pass before the open ocean reappears. Figure 18b shows the corresponding experiment performed by Semtner, where also a multi- year equilibrium cycle occurs.

(a)

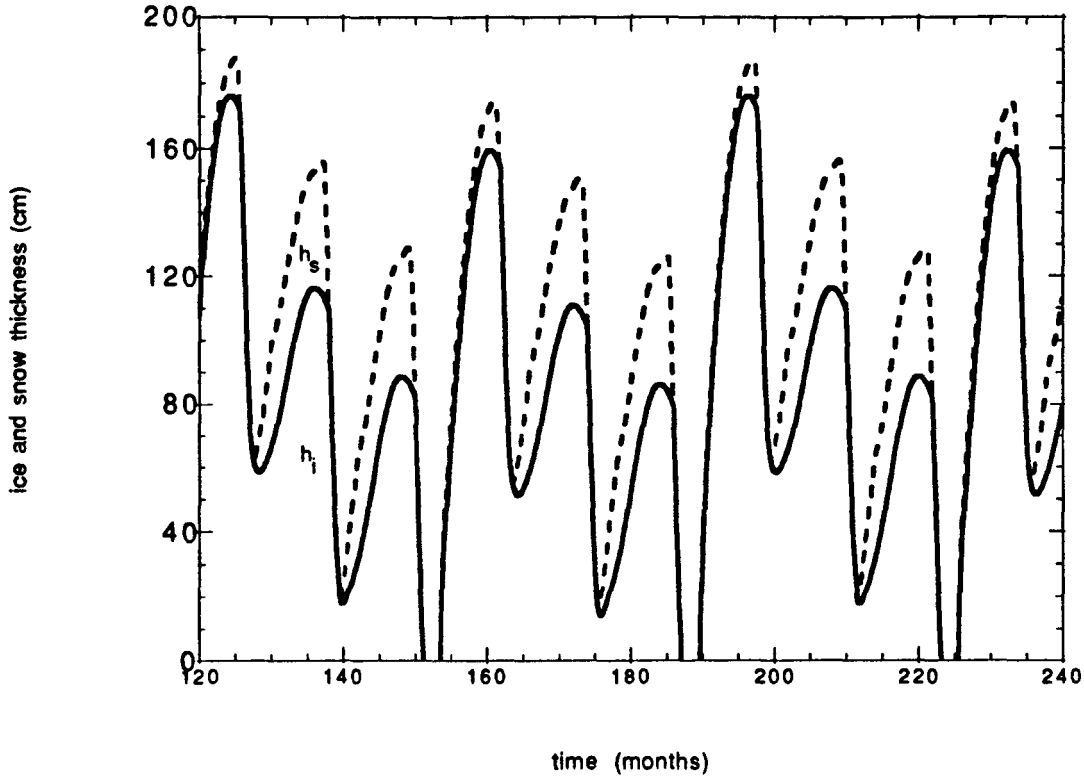

(b)

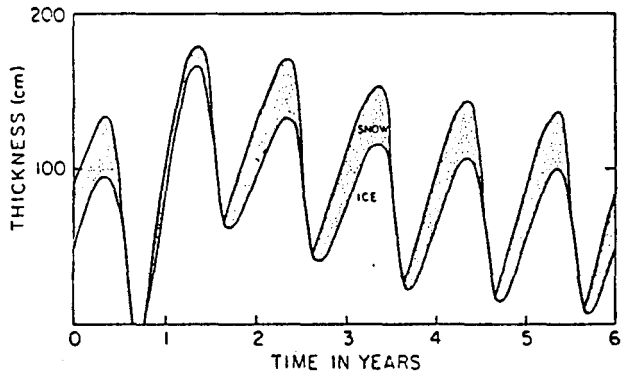

Fig.18 Multi- year equilibrium cycle of ice thickness, as predicted by (a) the thermodynamic ice model at 74° N and (b) the Semtner model (Appendix A) for the case in which the oceanic heat flux equals 8.074 $\cdot 10^{14}$ Wm^{-2}.

4.3. The heat balance of the ice

When the ice layer is not melting, the heat balance (1a.) must be valid at the top of the ice layer. During the melting period in summer, F_a-F_s does not equal zero, but this imbalance between the atmospheric and conductive heat flux then results in melting of the ice. Figure 19a displays the heat balance at the top of the ice in case of no snow cover. Figure 19b shows the corresponding ice thickness, atmospheric and surface layer temperature at 75° N. The atmospheric forcing is taken according to the Oort data in

section 3.2.5.. Note that downward heat fluxes are taken as negative and upward as positive.

The solar radiation is a smooth symmetric curve with value zero during the polar night. The maximum value occurs at approximately the 20th of June.

The net infrared radiation is composed of two components: the incoming longwave radiation and the outgoing black- body radiation (σT_s^4). The black body term remains constant during the melting season, because the ice surface- layer temperature remains constant during that period (see figure 19b). This explains the bubble in the net infrared radiation term.

The latent heat flux is positive during the whole year which means that the surface humidity q_s is always larger than the atmospheric humidity at anemometer level, q_a. In spring and summer this difference is the highest, because in that period the surface humidity increases due to damping of the ice. Due to the temperature difference (T_s-T_a) also a bubble occurs in the latent heat curve.

The sensible heat flux changes of sign due to the change of sign in the temperature difference (T_s-T_a). In winter and spring $T_s > T_a$, but in summer and autumn $T_s < T_a$. During the melting period, T_s remains at the melting point of ice, but T_a still continues to rise, which explains the bubble formation in the melting season here too.

The conductive heat flux reaches the highest downward value in winter, due to the large temperature difference between the bottom and top of the ice layer in winter. In summer, during the melting period, F_s becomes slightly positive as follows out of the formulation of F_s (equation 5.).

Figure 20 shows the heat balance of the ice model when snow is included. The latitude chosen is now 80° N and the mean atmospheric temperature is enlarged with two degrees. If no temperature increment is performed the melting period at high latitudes will become too short to melt away the snow cover on top of the ice layer entirely. Then the snow thickness can grow unlimited towards exceptionally large thickness.

The solar radiation is not symmetric anymore and its maximum is shifted to the beginning of July. This is caused by the changing albedo of snow as depicted in appendix A. The net infrared radiation, the latent and conductice heat flux have the same kind of behaviour as in the situation without snow. However, the sensible heat flux shows other characteristics. During most part of the year the sensible heat flux is directed downwards. Especially in spring this flux is large, which is due to the difference in (T_s-T_a), (figure 20b.). In winter still the atmospheric temperature is lower than the ice surface temperature, which is the same as in the situation without a snow cover.

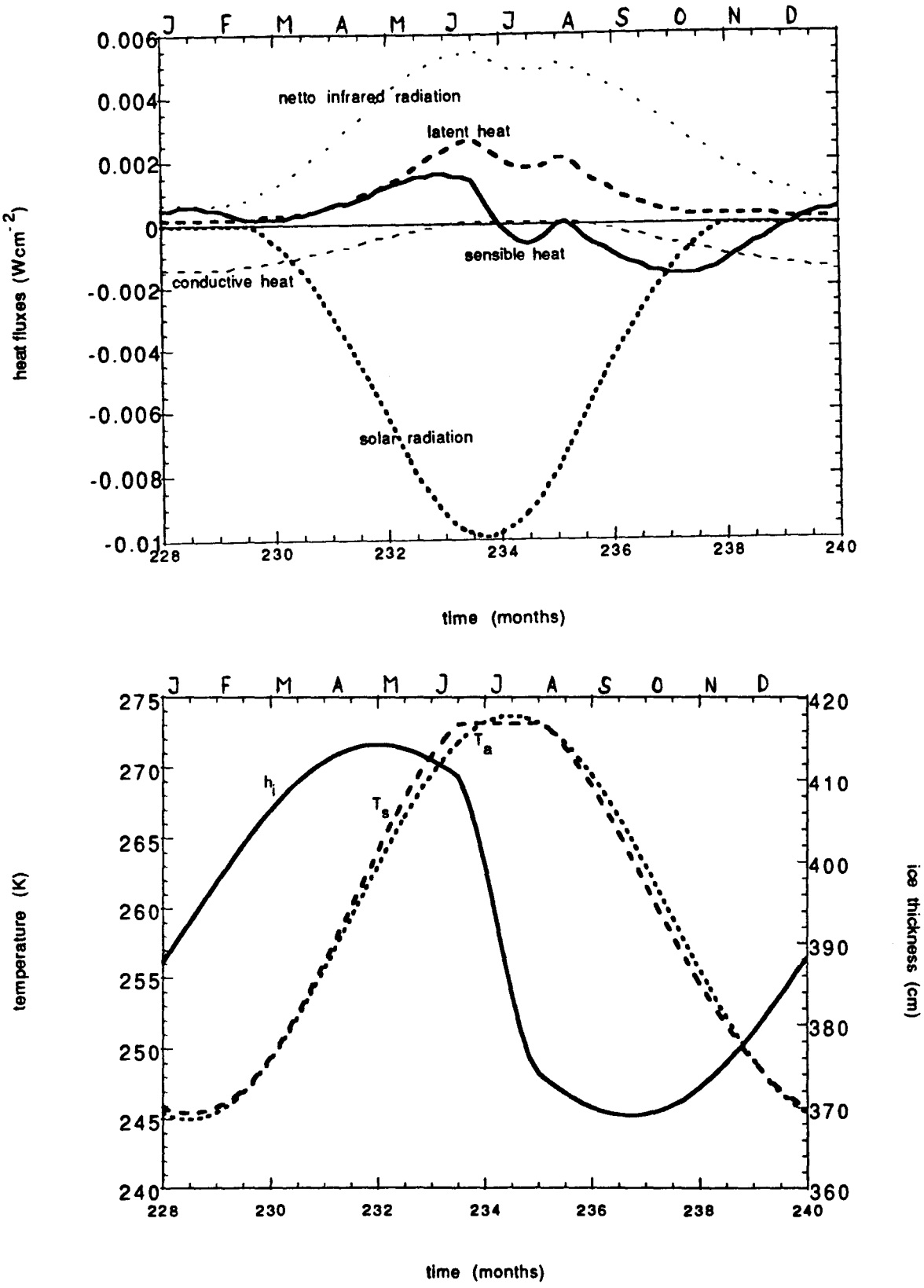

Fig. 19 Heat balance of the ice surface layer (a) and corresponding ice thickness, atmospheric and ice surface temperature (b), at 75° N latitude. Snowfall is not included and the atmospheric temperature forcing is according to the parameterization in section 3.2.5..

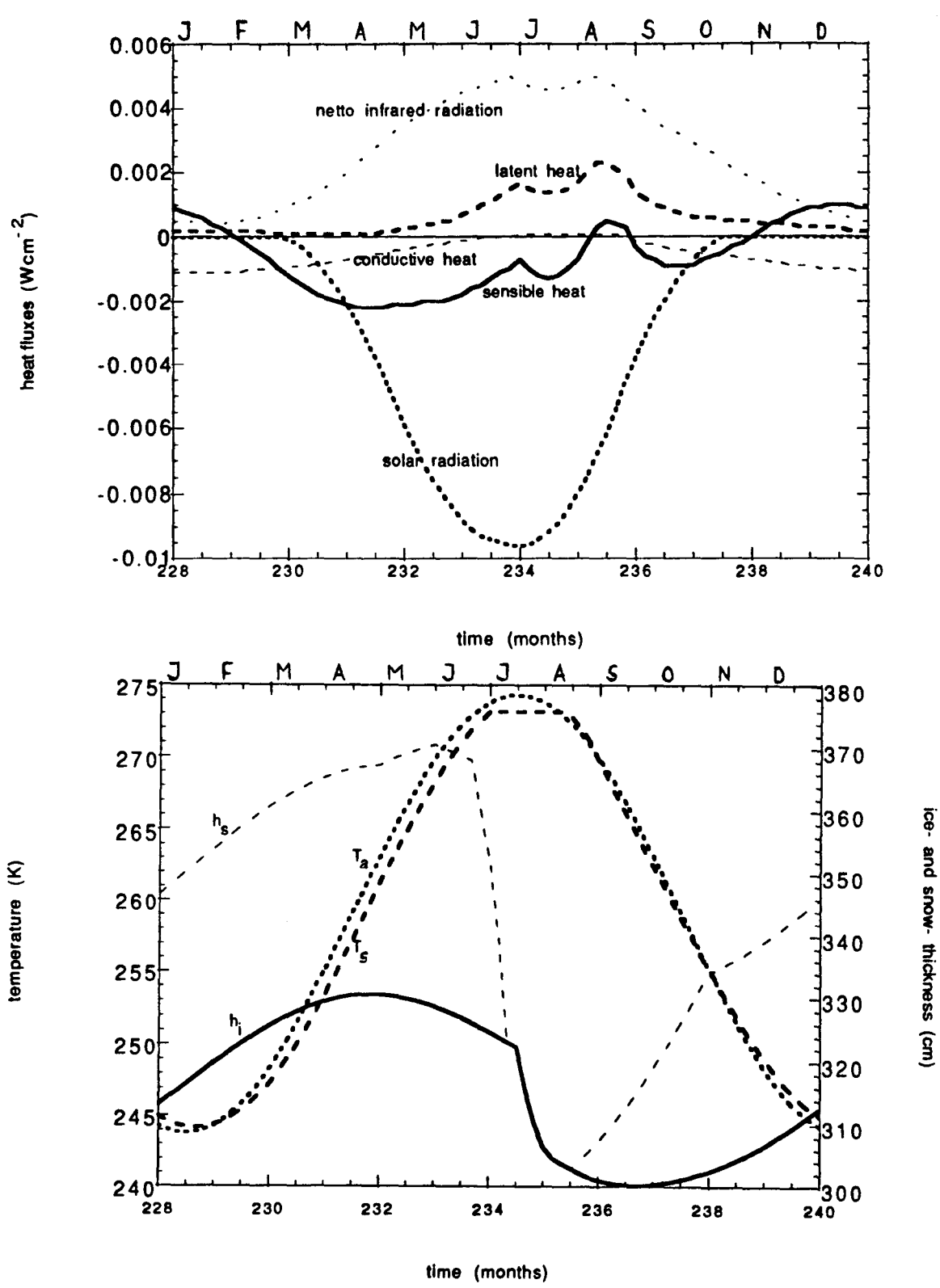

Fig. 20 Heat balance at the ice surface layer (a) and corresponding ice and snow thickness, atmospheric and ice surface temperature (b), at 80° N latitude. The atmospheric temperature forcing is according to the parameterization in section 3.2.5. plus an extra two degrees.

4.4. Ice thickness sensitivity to the atmospheric temperature

The atmospheric temperature is prescribed in section 3.2.5.. A more general expression for the atmospheric temperature is given by

$$T_a = 273.15 + T_{am} + T_{ampl}\sin\left(\frac{2\pi\ (t-105\ \text{days})}{360\ \text{days}}\right), \qquad (47.)$$

where T_{am} is the mean atmospheric temperature in °C and
T_{ampl} is the amplitude of the annual variation in T_a.

Figure 21a displays the dependence of the ice thickness when T_{am} is varied and T_{ampl} is held a constant (15.7 °C). The maximum, minimum, as well as the mean annual ice thickness are depicted. Snowfall is left out of consideration. As can be seen, there is a strong relation between h_i and T_{am}. 'High' T_{am} values cause small ice thicknesses and 'low' T_{am} values causes very thick ice slabs up to 7 meters. Another striking feature in figure 21a is that the annual variation in the ice thickness decreases for lower T_{am} values. The reason is that the period, in which the sea ice can melt, will become shorter for lower T_{am} values. If T_{am} will become even lower, there will be no melting period at all and ice can grow unlimited.

Figure 21b shows the sensitivity of the ice thickness on T_{ampl} when T_{am} is held constant (-14.8 °C). The relation is a bit weaker than observed in figure 21a, but it still is rather strong. Again the annual variation in h_i decreases for smaller values of T_{ampl}, for the same reason as mentioned before.

(a)

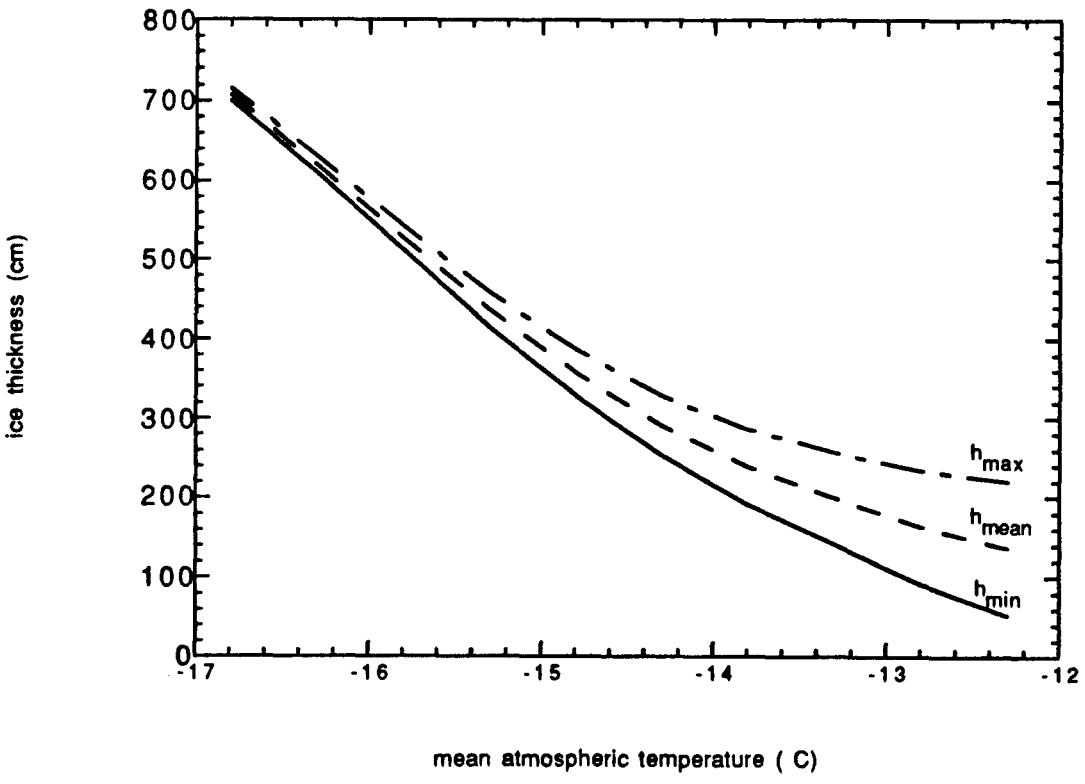

(b)

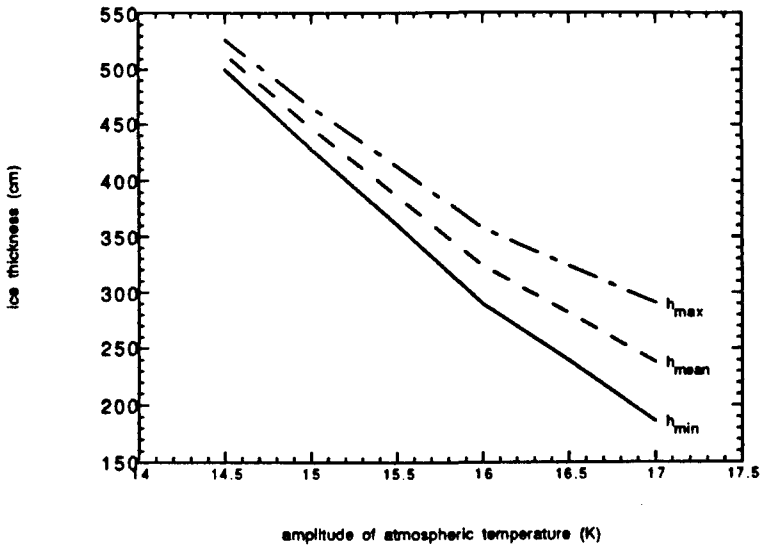

Fig.21 Ice thickness dependence on the mean atmospheric temperature (a), with T_{ampl} = 15.7 °C, and dependence on the amplitude of the annual variation in T_a (b), with T_{am} = -14.8 °C.

4.5. Ice thickness sensitivity to the advection flux

As can be seen in equation (8.) h_i is highly dependent on the oceanic bottom flux F_B. There is a lot of uncertainty about the value of the oceanic bottom flux and many different values for F_B are used in literature, as will be discussed in section 5.4.. For latitudes where ice is present during the whole year, the bottom heat flux equals the advection and diffusion flux F_H (section 3.3.). The ice thickness dependence on F_H is shown in figure 22.

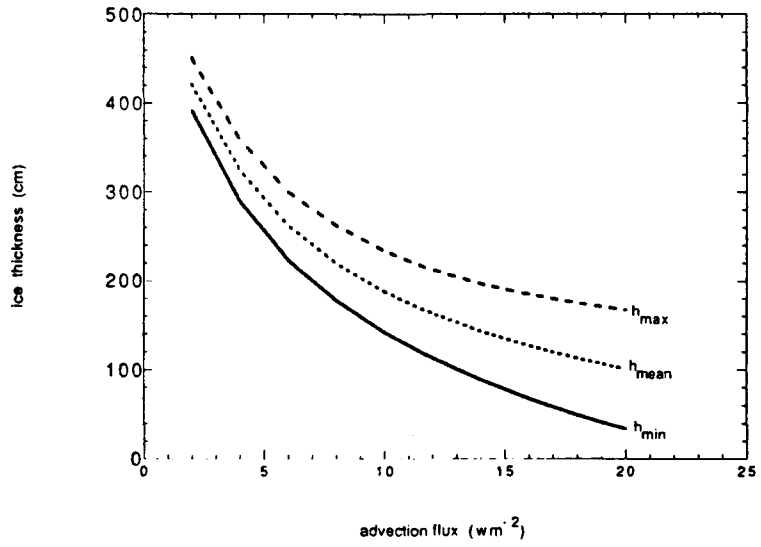

Fig.22 Ice thickness dependence on the advection and diffusion flux F_H. The atmospheric forcing is described by T_{am} = -14.8 °C and T_{ampl} = 16 °C.

Snowfall is left out of consideration. For very large values (> 25Wm^{-2}) of F_H the ice layer will vanish completely and a multi- year equilibrium cycle will be created. The amplitude in the annual ice- thickness variation decreases for small values of the advection flux F_H. This is caused by the decreasing ice- thickness change Δh_B at the bottom of the ice for decreasing F_H (thus F_B).

4.6. The mixed- layer salinity

The salinity of the mixed layer, as described in section 3.3., is directly proportional with the thickness change of the ice slab. Figure 23 displays the mixed- layer salinity as a function of time together with the ice accretion and ice melt during two years. During ice accretion the mixed-layer salinity increases, during ice melt the salinity decreases, as expected. There is no feedback mechanism of the mixed- layer salinity on the ice growth. An annual variation in h_i of 70 cm results in an annual variation in S_i of ± 0.2 PSU.

Figure 24 shows the dependence of mixed- layer salinity on the mixed-layer depth h_m and the salinity of the ice shelf S_i. If h_m is increased to 150 meters, the salt is distributed over a larger volume of water, resulting in a diminishing of the annual variability in the mixed- layer salinity. Decreasing the ice salinity to 3 PSU (instead of the usual 5 PSU), leads to a contrary result. The annual variability of S_i is enlarged, but not in a

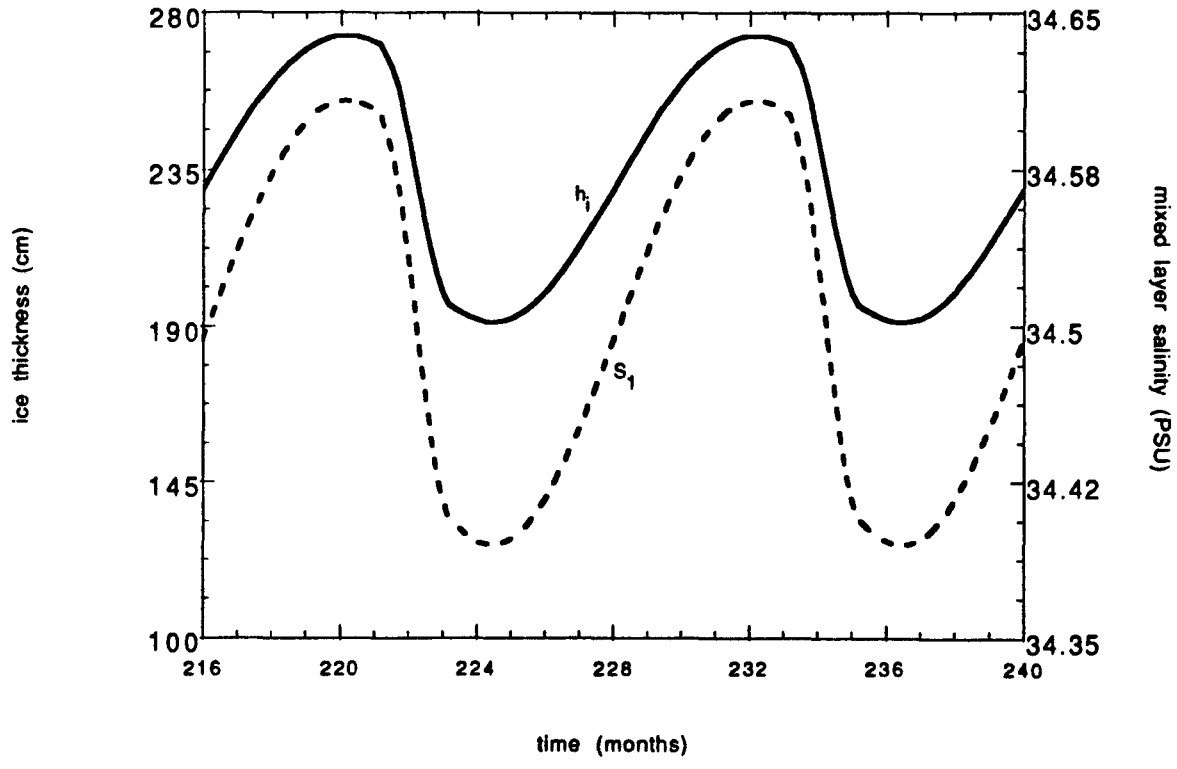

Fig.23 Relationship between ice thickness and mixed- layer salinity.

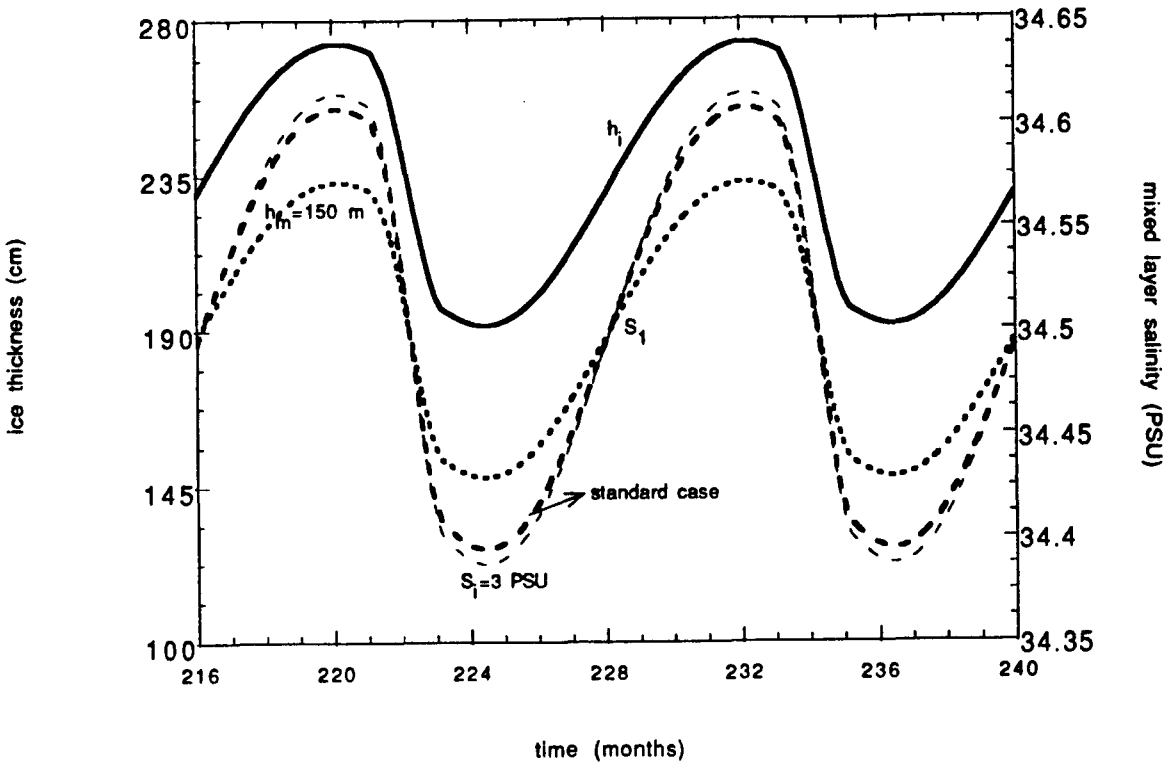

Fig.24 Mixed- layer salinity dependence on mixed- layer depth and ice salinity. The standard case is characterized by h_m=100 m and S_1=5 PSU.

spectacular fashion, although the change in the ice salinity is about 40%. However, the salinity flux is proportional with the salinity difference between ice shelf and mixed layer, and this salinity difference only changes 6% due to the change in S_1.

4.7. Time constants of the ice model

Figure 16 displays an integration of the ice model at a 80°N latitude. It shows us that the ice thickness is not immediately in an annual equilibrium cycle , but will gradually approach to that cycle when starting at an initial ice thickness $h_1(0)$. The ice- surface temperature is almost immediately settled in his annual equilibrium cycle. This temperature follows from the diagnostic equation (1a.). Now consider the situation in which snowfall is left out of the model and the atmospheric forcing K in equation (9a.) is constant in time. Then (1a.) can be written as

$$K + \sigma T_s^4 - F_s = 0. \qquad (48.)$$

The surface layer temperature is almost immediately in its annual equilibrium cycle. It is calculated with the use of the Newton- Raphson method as depicted in equations (11.) and (12.). The equilibrium value of the surface temperature is undependent of the ice thickness h_1 (equation (7.))

However the annual equilibrium cycle of the ice thickness is reached only after several years of integration. For constant atmospheric forcing and a matching surface temperature that is lower than the melting point of ice, only ice accretion takes place, so

$$\frac{dh_1}{dt} = \frac{F_s - F_B}{q_B} = \frac{\frac{k_1}{h_1}(T_B - T_s)}{q_B} - \frac{F_B}{q_B} = \frac{C_1}{h_1} + C_2 \qquad (49.)$$

where

$$C_1 = \frac{k_1}{q_B}(T_B - T_s) \qquad (50a.)$$

and

$$C_2 = -\frac{F_B}{q_B}. \qquad (50b.)$$

Because T_s is constant , C_1 and C_2 are both constants during the whole integration period. T_s is computed from equation (7.). If the total ice model is in an equilibrium situation (49.) equals zero, and thus

$$C_2 = -\frac{C_1}{h_e} \qquad (51.)$$

where h_e stands for the final equilibrium value for the ice thickness. Now consider a perturbation h' on the equilibrium value h_e, and suppose $h' \ll h_e$, then $h_1 = h_e + h'$. Now (49.) can be written as

$$\frac{dh'}{dt} = \frac{C_1}{h_e + h'} + C_2 = \frac{C_1}{h_e(1 + h'/h_e)} + C_2 = \frac{C_1}{h_e}\left(1 - \frac{h'}{h_e}\right) + C_2 \qquad (52.)$$

The last step is allowed because h' is much smaller than h_e. Rewriting (52.) and using (51.), we get

$$\frac{dh'}{dt} = -h'\frac{C_1}{h_e^2} + \frac{C_1}{h_e} + C_2 = -h'\frac{C_1}{h_e^2} \qquad (53.)$$

Integration of (53.) gives us

$$\int \frac{dh'}{h'} = -\int \frac{C_1}{h_e^2}\,dt \qquad (54.)$$

thus

$$\ln(h') = -\frac{C_1}{h_e^2}t + \text{const.} \qquad (55.)$$

Finally this results in

$$h' \sim e^{-t/\tau} \tag{56.}$$

where τ is a time constant equal to

$$\tau = \frac{h_e^2}{C_1} = \frac{q_B h_e^2}{k_1 (T_B - T_s)}. \tag{57.}$$

If we use the following mean parameter values for the atmospheric fluxes, respectively H = 4.3061, E = -3.6467, I = $-2.23 \cdot 10^2$ and Q = $-1.0146 \cdot 10^2$ Wm^{-2} and F_B equals 2.0185 Wm^{-2}, then $\tau \sim 1.6 \cdot 10^9$ sec. ~ 620 months. When an experiment is performed these same conditions as mentioned above, figure 25 will arise. With the use of the gradient at t = 0, it is possible to deduce the experimental time constant τ. The ice thickness at time t can be written as

$$h_1(t) = h_e - h'e^{-t/\tau} \tag{58.}$$

and

$$\frac{dh_1(t=0)}{dt} = \frac{h'}{\tau} \tag{59.}$$

where h' denotes the ice- thickness perturbation.

From (59.), the experimental time constant τ equals ~ 650 months, which is very close to the theoretical time constant as calculated above. The fact that the process towards an equilibrium ice thickness is very slow, is due to the small ice growth velocity, which is related with the latent heat of fusion of sea ice, q_B.

If we skip the condition of prescribed constant annual atmospheric forcing and return to the parameterizations with variable forcing as described in section 3.2., again an exponential behaviour towards an equilibrium cycle appears. On top of this exponent a yearly cycle is superposed, which can be regarded as a high frequency disturbance (figure 26). The final mean equilibrium ice thickness is ± 2.5 meters. This is a much thinner ice slab than in the case of the constant annual atmospheric forcing (approximately 12 m.).

The time constant τ is proportional with the equilibrium ice thickness squared , thus for a mean ice thickness of 2.5 meters τ equals

$$\tau \sim 620 \frac{(2.5)^2}{(12)^2} \sim 27 \text{ months.} \tag{60.}$$

From figure 26 an experimental time constant of approximately 39 months can be deduced using the gradient method as mentioned in (59.). This experimental value is in the same order as the theoretical value expressed in (60.). Differences between both values are due to the annual cycle in the atmospheric forcing and the simple assumption of a high frequency disturbance superposed on the exponential behaviour towards equilibrium.

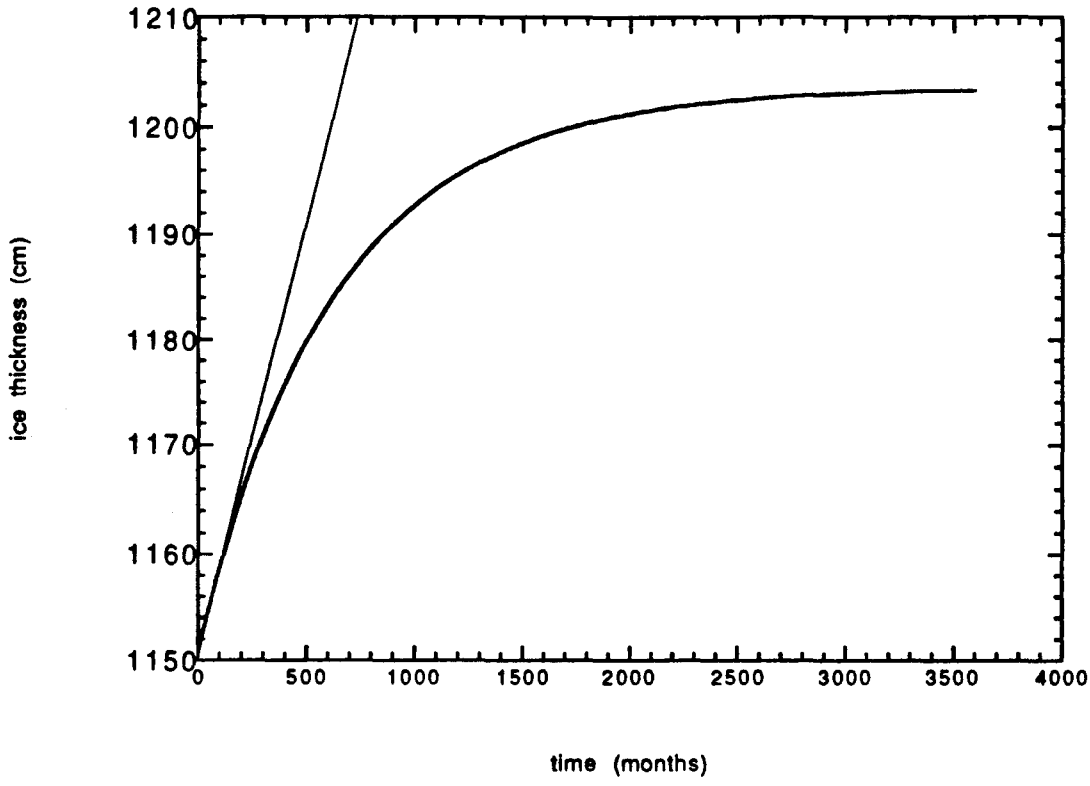

Fig.25 Ice thickness behaviour in time using constant annual atmospheric forcing (see text) and plot of the gradient at t=0.

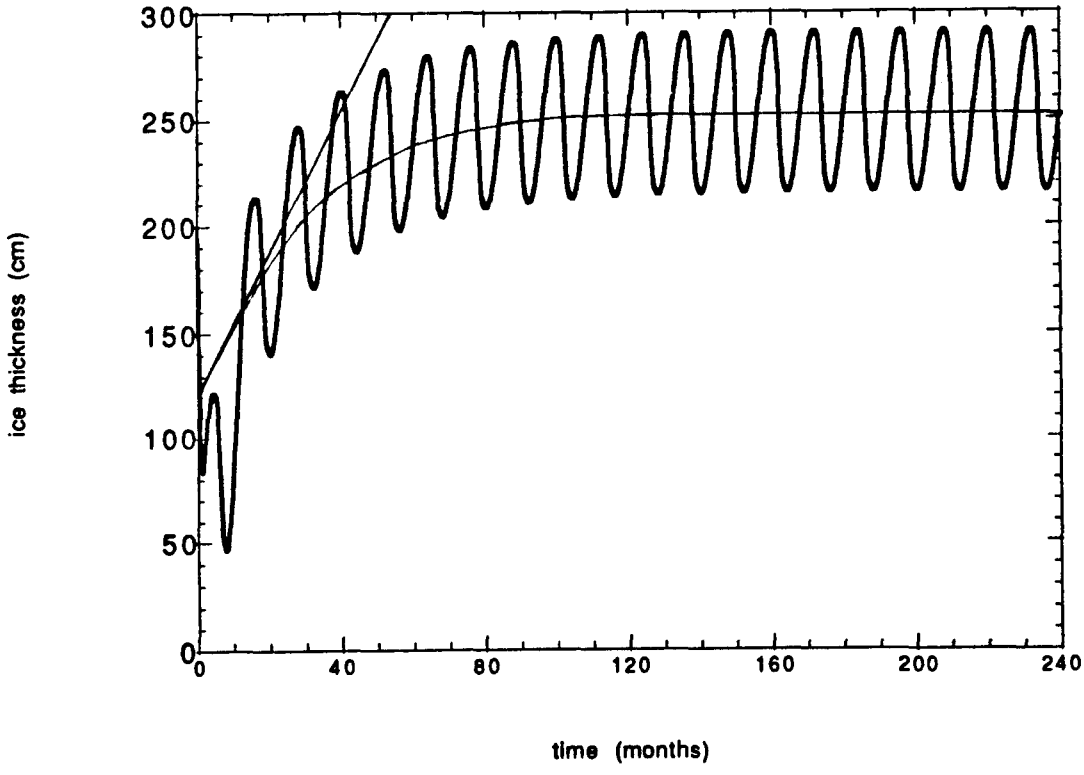

Fig.26 Ice thickness behaviour in time using the atmospheric forcing as described in section 3.2. with plot of exponent and gradient at t=0.

4.8. Two- dimensional ice experiments

4.8.1. The seasonal ice margin

Until now ice thicknesses have been given only as a function of time. When also the latitudinal dependence is taken into account, by using the parameterization of the atmospheric temperature as described in section 3.2.5., one obtains contour pictures as a function of time and latitude as in figure 27. The contour lines denote ice thickness values in centimeters. Snowfall is left out of consideration, but will be discussed later. The grid used for the latitude dependence equals 2.5°.

At the end of the winter and in the beginning of the spring, the ice margin lies at the lowest latitude, i.e. about 60° N. The margin is very flat during this period, which is caused by the latitude grid size. In autumn the ice margin is positioned at 67.5° N. This implies an annual variation in the ice margin of ± 8° in latitude.

When moving from low to high latitudes, ice becomes thicker and annual ice thickness variation decreases. A higher latitude implies a lower atmospheric temperature, so shorter melting periods of ice, and thus smaller annual ice thickness variation. At 80° N ice thicknesses equal up to 6 meters. Multi year equilibrium cycles do not occur, because snowfall is not included.

If we increase the mean atmospheric temperature T_{am} in equation (47.) with one or two degrees compared to Oort data, the following effects can be seen:

1. The ice margin is situated at higher latitudes during the whole year; approximately 2 degrees latitude increase for one degree temperature increase.
2. Ice thicknesses decrease at every latitude. At 80° N the ice thickness decreases from 600 cm to 340 cm for a two degree mean atmospheric temperature increase compared to the Oort data.
3. The annual ice margin variation remains ± 8° in latitude.

Figure 28 displays the salinity and mixed layer field corresponding to the ice thickness field depicted in figure 27. The salinity field shows us a salinity source at the ice margin latitude in march and a salinity sink at the ice margin latitude in september. When the ice thickness is increasing, during winter and early spring, the salinity of the mixed layer is increasing too, as explained in paragraph 4.6.. The largest salinity fluxes occur at the ice margin, because at these latitudes annual ice thickness variation is at a maximum (up to 1.5 meters). The maximum annual salinity variation is about 4 PSU. At every latitude the annual mean salinity flux must be zero during an equilibrium cycle. At very low latitudes, where no ice exists at all, the annual salinity variation is very small, because no salinity exchange occurs between an ice shelf and the oceanic mixed layer.

The initial salinity contents of the mixed layer is prescribed as a function of time and latitude in paragraph 3.4. and equilibrium salinity values depend on the initial ice- thickness parameterization.

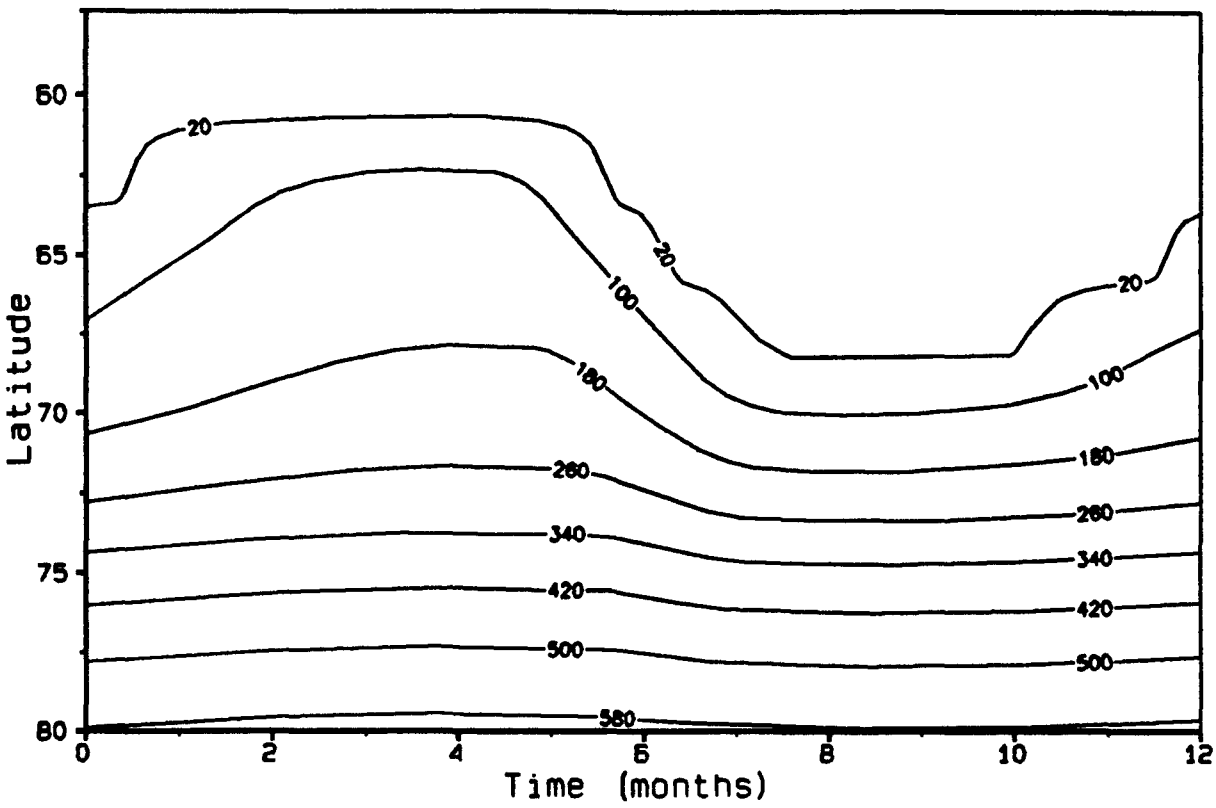

Fig. 27 Ice contours as a function of time and latitude with atmospheric temperature forcing according to Oort's data (Oort, Peixoto [1992])

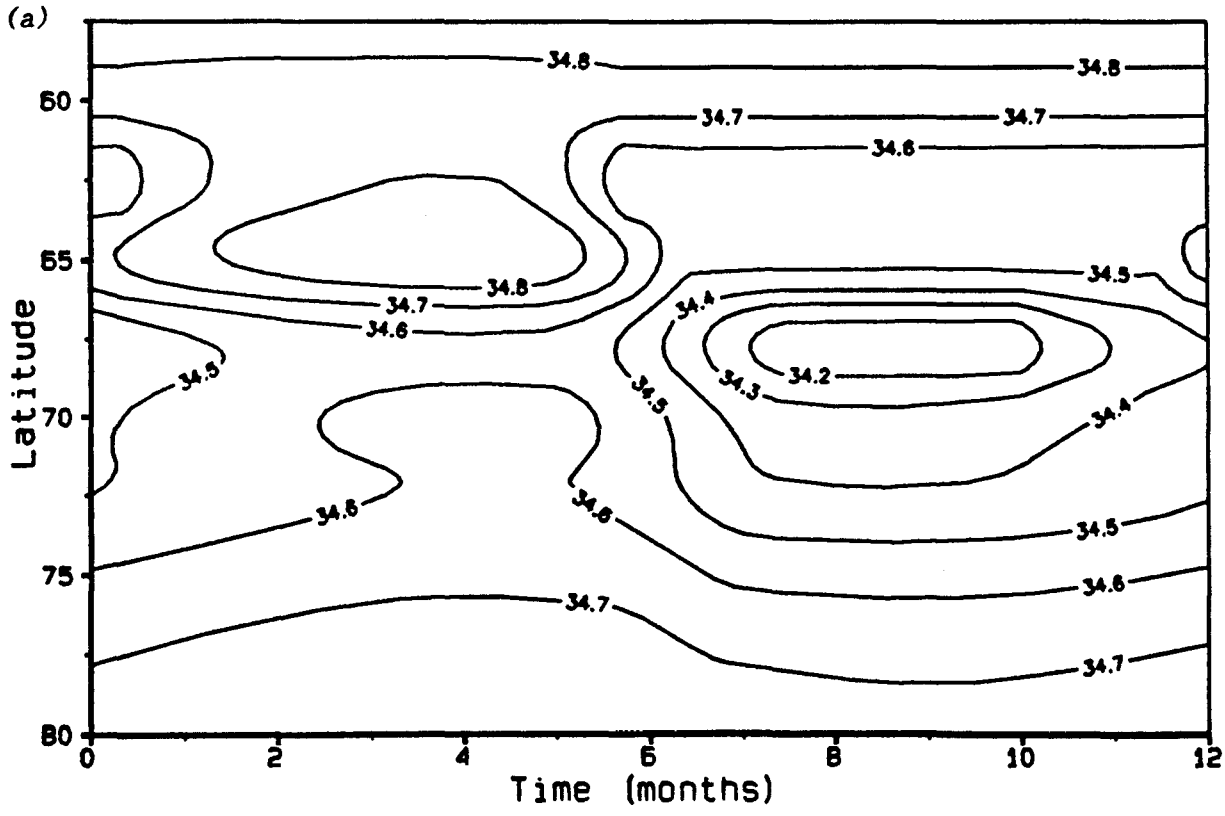

(b)

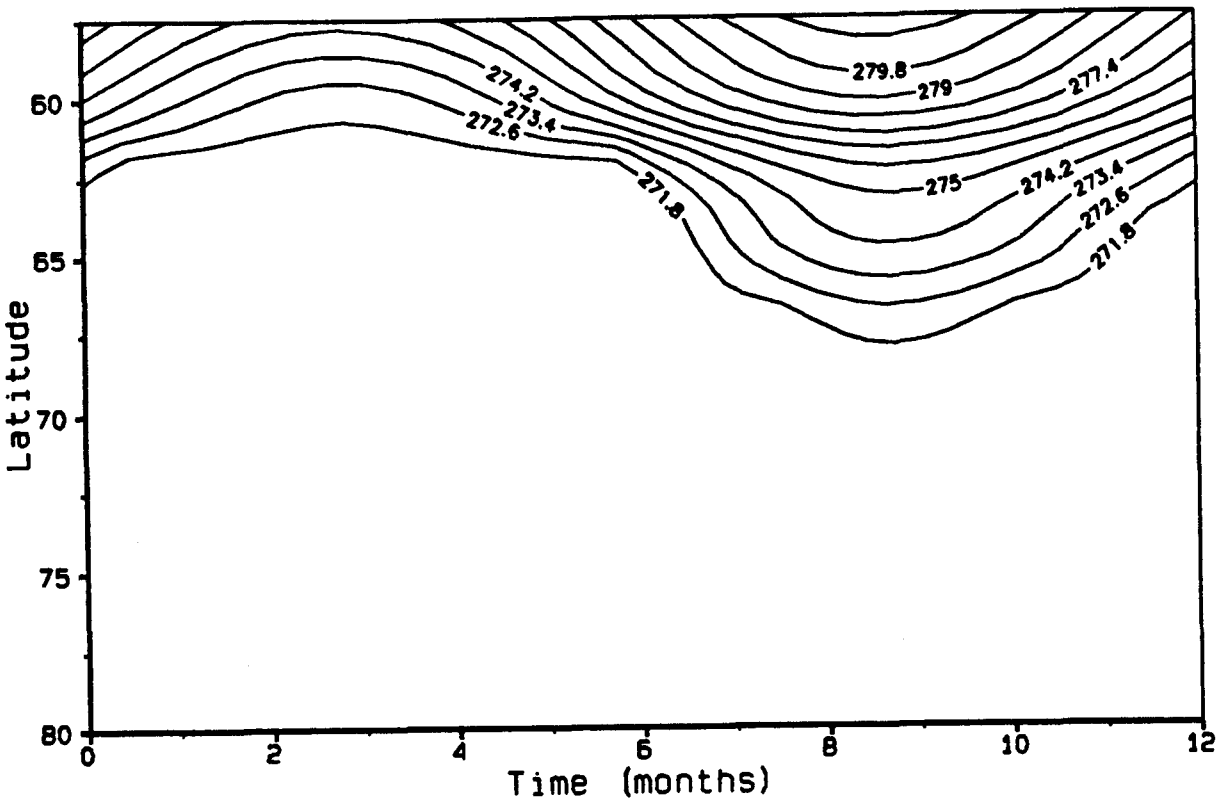

Fig.28 Mixed- layer salinity (a) and mixed- layer temperature (b) contours as a function of time and latitude, both corresponding to the ice thickness field as depicted in figure 27.

The mixed- layer temperature field is depicted in figure 28b. The mixed-layer temperature has a constant value on latitudes where ice is present. This temperature can be calculated with the use of equation (42.) which gives T_m = 271.17 K, i.e. just above the freezing point of sea water. At the ice edge and at lower latitudes the mixed layer can warm up and cool down due to the variation in the atmospheric fluxes. The lower the latitude on the Northern Hemisphere, the smoother the curvature of a mixed layer temperature contour, because ice influence vanishes.

4.8.2. Multi- year equilibrium cycles

If now the latitudinal dependence is introduced and snow is allowed to fall down at each latitude where ice is present (40 cm a year), figure 29 is obtained. The atmospheric temperature forcing equals the Oort data (Oort & Peixoto [1992]), plus an additional two degrees Kelvin at every latitude. If no temperature increment is performed the melting period at high latitudes will become too short to melt away the snow cover on top of the ice layer entirely. Thus the snow cover can grow unlimited towards exceptionally large thicknesses. Of course this is not realistic, since snow can be converted into ice and snow can sublimate.

Figure 29 shows the following features:

1. Several multi- year cycles can be distinguished on different locations. In this situation we have a one- year, two- year and four- year equilibrium cycle.
2. Ice thicknesses are a lot smaller than without a snow cover due to the difference in thermal conductivity of snow and ice.
3. The ice margin is not positioned at the same latitude every year after the melting period in summer, due to the multi- year cycle effect. The ice margin variation in latitude lies in between 9° and 13°, which is higher as in the case without snowfall.

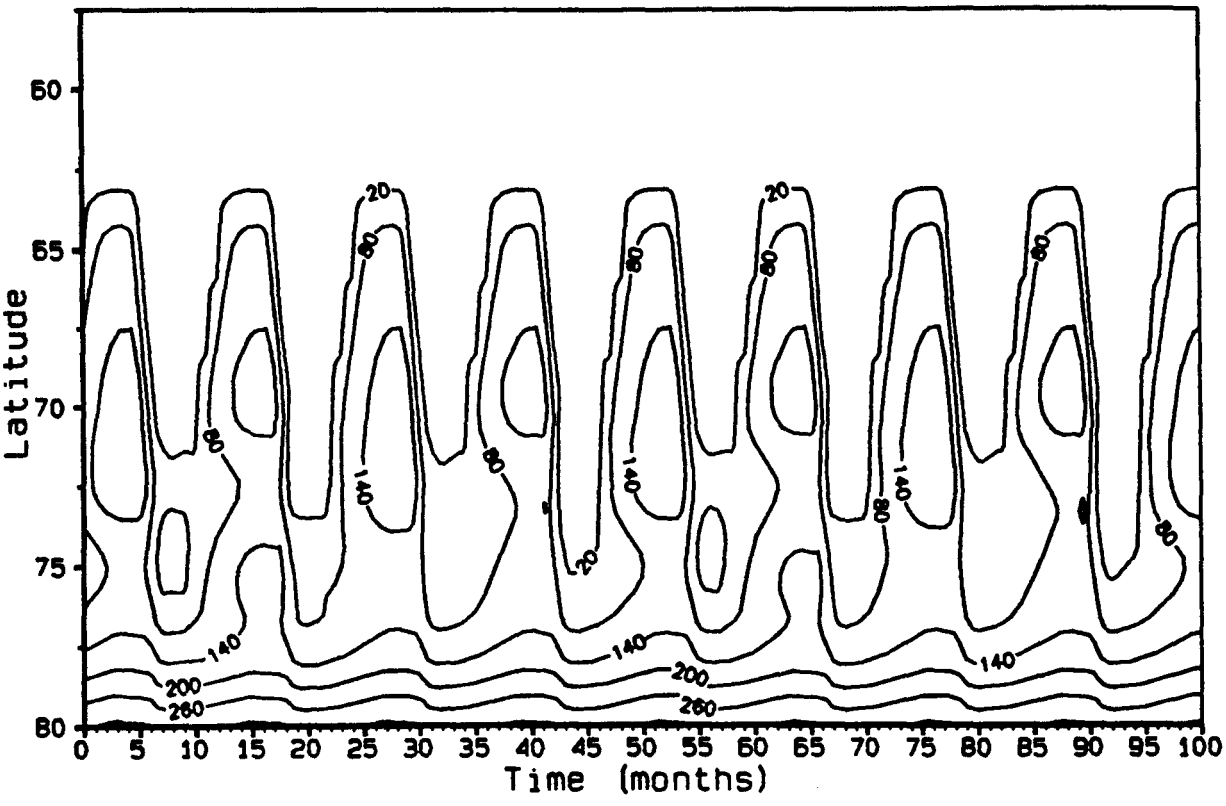

Fig.29 Ice thickness field with a yearly snow fall of 40 cm at every latitude where ice is present. Different multi- year cycles can be distinguished.

CHAPTER 5. DISCUSSION OF THE ICE MODEL

5.1. Introduction

The ice model described in this paper is a thermodynamic ice model. This implies that it only deals with thermodynamic or energetic parameterizations. It is a simple form of an Energy Balance Climate Model (EBCM) explicitly developed for sea ice modelling, as is illustrated in Harvey [1988a], [1988b]. Dynamics have no role at all in the developed ice model, so ice transport is not considered. The model is actually one-dimensional in space although applied at different latitudes. It is basically the Semtner [1976] zero- layer model which has been followed for the calculations related to the ice and snow. The Semtner model is the basic model in most of the ice models developed in literature. In these models the atmospheric fluxes are computed rather than specified as is done by Semtner.

Discussions of ice transport include a wide range of formulations. Certainly the simplest are those relating the speed and direction of the ice strictly to the speed and direction of the water. Other formulations include wind stress, water stress, Coriolis force, stress from the tilt of the sea surface and internal ice resistance. Such an elaborate ice model is the Hamburg Sea- Ice Model by A. Stössel [1991]. The sea ice model of Parkinson and Washington [1979] also includes sea ice dynamics, as does the model developed by Hibler [1978].

For simplicity and good understanding, and for implementation of the ice model into the ocean model developed by Haarsma and Lenderink [1992], all dynamics have been omitted. In first instance we are interested in the principal features of the influence of sea ice on the thermohaline circulation of the ocean. Complicated modelling makes explanations too elaborate and uncertain.

For the same reason other rather important ice features have not been considered, such as ice leads, brine pockets trapped within the ice and for example vertical variations in the ice density. Also sea ice interaction, related to plastic rheology as discussed by Hibler [1978] is left out of consideration. Furthermore the parameterizations and the constants used in the ice model are very much simplified and in most of the cases certainly not always in perfect correspondence with real climatic situations.

5.2. Ice characteristics in reality

Sea ice covers roughly 7% of the Earth's oceans and forms a very effective barrier between these oceans and the atmosphere. The distribution of sea ice undergoes large variations both seasonally and interannually.

Because of our interest in the behaviour of the ice slab in the Northern Hemisphere, the following ice characteristics only refer to the North Pole. Sea ice extent typically varies from a summer minimum of $8 \cdot 10^6$ km^2 to a winter maximum of $15 \cdot 10^6$ km^2, the latter being roughly 10% of the ocean area in the Northern Hemisphere. The Arctic Ocean itself remains covered with ice during most of the year and consists of a fairly compact ice mass called the polar cap. See figure 30 for average monthly sea ice extents.

Ice thicknesses in the Central Arctic average about 3 to 4 meter, while

those in the surrounding seas and in the Antarctic are more commonly 0.5 to 1 meter. Sea ice is distinct and far smaller than the occasional icebergs found in the polar waters of both hemispheres. Icebergs calve from land glaciers, are composed of fresh rather than salt water, and can be over 600 meter thick. Sea ice, in contrast, forms within the sea, and even with extensive ridging only very rarely has thicknesses exceeding 20 meters.

Sea ice influences the temperature and circulation patterns of both the atmosphere and the ocean. Sea ice diminishes the amount of solar radiation absorbed at the ocean's surface; it is a strong insulator, restricting exchanges of heat, mass and momentum. The reduction in heat exchange between ocean and atmosphere due to the ice cover is impressive. In the Arctic winter, air temperatures vary roughly from -20 °C to -40 °C, while water temperatures vary from 0 °C to -2 °C. This temperature contrast can lead to heat transfers in the order of 10^2 Wm^{-2} from the ocean to the atmosphere at locations where the two come in direct contact. Where direct contact is prevented by an ice slab, however, the heat transfer is only about 10 to 20 Wm^{-2}.

A reasonable value for the salinity of sea ice in numerical models is about 4-5 PSU. However the composition of sea ice depends on many factors, including the salinity of the water from which it is formed, the speed of freezing, the amount of any melting subsequent to freezing, the temperature, and the age of the ice. Older ice often has a lowered salinity contents, because brine pockets are frequently allowed to drop into the water underneath. Rapidly formed ice might have salinities as high as 20 PSU. The sea ice density depends largely on salinity. The most important fact regarding sea- ice density is that it is always lower than the density of the surrounding water, allowing the ice to float rather than to sink. Typical values range from 880 to 910 kgm^{-3}, with the differences depending primarly on the air and salt content. Ice density tends to increase with an increase in salinity.

Salt rejection processes result in increased salinities of the oceanic mixed layer in regions of ice formation and decreased salinities in regions of net ice decay. This salinity change of the mixed layer resulting from the formation of ice affects the vertical density of the mixed layer, and so increases the chances of an unstable density stratification which results into convective overturning with the underlying water. By this the total ocean circulation can be affected in the long run. This is most likely where the amount of ice formation is the greatest, which tends to be at the open ocean and at the edges of the ice pack. Although observations are limited, it is believed that a large part of the world's bottom water is formed at the polar regions (Washington & Parkinson [1986]).

Ice thicknesses computed with the thermodynamic ice model as described in chapter 3, depend on whether or not snowfall is included in the model. Without a snow cover the ice is rather thick, up to 6 meters at 80 °N latitude, which is not corresponding to the Central Arctic average which equals about 3 to 4 meters. Increasing the mean atmospheric temperature T_{am} with 2 °C results in more reasonable ice thicknesses.

Including snow fall, although at the same rate at every latitude (which is of course not very realistic), improves model simulations. Ice thicknesses at 80 °N equal about 3 meter, when the mean atmospheric temperature is increased by 2 degrees. If not done, the melting period of

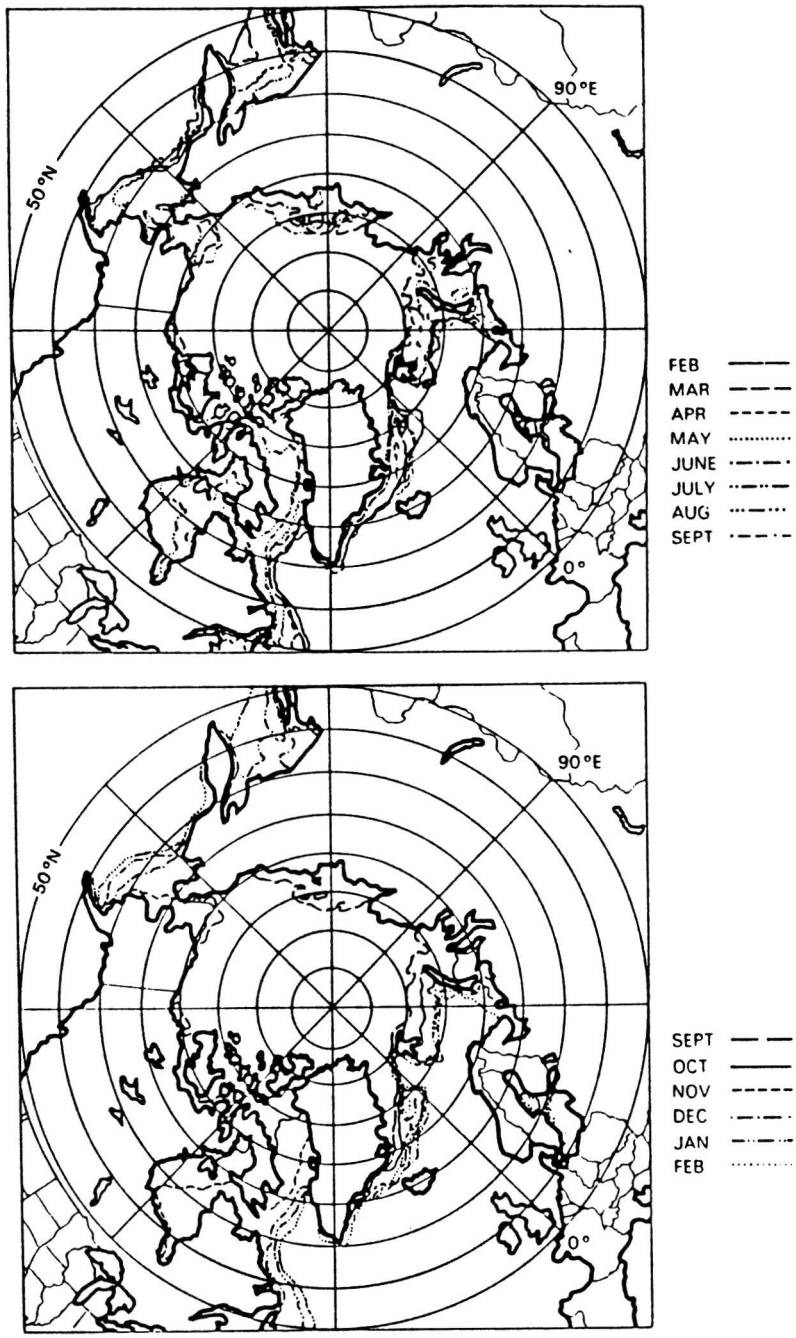

Fig.30 Average sea- ice extents in the Northern Hemisphere. These are averaged, by month, for the four years 1973-1976 from passive microwave data from NASA's Nimbus satellite. (From Parkinson and Washington [1986]).

the ice will become too short to eliminate the entire snow cover, which leads to immense unrealistic snow thicknesses in the following years. Since snow (ice) ablation and convertion of snow into ice are not included in the model, the atmospheric temperature had to be increased. Another possibility to temper the unlimited snow cover growth is to restrict it to a maximum value of, for example, 50 cm. When reaching this limit, no more snow is allowed to accumulate. The atmospheric temperature is now prescribed as in section 3.2.5.. This leads to ice thicknesses up to 4 meters at 80° latitude, which still are fairly realistic values.

The ice margin at 170°W longitude varies according to the observations of the Nimbus satellite, as depicted in figure 30, between 57.5°N in winter and 72.5°N in latitude in summer, so an annual variation of about 15°. Without a snow cover the calculated ice margin is positioned between approximately 60° and 67°N, which lies just in between the real ice margin variation. The annual variation is, however, far too small. The main causes for this difference are the neglect of ice dynamics, snowfall and the omitting of the formation of ice leads, which have a reasonable impact on the energetic balance at that location. When ice leads occur the atmosphere is in direct contact with the mixed layer of the ocean, although an ice cover is in the direct neighbourhood of these irregularities. The leads increase the melting rate of the surrounding ice slabs during the melting seasons.

With an additional snow cover the ice margin fluctuates between 62.5°N and an averaged 73°N (averaged due to the multi- year equilibrium cycles). Again the model with snowfall included leads to more realistic results. Nevertheless the unrealistic build- up of the snow remains a problem.

The ice salinity has been set at a constant value of 5 PSU. The age of the ice slab is assumed to have no influence on the salinity content of the ice slab. As discussed above this point of view is very simplistic.

The mechanism of the multi- year equilibrium cycles might be important in considering multi- year anomalies in the observed ice cover.

5.3. The atmospheric heat fluxes

5.3.1. The solar radiation

In section 3.2.2. the solar radiation incident on the surface under cloudless skies was defined as Q_o. Thus albedo and cloud effects are not yet implemented in this definition. When Q_o is averaged over the period of an entire year and computed as a function of latitude with the use of the zenith angle Z, figure 31 appears. At the equator the yearly averaged Q_o approximately equals 412 Wm^{-2}, while at the North Pole it amounts approximately 173 Wm^{-2}. Also in this diagram the maximum incident solar radiation (this is the case at 20 June) is plotted. An apparent feature is the fact that now the maximum Q_o increases for increasing latitude, except around 67.5°N where we observe a small decrease in magnitude. This is the region where the polar night starts to get involved in the yearly solar cycle.

Comparing the upper results with observational data from Campbell and Vonder Haar [1980], we see a lot of similarities, see figure 32. The yearly averaged curve of Q_o shows the same behaviour as computed above. The equator value equals ± 410 Wm^{-2}, the pole magnitude ± 180 Wm^{-2}, which is in perfect coincidence with the computational values. The maximum incident solar radiation in figure 31 can be compared with the observed June- July- August average curve in figure 32. Although the latter is a three- monthly averaged value it gives similar behaviour as the calculated maximum Q_o, which as expected gives higher incident solar radiation magnitudes. The dip is located at the same latitude.

The solar radiation absorbed at the surface, given by (17.) needs values of cloud cover, cloud albedo and surface albedo, which is either water, either sea ice, either snow. These parameters will be discussed in section 5.5..

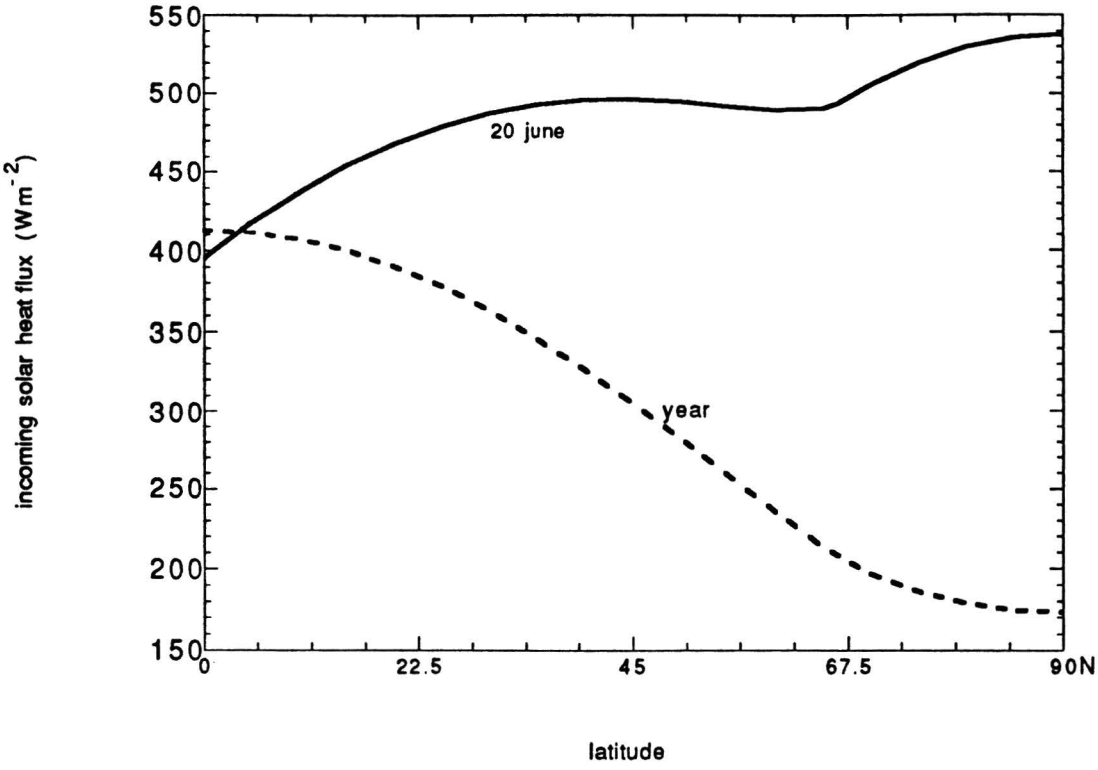

Fig.31 Computed meridional profile of the annual mean incoming solar radiation for clear skies and the maximum incident solar radiation on 20 June.

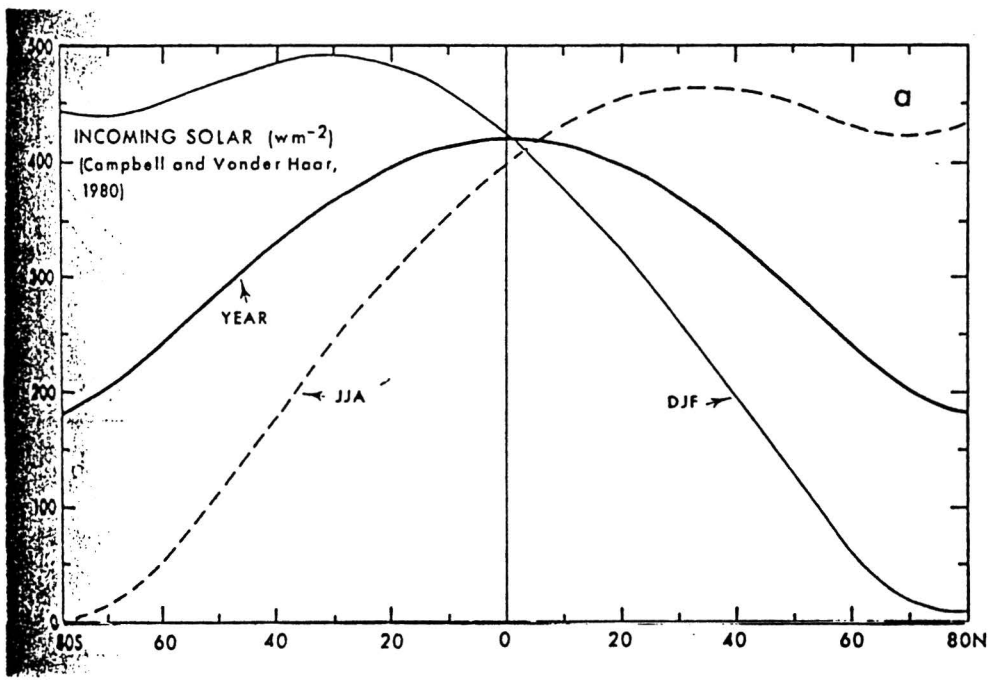

Fig.32 Meridional profiles of the zonal-mean incoming solar radiation at the top of the atmosphere in Wm^{-2} for annual, DJF and JJA mean conditions (based on data from Campbell and Vonder Haar [1980]).

5.3.2. The infrared radiation

Different parameterizations for the incoming infrared radiation exist. The parameterization introduced by Idso and Jackson [1969], IJ, is used in this sea- ice model and is descibed in section 3.2.3.. Idso and Jackson found their formulation through experimental considerations and used statistical analysis of experimental data at different latitudes and seasons. They compared previous formulas through a theoretical analysis of the atmospheric thermal radiation, and stated that their parameterization was the only one with universal applicability. Their parameterization is also used by Parkinson and Washington [1979], and in the Hamburg Sea Ice Model [1991].

However, Harvey [1992] uses the parameterization introduced by Berliand and Berliand [1953], (BB). The BB formula came out best of research work performed by Fung et al. [1984]. To judge whether there are significant differences and whether both definitions lead to different model behaviour, the BB parameterization is compared to the IJ parameterization. In first instance the cloudiness factor f_c is set equal to zero. The IJ parameterization is depicted in equation (27.). The general BB formulation is given by

$$I_o = - \sigma(T)_a^4 \left(0.61 + 0.05 \, (e_a)^{1/2} \right). \qquad (61.)$$

Three BB parameterizations are defined, all differing in the description of the vapour pressure e_a. BB1 corresponds to the formula in (61.) with e_a=0, BB2 idem but with e_a according to Haney [1992] (eq.(35.)), and BB3 idem but with e_a according to Parkinson and Washington [1979] (eq.(34.)). The result is shown in figure 33a.

The BB1 curve is parallel to the IJ curve. This is because both definitions exclude the vapour pressure e_a. However the BB1 values are a lot smaller than the IJ values. The difference between the BB2 and BB3 curve is minimal, which implies that the e_a definition by Parkinson and Washington is as good as the definition by Haney. In summer, during maximal downward infrared radiation, the BB2 and BB3 curves touch the IJ curve. During winter the difference in magnitude is up to 22%. Thus in summer the role of the vapour pressure e_a becomes significant, because during that period water vapour can easily enter the atmosphere. In winter this effect is minimal. The IJ description does not include this phenomena, thus keeps a rather small amplitude.

If the cloudiness factor is introduced the Berliand and Berliand formulation becomes:

$$I = \sigma(T_a)^4 \left(0.39 - 0.05(e_a)^{1/2}\right) (1-0.275f_c) - \sigma(T_a)^4. \qquad (62.)$$

Figure 33b plots the curves of BB2, BB3 and IJ with a cloudiness factor f_c = 0.5. The general effect is an increasing infrared radiation during the entire year for all parameterizations. But now the BB curves no longer reach to the maximum IJ value in summer. The reason for this is that in the BB definitions the cloudiness factor is multiplied only with the first term,

the second term $-\sigma T_a^4$ is not influenced by the cloud cover. In the IJ formulation the cloudiness factor affects the total magnitude of the incoming infrared radiation.

Some observational data for the atmospheric thermal radiation are available, and those are presented in Appendix B. These climatological data were originally delivered by Marushunova for Q and I, and by Doronin for H and E, both described in Russian papers, which are not available. Their data sets with monthly- averaged values are used by Maykut [1971], [1978], [1982] and Semtner [1975]. However, no information is given about the latitude or atmospheric conditions, and both data sets from Marushunova and Doronin are

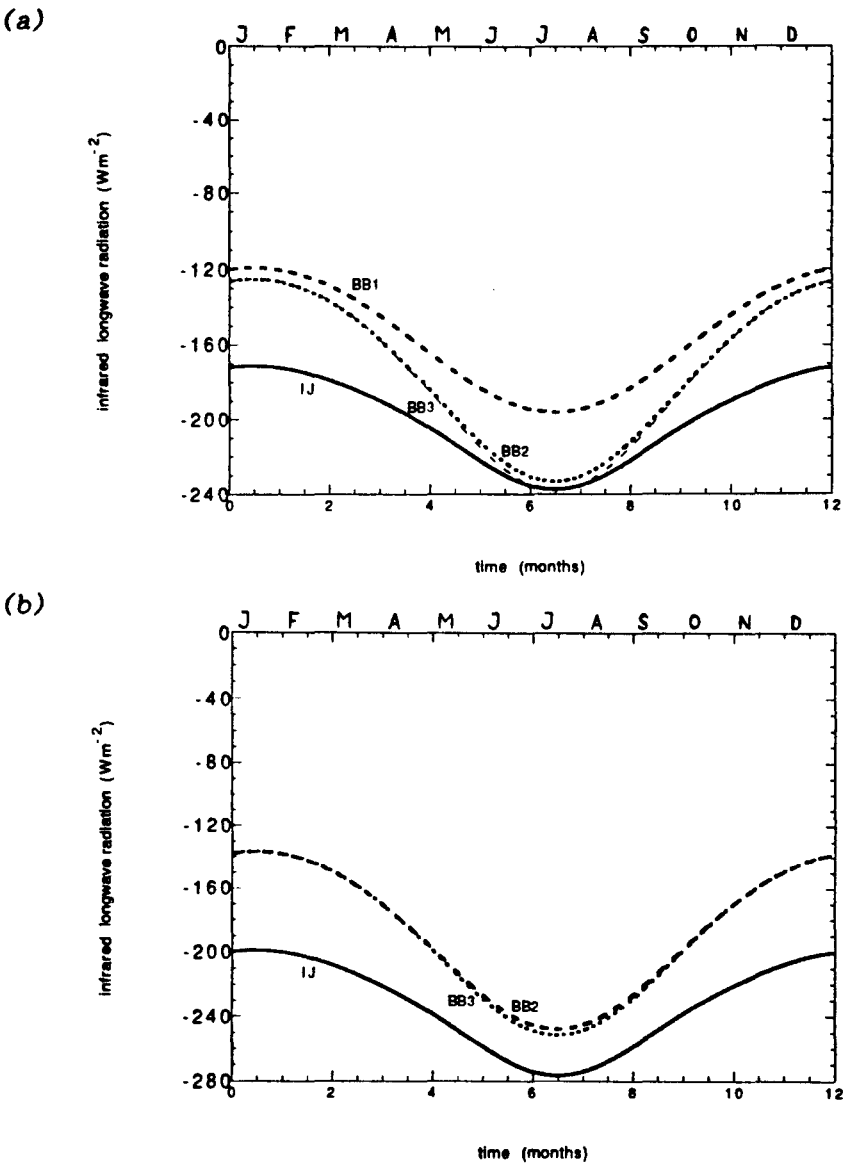

Fig.33 *(a) Incoming infrared radiation during a year according to definitions by Idso and Jackson (IJ) and Berliand and Berliand (BB) for clear skies. Further information see text. The atmospheric temperature is prescribed with $T_{am} = -14.8\,^{\circ}C$ and $T_{ampl} = -16\,^{\circ}C$.*
(b) Same as in (a) except now with a cloudiness factor $f_c = 0.5$.

old (1961 and 1963) and independent. So there is a lack of good observational data, and this makes it hard to judge whether the BB or the IJ formulation is most reliable. Nevertheless, when a comparison is made with figure A1, the IJ formulation predicts reasonably high incoming infrared radiation values which are more or less in the neighbourhood of the observational data. BB values are too low, although their amplitude is better.

When we compare ice thicknesses under the same experimental conditions, the BB formulation always predicts much larger thicknesses than the IJ formulation. At high latitudes the difference in ice thickness is more than two meters. The ice thickness in case of the BB description exceeds 5 m, although under moderate atmospheric conditions. Considering this the IJ definition seems more reasonable. Furthermore the heat balance shows us in case of the BB definition that the sensible heat flux is quite too large and always directed downward, which is not in correspondence with the few observational data, which always show a change in sign in the sensible heat flux during a year. The IJ definition gives rise to more realistic sensible heat flux values.

5.3.3. The latent and sensible heat flux

Regarding the behaviour of the latent heat flux, see figures 19 and 20, some remarks can be made. In summer the latent heat will rise to quite a high magnitude compared to the few observational data. The computed level is about two times higher. Uncertainties in the parameter values, such as the wind speed, the drag coefficient and the vapour pressure, contribute to this difference. The dip around June, caused by the stabilizing surface temperature in this melting period, is not very realistic either. Figures 19b and 20b show that the atmospheric temperature keeps rising above the melting point of ice (273.15 K), although the ice- surface temperature remains at this level. One should expect a feed-back from the ice to the atmosphere. This leads to a more moderate (T_s-T_a) difference. Thus the sudden dip in the latent heat, but also in the sensible heat and in the net infrared radiation, disappears and the curve will have a smoother behaviour in summer. These effects are not included in the ice model behaviour.

The value of the sensible heat flux is more or less corresponding with the data from Doronin, except upward values often become too large. The sensible heat flux always changes sign during a year of integration. Latitude and appearance of snowfall have influence on the time when this sign change in the sensible heat flux occurs. The quantity (T_s-T_a) plays a very important role in these computations.

5.4. The oceanic heat flux

Because of the difficulties in direct measurement, the magnitude of the oceanic heat flux is not precisely known. In the 'early' ice models the oceanic heat flux was taken a constant. Maykut and Untersteiner [1971] and Semtner [1975] indicated that the average value must lie close to 2 Wm^{-2} and they stated that lacking more precise information, this value was chosen and assumed to remain constant throughout the year. The choice of 2 Wm^{-2} was

predominantly based on its yielding the most satisfactory results. Parkinson and Washington [1979] also adapted this formulation of the bottom flux, although they mentioned that in some studies the flux from the mixed layer is directly proportional to the temperature difference between the water and the ice. However they state that the temperature directly underneath the ice remains practically at freezing level until the ice disappears, resulting in a zero calculated oceanic heat flux regardless of the proportionality factor (this reasoning does not seem to be very justified, because not only the temperature directly underneath the ice is of importance for the oceanic bottom flux, also the ocean water below the surface plays a role). Furthermore, an accurate calculation of the energy from ocean to ice would require incorporation of ocean salinity and a variable mixed- layer depth. For these reasons, they used the 2 Wm^{-2} for the oceanic heat flux in the Central Arctic (Typical fluxes from water to ice are believed to be much greater in the Antarctic than in the Arctic, namely up to 25 Wm^{-2}. This large difference is believed to be due to the different type of deep convection in the Arctic and the Antarctic. Both polar regions have different salt discharges to the deep ocean and different densities of the mixed layer, resulting in quite different deep convection.).

Harvey [1990] tested alternative parameterizations of the upward oceanic heat flux in a thermodynamic sea ice model. He found that the different parameterizations for this process can lead to dramatically different results in simulated sea- ice area, sea- ice thickness, or both. Furthermore, he stated that equatorward sea ice will be in contact with increasingly warmer mixed layer water, and that it is unrealistic to prescribe a fixed F_B in this case. Harvey tested seven different parameterizations of the heat flux F_B and found that in most of the cases the oceanic heat flux is much higher than 2 Wm^{-2} in the Arctic. In some cases it amounts up to 16 Wm^{-2} at certain latitudes.

Omstedt and Wettlaufer [1992] related ice growth to oceanic heat flux and introduced a bulk formulation, which very much resembles the definition given in equation (6.). Their model predicts oceanic heat fluxes that are quite variable in time due to short-term variations in ice drift. They also introduce observed values of the oceanic heat flux, which show a minimum level of about 5 Wm^{-2} and going up to even 30 Wm^{-2}.

The oceanic heat flux descibed in this paper originates from Pease [1964]. It is proportional to the temperature difference (T_m-T_B). In case an ice cover exists at any time of the entire year at a certain latitude, the mixed- layer temperature will tend to reach an equilibrium value which follows from (42.). The oceanic heat flux then equals the advection flux F_H. A value of 4 Wm^{-2} was chosen for this advection flux F_H. It is an agreement between the constant value given by Maykut and Untersteiner [1971], and the observational minimum as in Omstedt and Wettlaufer [1992]. For this magnitude, reasonable ice thicknesses were found as shown in section 4.8..

5.5. Deficiencies of the input parameters

In chapter 3 the thermodynamic ice model is described with the use of many different parameterizations. These parameterizations include many constants. However, in reality these quantities seem to be rather variable in time, sometimes changing over 100%. To give an estimate of the variability of the different 'constants', a survey of the most important changes in some

quantities will be discussed next.

First of all, the sea- ice model consists of only a single ice layer. The conductive heat flux F_s through this ice layer is caused by the temperature difference between bottom and top of the ice layer. This is a linear temperature profile through the ice. If we increase the vertical resolution of the ice layer, the differentation proces of ice growth and melt now will become more accurate. However, Semtner [1975] showed that the vertical diffusion process in ice can be treated quite accurately with only two temperature points in the ice. The physical processes remain the same, ice thicknesses only become about 10% smaller than with more than two grid points for temperature in the ice slab.

When adding snowfall to the sea- ice model, more realistic ice thicknesses are obtained (see section 5.2.). Snowfall is assumed to consist of a linear accumulation in different periods of the year, to a total yearly snowfall of 40 cm at any latitude where an ice slab is present. Of course this representation is not correct. Snowfall depends on latitude. Furthermore snowfall can be regarded as a fresh- water supply for the mixed layer of the ocean on the longer term. In the discussed ice model, however, the snow does not contribute to this salinity flux. If a salinity flux from the atmosphere was admitted, then the mixed- layer salinity would decrease constantly due to the precipitation, unless vaporazation of snow, ice and ocean water was implemented in the model. Another shortcoming in the current model is that snow cannot be converted into ice. In case of large build- ups of snow this should be possible.

The depth of the mixed layer underneath the ice is taken to be 100 meters. Pollard et al [1983] and Lemke [1987] use a variable mixed- layer depth that depends on profiles of temperature and salinity in the mixed layer. Mixed- layer depths increase in winter, while the layer becomes shallower in spring and early summer. Cold and saline water tends to sink into the deeper ocean, while warm and fresh water tends to stay at the surface of the ocean. This process also contributes to the thermohaline circulation in the ocean. Thus, taking h_m as a constant is not quite in correspondence with reality.

The magnitudes of the albedos of the different quantities in the model, such as ice, snow, water and clouds, are submitted to changes too. A small change in for example the ice albedo can have a large impact on the ice thickness, as can be seen in figure 34. Snow albedo is prescribed in Appendix B, but should depend directly on snow thicknesses. Cloud albedo values are very uncertain, because their radiative properties are not fully understood. Cloud albedos depend on the zenith angle and the optical depth of the clouds, which is a function of a moisture parameter such as the relative humidity.

The bottom temperature of the ice equals $-2^{\circ}C$. In fact the bottom temperature depends on the interfacial salinity between mixed layer and ice slab. Omstedt and Wettlaufer [1992] use an empirical freezing temperature. Their description couples the salt and temperature fields and has important effects on the heat flow to the ice. If the interfacial salinity increases, the freezing temperature will decrease and more heat becomes available for melting. An assumption made is that the interfacial temperature between the mixed layer and the ice layer is always that of freezing.

Cloud cover also plays an important part in the sea- ice model. It affects the incoming solar radiation and the multi- scattered incoming infrared longwave radiation. Often monthly fractional cloud covers f_c are

determined from satellite data. They have a large dependence on latitude and season. Parkinson and Washington [1979] used Arctic fractional cloud covers for each month. Intervening periods cloud cover amounts were obtained through linear interpolation. Figure 34 gives the influence on the ice thickness using a cloud cover percentage of 0.7 instead of the value 0.5 used in the standard case.

The wind speed v_a is a very variable parameter. It changes in magnitude and direction every day and depends on surface type (water, ice or ice edges). In some papers monthly- averaged values are chosen. For simplicity v_a is taken constant throughout the whole year, and 5 ms^{-1} is a reasonable value for the yearly- averaged wind speed. Figure 34 shows us the ice thickness in case of a wind speed of 7 ms^{-1}. In that case sensible and latent heat flux become quite large.

The drag coefficient C_D depends on the wind speed and surface type. Haney [1971] proposed a variable drag coefficient over the ocean, linearly depending on the wind speed. Generally the value over the open ocean falls between $1.1 \cdot 10^{-3}$ and $1.7 \cdot 10^{-3}$. For ice and snow the transfer coefficient is larger than for open ocean. Most of the papers use a drag coefficient of $1.75 \cdot 10^{-3}$.

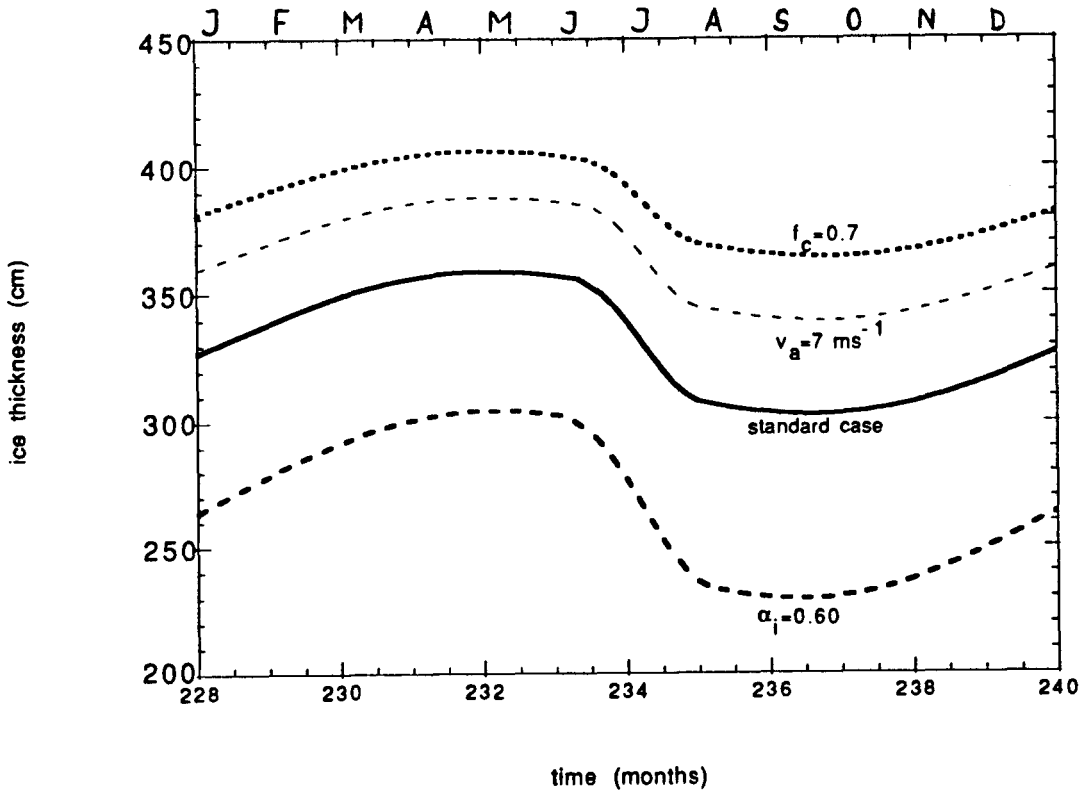

Fig.34 Ice thickness dependence on ice albedo α_I, fractional cloud cover f_c, and wind speed v_a. Also depicted is the equilibrium cycle of the standard case characterized with α_I=0.64, f_c=0.5 and v_a=5 ms^{-1}. The latitude is 74° N and snowfall is not included.

Also uncertainties exist about the magnitude of the ice density, ice salinity, saturation vapour pressure and other empirical formulations. In spite of all these shortcomings, the model predicts reasonable results. The simplicity of the model is a very important property, because this implies that physical processes can be understood more easily and implementation of the ice model into the ocean model is more or less straightforward.

Chapter 6. CONCLUSIONS

This last chapter will resume all the most important features of the presented thermodynamic ice model, and it will give a survey of the most important conclusions. The model is based on the 'zero-layer' ice model of Semtner [1976]. It is a thermodynamic sea- ice model: dynamics are not included, although in reality dynamic processes, such as drift and deformation, are quite important. The sea- ice model includes an upper ocean layer, the mixed layer, which delivers energy to the ice shelf by a bottom flux, and furthermore the ice model is forced with a temporally and latitudinally dependent atmospheric temperature, which applies to the 170° W longitude on the Northern Hemisphere. At this longitude no land is present. Through the Bering Strait the ocean flows in between the continents of Russia and Northern America.

The purpose of building this sea ice model was to investigate the impact of an ice cover on the energy balance between the atmosphere and the ocean: a sea- ice cover forms a very effective barrier between the ocean and the atmosphere. Furthermore the sea- ice model is meant to be implemented in a three-level ocean model to investigate the response of the ocean to this insulating ice shelf, especially considering the thermohaline circulation. Mixed- layer temperature and mixed- layer salinity are important quantities involving the thermohaline circulation and these quantities can be considerably influenced by the ice shelf.

The main features of the sea- ice model are the following:

1. The model predicts a reasonable realistic description of the seasonal cycles of ice and snow thickness and ice surface temperature. It contains ice growth and ice melt, snowfall and snow melt and computes the surface- temperature behaviour using energy balance equations.
2. Multi- year equilibrium cycles of ice thickness occur at the ice edge due to the additional snow cover. Semtner found the same kind of ice- thickness behaviour. This mechanism of the multi- year equilibrium cycles might be important in considering multi- year anomalies in the observed ice cover.
3. The heat balance of the ice is in equilibrium after each integration time step, except during the melting period, where the imbalance in the heat fluxes is used for melt of the ice and the snow layer. The incoming solar radiance is quite realistic. The behaviour of the incoming longwave infrared radiation is hard to verify with the very few observed data, but its parameterization is commonly used in most of the existing sea- ice models. The latent and sensible heat flux have reasonable directions (upward or downward) during the entire year, but their magnitudes are somewhat too large.
4. Ice thicknesses strongly depend on the value of the mean forcing atmospheric temperature and also on the annual amplitude of the atmospheric temperature. This implies a strong latitudinal

dependence on the ice thickness.

5. Ice thicknesses strongly depend on the value of the bottom and advection flux in the oceanic mixed layer. Experimental data on the bottom flux are very scarce and uncertain, thus verification is quite difficult.
6. Ice grow and ice melt influence the salinity flux into the mixed layer. The salinity contents of the mixed layer varies most at the ice edge. In summer the ice edge acts as a large fresh- water flux region, in winter as a salt- water flux region. The salinity contents of the mixed layer has no feedback on the ice growth or the freezing point of the sea water in the current model.
7. The seasonal ice- thickness cycle starting at a certain initial ice thickness at the beginning of integration towards an equilibrium ice- thickness cycle, shows high- frequency behaviour superposed on exponential behaviour in time with a certain time constant. This time constant depends on ice thickness and the temperature difference between the bottom and the surface of the ice layer. Spin- up times of the model vary between 5 and 20 years.
8. Mixed- layer temperatures underneath the ice tend to go to equilibrium values just above the freezing point of sea water. With partial or no annual ice cover the mixed layer temperature shows variations corresponding to the atmospheric forcing.

The presented thermodynamic sea ice model has the following advantages: It contains a clear and reasonable physical mechanism, in which energy transport and energy exchange are very important. Furthermore, the model has a very simple design, which facilitates understanding and eventual implementation of the model into an ocean model. The model is not built to get extremely good representations for certain polar regions, as in Mysak et al. [1991a], [1991b], Willmot [1988] and Wood [1989]. Nevertheless, the model is able to simulate a fairly realistic ice cover, and makes it possible to study on the main physics of a growing or melting ice shelf.

Acknowledgements

The first line of the 'acknowledgements' always is the most difficult line to start with. However..., as you can see, this first line already appears to be written down. So now I can start to send my gratitude to the following persons.

I would like to thank Bart van der Sijde, for giving me the opportunity to perform my graduate research at the KNMI in de Bilt, and for his interest and support in my work. I am also grateful to Gert Jan van Heijst, for his enthusiastic contribution and his useful comments during the informal meetings at the University of Eindhoven.

At the KNMI, I was surrounded by several very kind and helpful people and they created a very pleasant working environment.

First of all, there is Rein Haarsma, my 'supervisor' during my graduate research, mister Salsa with the large moustache, conga minded, and laughing loudly down the hall when responding to a telephone call. Rein, I really enjoyed your leading role in my work. You were always helpful, patient and enthusiastic, even when my 'Gammon' project created ice thicknesses up to several thousands of kilometers.

I would like to thank Theo Opsteegh, head of the fundamental research department of the KNMI, for allowing me to stay for one year in room 259. You always greeted me with a smile: 'hello, Laurens!' I liked that very much.

Furthermore I want to name all my working mates for their help, their company and their friendship. We have

skating room-mate Geert 'wat? hole in one' Lenderinkson,
how much Ding Dong 'maybe garlic, whaaaarghh' HongNian,
(non) smoking bold Roger 'you're in the army now' Salden on the move,
dangerous driving Frank 'flying frisby' daddy Selten,
I want to do some ballsports Jan 'met andere woorden' Barkmeijer,
Dutch piano fireman Xueli 'negga negga twin bike' Wang,
(Dutch) kwin Liu 'walk in, sjing sjeng gwoa' Lientje Qing,
the hardest working man in show business Wim 'jumpin'jack' Verkleij,
running Robert 'an Englishman in de Bilt' Mureau ECWMF,
desk thief Maarten 'zooooooo, koffie' Ambaum,
Japanese Ruben 'beardy' Pasmanter,
Canadian wait a minute Peter 'what a beard!' Houtebovenkamer,
hihihihi Helena 'Russian pancakes with wodka' Karthasjova,
blablablabla... Eduard 'blabla..modon..blabla' Nephews

Of course there are many persons more to be named. Thank you for being there! I'll will miss you all!!!

APPENDIX A Check of the thermodynamic ice model

In order to see if the numerical procedure gives correct predictions of the ice thickness, the sea- ice model has been run using constant annual atmospheric fluxes and an annual- averaged snow albedo. In this case the results of the numerical computations should be equal to the equilibrium values. The results are shown in table A1. Two cases have been investigated, one without snow cover and one with a yearly snowfall of 40 cm.

The surface temperature values are perfectly matching. The ice thickness values only differ very slightly (0.3%), which is presumably due to truncation in the several numerical procedures.

The annual atmospheric fluxes are respectively H = 4.3061, E = -3.6467, I = $-2.23\ 10^2$, and $Q_o = -1.0146\ 10^2$ W m^{-2}, and the snow albedo has been set on 0.7825.

Table A1. Check of the numerical ice thickness h_i

No snow cover	exact equilibrium solution	numerical computed solution	difference in %
h_i (cm)	$1.2158 \cdot 10^3$	$1.2121 \cdot 10^3$	0.31
Ts (K)	$2.5982 \cdot 10^2$	$2.5982 \cdot 10^2$	0.00
With snow cover			
h_i (cm)	$1.4257 \cdot 10^3$	$1.4209 \cdot 10^3$	0.33
T_s (K)	$2.5542 \cdot 10^2$	$2.5542 \cdot 10^2$	0.00

APPENDIX B Heat fluxes according to Maykut and Untersteiner

Maykut and Untersteiner [1971] prescribed a standard atmospheric forcing. Fluxes are taken to be positive when directed upward. In table A2 monthly-averaged values of H, E, I and Q_o are given. Instantaneous values of these surface fluxes are deduced using linear interpolation between monthly-averaged values. Also the monthly- averaged values of the snow albedo are depicted in table A2. As can be seen the incoming solar shortwave radiation is zero during the polar night. The exact latitude is unknown.

Table A2. Prescribed standard forcing

	$-Q_o$ (W m^{-2})	- I (W m^{-2})	- H (W m^{-2})	- E (W m^{-2})	α_s
Jan	0	168.0	19.1	0	0.83
Feb	0	166.3	12.3	-0.32	0.83
Mar	30.7	166.3	11.6	-0.48	0.83
Apr	160	187.3	4.68	-1.5	0.81
May	286	243.8	-7.27	-7.4	0.82
Jun	310	290.7	-6.30	-11.3	0.78
Jul	220	308.4	-4.84	-10.3	0.64
Aug	145	302.0	-6.46	-10.7	0.69
Sep	59.7	266.4	-2.75	-6.3	0.84
Oct	6.5	224.5	1.61	-3.1	0.85
Nov	0	180.9	9.04	-0.16	0.85
Dec	0	176.0	12.8	-0.16	0.85
Year	101.9	223.4	3.62	-4.31	—

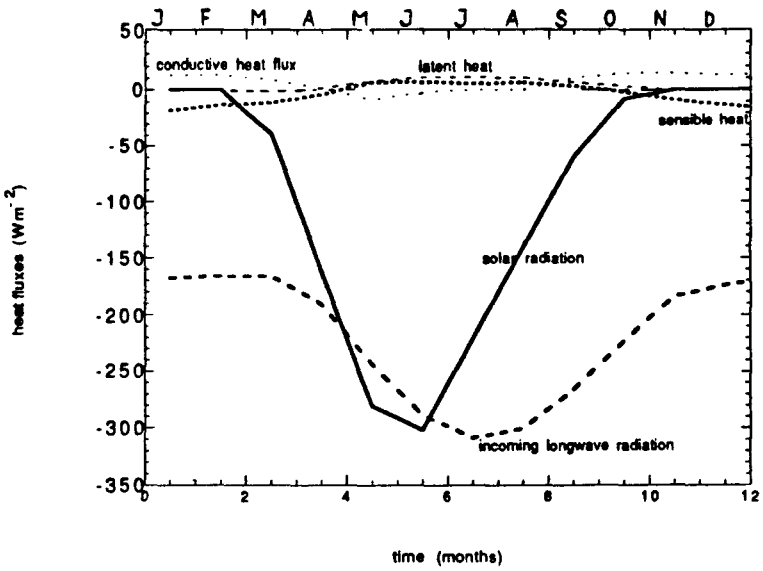

Fig.A1 Prescribed standard forcing by Maykut and Untersteiner.

APPENDIX C Parameter sensitivity according to Semtner

In this appendix we will give a survey of the influence of the magnitude of several parameters using the atmospheric forcing as prescribed in appendix B. In table A3 all the different experiments are summarized. This table also displays the mean annual ice thickness as computed by Semtner [1976] for the same parameter values.

Table A3. Summary of cases

case no.	ice model mean annual thickness (cm)	Semtner mean annual thickness (cm)
1	265	289
2	413	-
3	316	333
4	225	243
5	465	504
6	153	172
7	85	97
8	114	148
9	173	177
10	178	-

characteristics of case no.:

1. *heat budget as prescribed in table A1 and* F_B*=2.0185* Wm^{-2}*;*
2. σ*=5.79·10*$^{-8}$ $Wm^{-2}K^{-4}$ *instead of the normal Stefan- Boltzmann value;*
3. *near- fresh water below the ice (*T_B *= -0.1* °*C);*
4. P_o*=0% of* Q_o*, so no fraction of the shortwave radiation penetrates the ice;*
5. F_B*=0; no heat flux from the ocean;*
6. F_B*=4.0369* Wm^{-2}*;*
7. F_B*=6.0554* Wm^{-2}*;*
8. *H= E= 0, so no sensible or latent heat flux;*
9. Q_o *increased by 10%;*
10. *ice albedo = 0.58;*

In the standard case the mean annual thickness is 24 cm lower than computed by Semtner. This small difference can be due to differences in the Stefan-Boltzmann constant and in the numerical procedures. His paper contains some errors concerning the exact value and the dimension of σ (see note). It is not clear which value of σ he used in his computations.

Experiment 2 shows the sensitivity of the ice thickness to σ. Here the Stefan Boltzmann constant σ has been increased by 2%. Compared with the usual σ value, as in experiment no. 1, the ice- layer thickness has increased more than 140 cm. This large impact of the σ value can be

explained by the black- body emission term in (2.) and (3.), which is proportional with T_s^4.

Similar as in case no.1 the sea- ice thicknesses simulated in the other experiments are slightly lower than computed by Semtner.

note, Semtner used for σ a value of 1.385 10^{-12} erg $cm^{-2} K^{-4} s^{-1}$ which equals 1.385 10^{-1} $Wm^{-2} K^{-4}$ in SI-units. It is assumed that the author used the 'correct' value of σ (which is still 2% higher than usual as stated by Semtner) in his experiments.

APPENDIX D Ice- thickness sensitivity to the snowfall rate

Until now the annual snowfall was equal to 40 cm. If we consider this amount of snowfall to correspond to a snowfall rate equal to 1, we can investigate the ice- thickness sensitivity to other values of the snowfall rate. Figure A2 shows this dependency. The experiments are performed at 78° N and the mean atmospheric temperature is according to Oort's data plus an additional two degrees Celcius. The time- step size of integration had to be lowered from 5 days to 1 day, because otherwise numerical instabilities occurred. As can be seen, the ice thickness linearly decreases when increasing the snowfall rate. Equation (8.) shows that the equilibrium ice thickness is indeed linearly dependent on the snow- layer thickness.

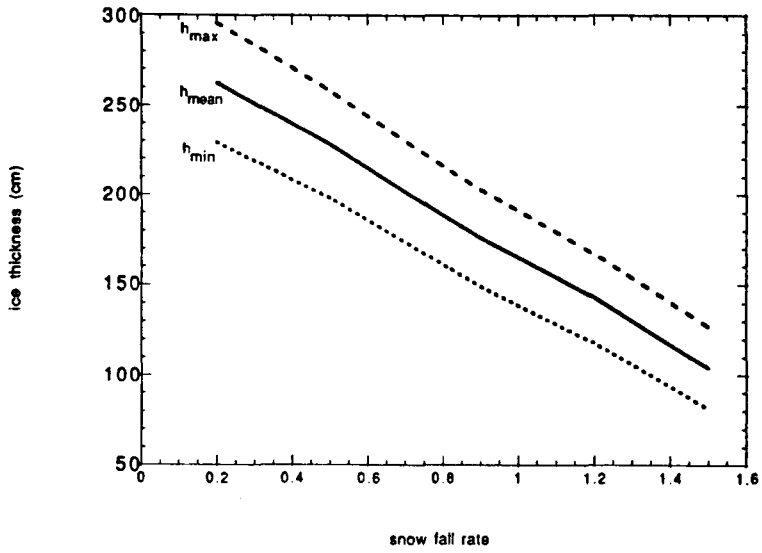

Fig.A2 Ice thickness- sensitivity to the snowfall rate at 78° N. A snowfall rate of 1 corresponds to an annual snowfall of 40 cm. The atmsopheric temperature is according to Oort's data plus an additional two degrees Celcius.

Now we consider a latitudinally dependent snowfall rate, for example in the following way

$$h_s(t+\Delta t) = h_s(t) + \Delta h_s \cdot \sin\left(\frac{\pi}{180}(-4\phi + 30)\right) \qquad (63.)$$

where Δh_s is the change in snow layer thickness due to snowfall as prescribed in section 3.4. and ϕ is the northern latitude in degrees. At 75° N latitude the snowfall rate is at a maximum. The consequenses for the multi- year equilibrium cycles are shown in figure A3. There are clear differences with the situation of non- latitudinally dependent snowfall as shown in figure 27, concerning sea- ice extent and multi- year cycles.

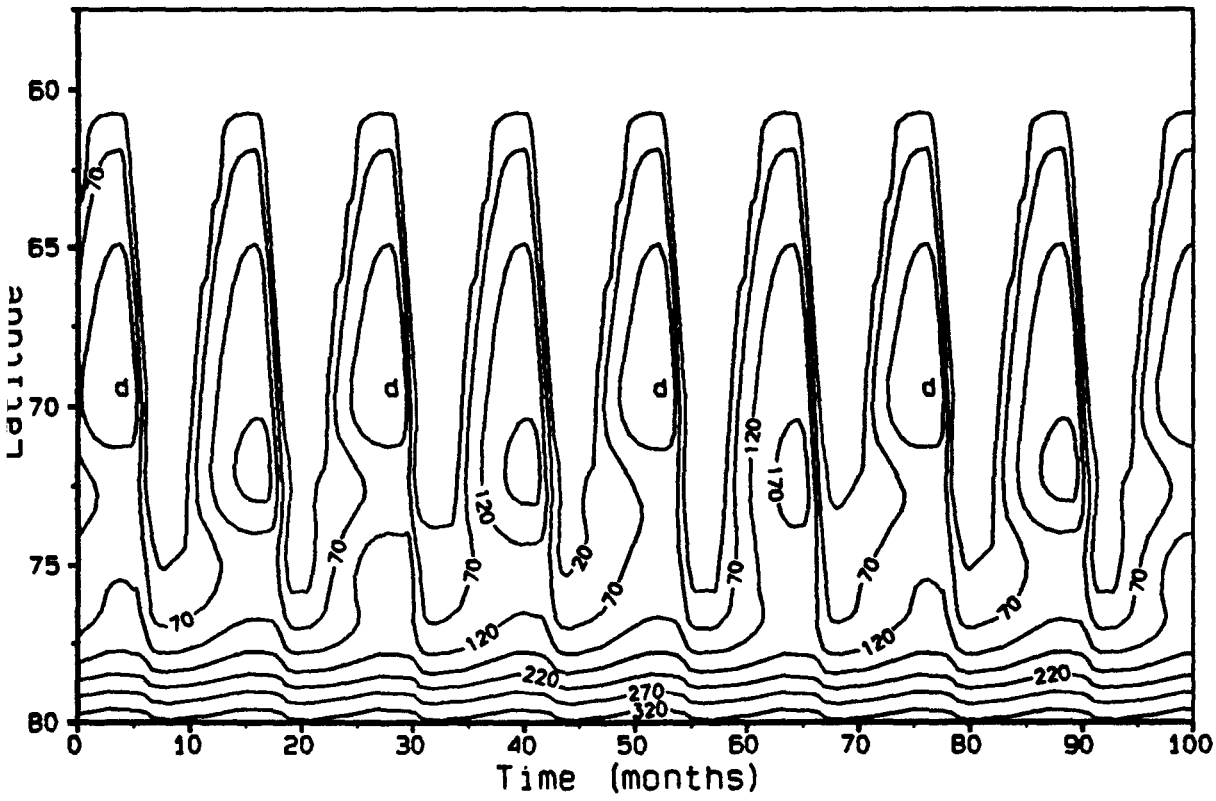

Fig.A3 Ice- thickness field with a latitudinally dependent annual snow fall. The atmospheric temperature is according to the Oort data plus an additional two degrees Celcius. Several multi- year cycles can be distinguished.

APPENDIX E Emission scenarios of the IPCC

Here follows a brief description of the emission scenarios as mentioned in the IPCC report [1990]. Growth of the economy and population was taken common for all scenarios. Population was assumed to approach 10.5 billion in the second half of the next century.

In the *Business- as- Usual scenario* the energy supply is coal intensive and on the demand side only modest efficiency increases are achieved. Carbon monoxide controls are modest, deforestation continues until the tropical forests are depleted and agricultural emissions of methane and nitrous oxide are uncontrolled. For CFCs the Montreal Protocol is implemented albeit with only partial participation.

In *scenario B* the energy supply mix shifts towards lower carbon fuels, notably natural gas. Large efficiency increases are achieved. Carbon monoxide controls are stringent, deforestation is reversed and the Montreal Protocol implemented with full participation.

In *scenario C* a shift towards renewables and nuclear energy takes place in the second half of the next century. CFCs are now phased out and agricultural emissions limited.

For *scenario D* a shift to renewables and nuclear in the first half of the next century reduces the emissions of carbon dioxide, initially more or less stabilizing emissions in the industrialized countries. Carbon dioxide emissions are reduced to 50% of 1985 levels by the middle of the next century.

APPENDIX F Word list

advection flux: the advection and diffusion flux of sea water from nearby regions and from deep oceanic layers;

albedo: the percentage of incident solar radiation that is reflected at a certain surface;

bottom flux: heat flux from the upper ocean layer into the bottom of the covering ice slab;

brine pocket: small pocket of concentrated salt within an ice slab;

cryosphere: climate component which includes all the elements of the current climate which are related to frozen water, such as sea ice, snow, ice sheets, glaciers and permafrost;

ice leads: large open ocean areas in between enormous ice covers;

latent heat: atmospheric heat flux which arises due to humidity differences between surface and anemometer level of the air;

latent heat of fusion: the heat that is necessary to melt one cubic metre of ice or snow;

mixed layer: the upper ocean layer (in this report the upper 100 m), where temperature and salt exchange with the atmosphere or covering ice slab is realised;

sensible heat: atmospheric heat flux which arises due to temperature differences between the surface and the overlying atmosphere;

thermohaline circulation: ocean circulation on a global scale, induced by temperature and salinity gradients;

zenith angle: angle over which the solar radiation enters the Earth's surface. It depends on latitude, time of the year, and hour of the day.

BIBLIOGRAPHY

Berliand, M.E., and Berliand, T.G., 1952: Measurement of the effective radiation of the earth with varying cloud amounts (in Russian). *Izv. Akad. Nauk. SSSR Ser. Geofiz.*, no.1.

Berger, A., Imbrie, J., Hays, J., Kukla, G. and Saltzman B., 1984: Milankovitch and climate, part 1, Understanding the response to astronomical forcing. Dordrecht /Boston /Lancaster.

Fung, I.Y., Harrison, D.E. and Lacis, A.A., 1984: On the variability of the net longwave radiation at the ocean surface. *Rev. Geophys. Space Phys.*, 22, 177-193.

Haney, R.L., 1971: Surface thermal boundary condition for ocean circulation models. *J. Phys. Oceanogr.*, 1, 241-248.

Harvey, L.D.D., 1988(a): A semianalytic energy balance climate model with explicit sea ice and snow physics. *J. Climate*, 1, 1065-1085.

Harvey, L.D.D., 1988(b): Development of a sea ice model for use in zonally averaged energy balance climate models. *J. Climate*, 1, 1221-1238.

Harvey, L.D.D., 1990: Testing alternative parameterizations of lateral melting and upward basal heat flux in a thermodynamic sea ice model. *J. Geophys. Res.*, C95, 7359-7365.

Harvey, L.D.D., 1992: A two-dimensional ocean model for long-term climate simulations: stability and coupling to atmospheric and sea ice models. *J. Geophys. Res.*, C97, 9435-9453.

Henderson-Sellers, A. and McGuffie, K., 1979: A Climate Modeling Primer. Wiley, Chichester, GB.

Hibler, W.D.: Modeling sea ice thermodynamics and dynamics. *Survey report*, Hannover, NH 03755, 1-48.

Hibler, W.D., 1978: A dynamic thermodynamic sea ice model. *J. Phys. Oceanogr.*, 9, 815-845.

Hibler, W.D., 1980: Modeling a variable thickness sea ice cover. *Mon. Weather Rev.*, 108, 1943-1973.

Holton, J.R., 1979: An Introduction to Dynamic Metereology. *International Geophysics series, volume 23, second edition.* Academic Press, New York.

Idso, S.B. and Jackson, R.D., 1969: Thermal radiation from the atmosphere. *J. Geophys. Res.*, C74, 5397-5403.

Intergovernmental Panel On Climate Change, 1990: Climate change, the IPCC Scientific assessment. Edited by J.T. Houghton, G.J. Jenkins and J.J. Ephraums.

Kipfstuhl, J., 1991: On the formation of underwater ice and the growth and energy budget of the sea ice in Atka Bay, Antarctica. *Ber. zur Polarf.*, 42-65.

Lemke, P., 1987: A coupled one-dimensional sea ice-ocean model. *J. Geophys. Res.*, C92, 13164-13172.

Lenderink, G., 1992: Sensitivity and internal variability of the thermohaline circulation. *Afstudeerverslag TU Delft.*

Maykut, G.A. and Untersteiner, N., 1971: Some results from a time-dependent thermodynamic model of sea ice. *J. Geophys. Res.*, C76, 1550-1575.

Maykut, G.A., 1978: Energy exchange over young sea ice in the Central Arctic. *J. Geophys. Res.*, C83, 3646-3658.

Maykut, G.A., 1982: Large-scale heat exchange and ice production in the Central Arctic. *J. Geophys. Res.*, C87, 7971-7984.

Mitchell, J.F.B., 1989: The "Greenhouse" effect and climate change. *Rev. Geophys.*, 27, 115-139.

Mysak, L.A., Power, S.B., 1991(a): Greenland sea ice and salinity anomalies and interdecadal climate variability. *Climatological Bulletin*, 25(2), 81-91.

Mysak, L.A., Peng, S. and Wood, R.G., 1991(b): Application of a coupled ice-ocean model to the Labrador sea. *Atmosphere-Ocean*, 29(2), 232-355.

Omstedt, A. and Wettlaufer, J.S., 1992: Ice growth and oceanic heat flux: models and measurements. *J. Geophys. Res.*, C97, 9383-9390.

Oort, A.H. and Peixoto, J.P., 1992: Physics of Climate. American Institute of Physics, New York.

Parkinson, C.L. and Washington, W.M., 1979: A large-scale numerical model of sea ice. *J. Phys. Oceanogr.*, 84, 311-337.

Pease, C.H., 1975: A model for the seasonal ablation and accretion of the Antarctic sea ice. *AIDJEX Bull.*, No.29, 151-172 (unpublished manuscript).

Pollard, D., Batteen, M.L. and Han, Y.J., 1983: Development of a simple upper-ocean and sea-ice model. *J. Phys. Oceanogr.*, 13, 754-768.

Press, H.P., Flannery, B.P., Teukolsky, S.A. and Vetterling, W.T., 1986: Numerical Recipes. Cambridge University Press.

Saltzman, B., 1978: A survey of statistical-dynamical models of the terrestrial climate. *Adv. Geophys.*, 20, 281-290.

Semtner, A.J., 1976: A model for the thermodynamic growth of sea ice in numerical investigations of climate. *J. Phys. Oceanogr.*, 6, 379-389.

Stössel, A., 1991: The Hamburg sea-ice model. *Technical Report No.3*, 1-41.

Various authors, 1990-1992: World climate research programme: Sea ice and climate, WRCP-41, -45, -62, -65.

Various authors, 1990: Milieu en Energie. Collegedictaat TUE, nr. 3472.

Washington, W.M. and Parkinson, C.L., 1986: An introduction to three-dimensional climate modeling. Oxford University Press.

Wilmott, J. and Mysak, L.A., 1988: A simple steady-state coupled ice-ocean model, with application to the Greenland- Norwegian Sea. *J. Phys. Oceanogr.*, 19, 501-518.

Wood, R.G. and Mysak, L.A., 1989: A simple ice-ocean model for the Greenland Sea, *J. Phys. Oceanogr.*, 19, 1865-1880.

Yuen, C.W., Cherniawsky, J.Y., Lin, C.A. and Mysak, L.A., 1992: An upper ocean general circulation model for climate studies: global simulation with seasonal cycle. *Climate Dyn.*, 7,1-18.